Master’s Thesis

PCRGLOB-SET –

DEVELOPMENT AND VERIFICATION OF A GLOBAL SEDIMENT SUPPLY MODEL

Jannis Hoch

UNIVERSITY OF TWENTE.

Master's Thesis

"PCRGLOB-SET –

DEVELOPMENT AND VERIFICATION OF A GLOBAL SEDIMENT SUPPLY MODEL"

Jannis Hoch

B.Sc. Environmental Engineering (TU Munich, Germany)

In partial fulfilment of the requirements
for the degree of

Master of Science in Civil Engineering and Management

University of Twente, November 7, 2014

Under supervision of the following committee:

Dr. ir. J.C.J. Kwadijk
University of Twente, Department of Water Engineering and Management
Stichting Deltares

Dr. ir. D.C.M. Augustijn
University of Twente, Department of Water Engineering and Management

Dr. M.S. Krol
University of Twente, Department of Water Engineering and Management

Abstract

Sound knowledge of sediment transported along rivers and into the oceans is a relevant factor for the assessment of coastal erosion as well as for the maintenance of important ecosystems. Along with the increase of the World's population, human actions have continuously impacted the detachment of soil and its transport towards the coast. The main interferences are the constructions of dams, the application of soil conservation practices as well as the intensification of land-use. In order to determine the global sediment flux into the oceans, models of soil erosion and sediment transport are needed. Therefore, the global sediment supply model PCRGLOB-SET has been developed. It is based on the RECODES model and uses equations of the RUSLE with some adaptions and extensions required for the large-scale application. The developed model is capable of producing monthly and annual output at a 0.5° grid cell resolution. Comparing the model output with observed values yields a coefficient of correlation of r=0.62. Thereby the main continental contributors of sediment into the oceans are correctly resembled with Asia delivering 41% of the global annual value. Since PCRGLOB-SET is a first-order model, it computes only unaffected sediment supply. The global annual sediment supply is determined to be between 150 GT/year and 195 GT/year which is, given the absence of important influences, a good estimate. The monthly output of PCRGLOB-SET has been compared to measured values in four river basins. Generally, the model is capable of representing the monthly fluctuations with most coefficients of correlation lying above 0.5. A sensitivity analysis revealed that the model output is less sensitive towards changes in the slope angle and temperature, but more sensitive towards variations in precipitation and vegetation cover. The intensity of these responses differs between continents. While precipitation changes strongly affect sediment supply in Africa while fluctuations of vegetation cover leads to considerable responses of computed sediment supply in South America. Model results are discussed in the light of model limitations such as the constricted representation of human influences and natural alluvial processes as well as in the model formulation. Eventhough these impacts cannot be explicitly quantified, it is concluded that PCRGLOB-SET provides a good starting point for further developments. In order to obtain more accurate results, it would be necessary to implement dams and reservoirs and to use a finer spatial resolution. Moreover, some equations applied in PCRGLOB-SET need to be tested more closely in order to apply them on the global scale. Nevertheless, the developed model shows potential for further improvements which are facilitated by the fact that the model has been coded in PCRaster which is a freely available and easily accessible tool for environmental modelling.

Preface and Acknowledgments

This Thesis marks not only the end of a long process of researching but also of my study time. While always looking on the global scale, the topic of my Thesis turned from the investigation of reservoir sedimentation towards the development of a sediment supply model. It is the purpose of this model to produce both monthly and annual values of sediment supply by applying the RUSLE on the global scale. To that end, a lot of different data sets had to be acquired, manipulated and processed.

I want to sincerely express my gratitude to my supervisors Jaap Kwadijk, Denie Augustijn and Maarten Krol. Without their valuable input and effort throughout the entire process, it would not have been possible to bring this Thesis to a satisfying end. Thank you!

Besides from my supervisors, I received a lot of input, inspiration and ideas from other persons which have to be acknowledged here of course as well. First of all, I need to mention Rens van Beek of the University of Utrecht who provided important information about and data from PCRGLOB-WB which I used in my Thesis. In addition, he helped me out with some struggles with PCRaster. Next, I own my thanks to Mesfin Mekonnen of the University of Twente and Stefan Kern of the University of Hamburg who kindly helped me out with the acquisition and manipulation of important input data. Last but not least, I thank Hessel Winsemius and Frederiek Sperna Weiland from Deltares as well as Paul van Dijk for their contributions to this Thesis.

And now that 5 years of studying come to an end, I can finally thank my family, especially my parents Ellen and Berti as well as my grandfather Walter, for their support during this time. I am more than grateful that you made this possible for me.

Jannis Hoch

Enschede, November 07, 2014

Table of Content

1. Introduction

1.1. Background

"Understanding the redistribution of continental substrate through weathering and erosion is one of the fundamental goals of geological sciences (Syvitski & Milliman, 2007)". Besides its importance in geological sciences and other scientific fields, sediment transport and distribution plays a crucial role in the field of civil engineering as well. For instance, sound knowledge of the amount of transported sediment facilitates the assessment of morphological changes both in rivers and at the coast and therefore the design of appropriate flood protection measures. However, estimating the distribution of sediment is challenging due to the complex nature of soil erosion and sediment transport. Additionally, human activities severely affect these processes. On the one side, deforestation and extensive agriculture accelerate soil erosion while on the other side the continued construction of reservoirs hinders the transport of sediment along rivers (Syvitski *et al.*, 2005). Additionally, projected changes in precipitation and temperature will most likely influence the weathering of rocks and detachment rate of soil as well.

As insinuated, these interferences may have serious implications. Amongst others, less sediment supply facilitates coastal erosion and affects wetlands and aquatic habitats (Syvitski, 2008; Yang *et al.*, 2006; Yang *et al.*, 2007). In case of increased sediment transport, reservoirs will be siltated at an accelerating rate, leading to a reduction in storage capacity. Consequently, freshwater distribution for agriculture is hampered and the potential for hydropower generation is reduced, risking social and economic cuts (Morris & Fan, 1998; Palmieri *et al.*, 2001; Wisser *et al.*, 2013). As a result of the aforementioned complexity of sediment supply, the spatial distribution and magnitude of these impacts will differ for different areas (Walling, 2006). Hence, it is decisive to achieve knowledge about the distribution, amount and timing of sediment discharges.

Traditionally, sediment fluxes were obtained by field measurements. However, in times of limited funding and increased computational power, extensive field studies are only rarely economically viable and hence can largely be replaced by the application of computer models. Computer models are furthermore advantageous because they enable researchers and policy makers to investigate the impact of changed parameters on the system and can contribute in collaborative learning processes (Brugnach *et al.*, 2007; Stahl *et al.*, 2006). In turn, better insight in dynamics and decisive hot-spots within a system can be obtained and policy-making can be built on sound knowledge.

However, the scale on which computer models are applied is often small and reduced to single river basins or even sub-catchments. This severely limits the potential of global assessments of sediment supply which are needed to investigate global processes, changes and adaptions. These changes could for example result from climate change impact (Asselman *et al.*, 2003; Goode *et al.*, 2012; Mukundan *et al.*, 2013) or continued human interference with the natural systems such as river impoundments (Miao *et al.*, 2011; Syvitski *et al.*, 2005; Vörösmarty *et al.*, 2003; Yang *et al.*, 2006).

More globally oriented assessments will most likely become increasingly essential in the future because the magnitude and extent of many problems cannot be estimated on the basin scale anymore but require a bigger scale picture. What is more, modelling sediment discharge only in individual basins and sub-catchments does not add to the assessment of sediment discharge in more remote or ungauged areas. Here, the development of global sediment supply models can ease the problem of lacking information.

1.2. Research motivation

Global sediment supply models focus more on annual totals and often neglect the temporal variability of sediment supply. This is a major disadvantage as knowledge of the variations in sediment supply can be applied in various fields. For example, sediment removal techniques of reservoirs such as sediment routing by flood drawdown can be timed better which leads to less loss of storage water (for detailed information see Morris and Fan (1998)). In addition, annual totals based on monthly output are superior to annual averages as the effect of monthly variations in rainfall and vegetation on soil erosion is captured better (Pelletier, 2012). Transported sediment is furthermore subject to temporal storage. In order to be able to implement this process correctly into any model, temporal model output is a prerequisite.

Some global models use geomorphic features of individual river basins to determine a global value which ties up a lot of capacity such as the just recently published WBMsed model by Cohen *et al.* (2013). Thus, there is the need of a global model that is capable of determining sediment supply at different temporal resolutions while considering only the most important drivers of sediment supply. As a first approach, it seems appropriate to build upon an already existing model structure. Since it is only a first-order modelling approach and unlike other current models (for example from Pelletier (2012)), the model should be accessible and manipulable by others for further improvements and adaptions. Another issue that recently gained importance is the accessibility and transferability of scientific data and models. This motivates the development of a model that does not require specific computational preconditions, has little demand regarding the accessibility of the input data and can be coded and manipulated with open source software.

1.3. Research objective and questions

It is the objective of this Thesis to develop a global sediment supply model which is based on existing model formulations of basin-scale sediment supply models. Besides annual totals, the model should be able to produce monthly values of sediment delivery as well. Furthermore, the model is required to work with readily available and easily accessible data sets. For coding the model, open source software will be used. Finally, the model will consider only the most important drivers of sediment supply due to the limited scope of this Thesis.

Based on this model, the following research questions shall be answered in this Thesis:

a) *How much sediment is delivered throughout a year at different spatial scales?*
b) *What are the monthly variations of sediment supply within a year?*
c) *Which basins are main sources of sediment transport to the oceans?*
d) *How well does the developed model perform?*

1.4. Methodology

The model developed in this Thesis is named "PCRGLOB-SET"[i] and works at a spatial resolution of 0.5° to 0.5° which is around 55 km to 55 km at the Equator. This name has been chosen as the model is strongly linked to the PCRGLOB-WB model (van Beek & Bierkens, 2008) which runs at the same spatial resolution and computes global water balances. Moreover, both models are coded with the same programming language, namely "PCRaster"[ii] (Wesseling *et al.*, 1996) which is explicitly written for environmental modelling purposes. With this freely available programme it is possible to manipulate data directly within a raster GIS environment at various temporal and spatial resolutions.

The model set-up of PCRGLOB-SET is based on the RECODES[iii] model which has been developed by van Dijk (2001). In turn, the RECODES model is strongly linked to the GAMES[iv] model (Dickinson *et al.*, 1986; Dickinson *et al.*, 1992). RECODES was chosen because it requires, unlike other erosion models, relatively little data that is globally available while it allows for simulating sediment fluxes on a monthly basis. The GAMES model

[i] PCRaster GLOBal SEdiment Transport
[ii] More information and the freely available software itself can be found on: http://pcraster.geo.uu.nl/
[iii] Rhine model for evaluating effects of Environmental Change On Delivery of Eroded soil to Streams
[iv] Guelph model for evaluating effects of Agricultural Management systems on Erosion and Sedimentation

assumes that sediment source areas do not necessarily coincide with major soil erosion areas, due to variations in the capacity of different parts in a basin to transport sediment. Hence, it consists of two modules, namely a Sediment Production Module and a Delivery Ratio Module. In RECODES, these main ideas of GAMES have been used and extended by equations taken from other models such as USLE (Wischmeier & Smith, 1978), SWAT[v] (Arnold *et al.*, 1998) and SWRRB[vi] (Arnold *et al.*, 1990).

With the RECODES model, it was the objective of van Dijk (2001) to detect the main sediment source areas in the Rhine Basin and to model the amount of sediment entering the stream channels. Moreover, the effect of environmental change on these two questions has been determined. In order to run the RECODES model, data input of the relief, the soil characteristics, the land use, the drainage network and the climate in the study area is required. A sensitivity analysis showed that modelled sediment supply is strongly related to the slope angle, the precipitation amount and the temperature as it triggers snowmelt. The model evaluation shows that the modelled erosion rates agree reasonably well with values found in literature. However, large differences between modelled amount of sediment and measured sediment yield have been brought to light. It is assumed that these differences result from the exclusion of alluvial processes in the model (van Dijk, 2001).

In order to formulate PCRGLOB-SET, the approach and equations of RECODES are adopted as far as possible. For some parameters alternative equations have to be used due to the coarser spatial resolution and the global application of PCRGLOB-SET. These equations are mainly taken from various studies that link erosion and sediment transport modelling with Geographic Information Systems (GIS). Consequently, the input data is chosen according to the equations. Due to the improvements of remote sensing technology and computational power, manifold of global data on a multitude of parameters is freely and online provided by scientific institutions. Besides the online datasets, various input files are used from the PCRGLOB-WB model.

The results of PCRGLOB-SET are separately assessed for annual totals and monthly fluctuations in sediment supply at different spatial scales. First, global results illustrate the overall pattern and magnitude of modelled sediment supply. Besides, the continents which contribute most to the global sediment supply are determined. For a more detailed look, results and their correspondence to input factors are assessed on the river basin scale.

[v] Soil and Water Assessment Tool
[vi] Simulator for Water Resources in Rural Basins

In a second step, the results are verified by comparison with sediment supply values found in scientific literature. This is done on the global scale, the continental scale as well as for individual river basins. On both the global and the continental scale, model results are compared to values reported in the M&S92+ database published by Milliman and Syvitski (1992). On these spatial scales, verifying monthly fluctuations is not sensible. Therefore, the monthly output is solely verified at the river basin scale. To that end, two single-objective functions are applied and modelled values are compared to observed time series of sediment supply.

As already indicated before, sediment supply is the result of many, partially interconnected, factors. In order to examine the performance of the individual model parameters separately, a coarse sensitivity analysis is performed. It is the goal to discover the main drivers of sediment supply in different river basins around the globe.

Last, the model results and the model itself are discussed and recommendations are given. This aims to discover strengths and weaknesses of the model formulation and to find opportunities for future improvements and adaptions.

1.5. Report outline

In chapter 2, the model formulation of PCRGLOB-SET is described including a discussion of the data used and assumptions made. Research questions a) to c) are answered in chapter 3 where the model results are presented on the global, continental and river basin scale. Chapter 4 deals with the verification of the model results with field data which answers research question d). The outcome of a short sensitive analysis of the model parameters is given in chapter 5. The findings made are subsequently discussed in chapter 6. Last, conclusions are drawn in chapter 7 and recommendations for further research are made in chapter 8.

2. Model formulation

Analogue to RECODES, PCRGLOB-SET consists of three modules: the Soil Loss Module, the Delivery Ratio Module and the Hillslope Delivery Module. In the first module, the soil loss per area will be calculated, using the Revised Universal Soil Loss Equation (RUSLE). While this only gives the potential erosion of sediments, the Delivery Ratio Module yields the fraction of actually transportable material. Last, the Hillslope Delivery Module combines both modules to obtain the sediment actually delivered. The actual amount of sediment reaching the water bodies is calculated by aggregating the delivered sediment along its path of flow.

In this chapter, these three modules will be explained in detail. In general, the same approach as in RECODES is followed. Due to the coarser spatial resolution, some assumptions and equations of RECODES are not applicable for PCRGLOB-SET which runs at a 0.5° resolution instead of 1 km^2. If this is the case, alternative routes have been chosen.

In Appendix A, the input data is listed, in Appendix B the model parameters are tabulated and in Appendix C the model script is provided.

2.1. Soil Loss Module

The Soil Loss Module in PCRGLOB-SET is basically a monthly application of the Revised Universal Soil Loss Equation (RUSLE) (Renard *et al.*, 1997). Originally, the RUSLE was applied for agricultural purposes, namely to assess the impact of conservation practices and to evaluate the erosion potential for various cropping intensities. To that end, long-term average annual soil loss under certain cropping and management practices is predicted. Nowadays the RUSLE is often used to determine soil loss rates in catchments (for instance Millward and Mersey (1999) for a tropical watershed or Prasannakumar *et al.* (2012) for a catchment in India) or to investigate impacts of future climate change (Yang *et al.* (2003)).

It may be argued whether it is a valid approach to use a method that aims to produce long-term annual averages for the prediction of monthly sediment supply. Based on the accuracy of RECODES, it can be stated that the chosen model structure should be able to produce reasonable monthly output. Differences between the output of RECODES and measured values are stronger associated to the absence of alluvial processes in the model formulation than to the application of RUSLE.

The Soil Loss Module is mathematically expressed as follows.

$$A_m = L \times S \times R_m \times K_m \times C_m \times Y \quad (1)$$

In order to obtain the amount of soil loss A [T ha^{-1} month^{-1}], the equation considers six factors: the slope length L [-], the slope steepness S [-], the rainfall-runoff erosivity R [MJ mm ha^{-1} h^{-1} month^{-1}], the soil erodibility K [T ha h ha^{-1} MJ^{-1} mm^{-1}], land cover and management practices C [-] and supporting conservation practices Y [-][vii]. The subscript m indicates thereby monthly variability. In analogy to RECODES and due to the fact that data about supporting conservation practices is lacking for the global scale, Y has been set to 1 in PCRGLOB-SET.

Hereafter, the individual factors will be explained shortly. In addition, the equations used in order to calculate the factors are presented and underlying assumptions as well as constraints are discussed. Moreover, the input data used for the individual factors will be examined and the performed format conversion outlined.

2.1.1. Slope length L

The slope length factor L is constant throughout the year and reflects the impact of slope length on erosion – the longer the slope length, the more erosion takes place. Traditionally, it is defined as the horizontal distance from the origin of overland flow to the point where "either (1) the slope gradient decreases enough that deposition begins or (2) runoff becomes concentrated in a defined channel (Wischmeier & Smith, 1978)".

Both van Dijk (2001) and Renard *et al.* (1997) use the same equation to determine L:

$$L = \left(\frac{l_c}{22.13} \right)^{\gamma} \tag{2}$$

Here l_c is the contributing slope length in horizontal projection in metres, 22.13 is the RUSLE unit plot length in metres and γ is a variable slope length exponent. While equations to calculate the exponent are mentioned in the RUSLE handbook, RECODES uses tabulated relations to determine the exponent (see Table 1). For PCRGLOB-SET the latter option has been chosen as it is the aim to formulate the model as similar to RECODES as possible. The input map of slope angles has been taken from PCRGLOB-WB and is depicted in Figure 1A. It has been derived using the equidistant hydro1k dataset which is at a 1 km^2 resolution (U.S. Geological Survey, 2004). Slopes have first been calculated and subsequently been aggregated to the 0.5° resolution. This has been done by first aggregating the slopes at sub-catchment level, then assigning them by averaging to a half-degree cell delineated on the equal-area projection and finally projecting these grids back to the geographic projection. As a result, each cell has become a true 0.5° cell. Subsequently, each grid cell has been

[vii] In the original equation, supporting practices are represented by P. In order to avoid any confusion with the precipitation P, it is named Y here instead

assigned a value for γ, depending on the slope angle. One should not be confused by the fact that the slope steepness is also accounted for in the slope length factor L. The resulting map is presented in Figure 1B with high gamma-values in mountainous areas such as the Andes and the Rocky Mountains and low values in flatlands such as Greenland and Australia.

Table 1: Slope length exponent γ as a function of slope angle (from van Dijk (2001))

Slope angle [%]	**≤ 0.5**	**> 0.5 - ≤ 1.0**	**> 1.0 - ≤ 3.4**	**> 3.4 - ≤ 5.0**	**> 5.0**
Exponent γ	0.15	0.2	0.3	0.4	0.5

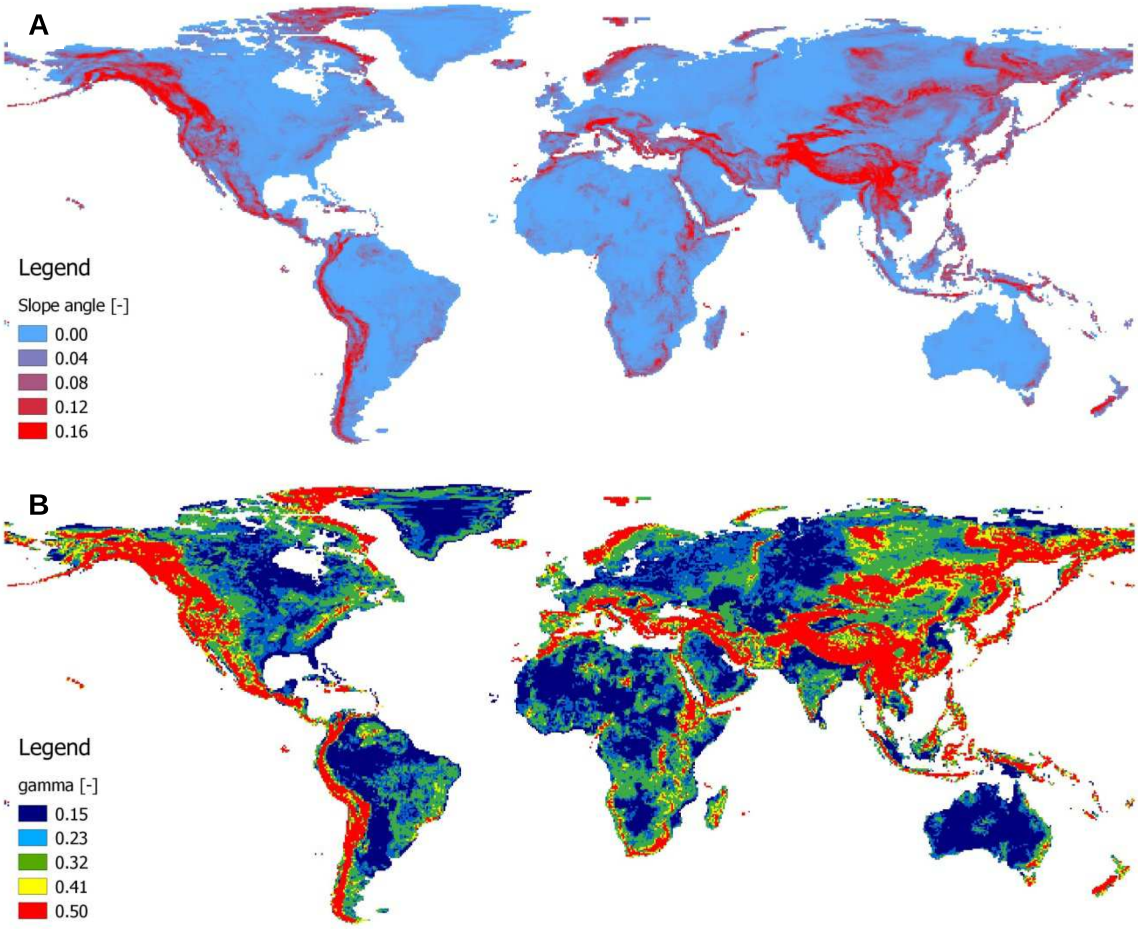

Figure 1: (A) global map of slope angle s projected at a 0.5 degree resolution, taken from PCRGLOB-WB; (B) resulting map of gamma factors, using the relations of Table 1

While assigning a value to γ is quite a straightforward operation, the determination of the contributing slope length l_c is not – see its rather vague definition. This is underlined by the statement of van Dijk (2001), that “the contributing slope length is one of the most difficult [R]USLE parameters to assess”. Due to this, l_c was set constant to 100 m in RECODES after reviewing scientific publications. Fortunately, the PCRGLOB-WB model provides slope length values in metres and at a 0.5° resolution. Since PCRGLOB-SET works on the same spatial resolution, the latter is chosen as input data. In general, these slope lengths are longer than 100 m, ranging from 16 m up to 93.000 m in very flat areas. Despite these differences, it is assumed that the contributing slope length l_c taken from PCRGLOB-WB is more realistic than the 100 m estimate of RECODES because it has been directly derived from the Earth’s elevation and not from literature.

2.1.2. Slope steepness S

By incorporating the slope steepness factor *S*, the influence of slope on erosion is reflected – the steeper the slope, the more erosion can occur. Generally, slope steepness has more impact on soil loss than slope length (Renard *et al.*, 1997). For slope angles up to 9 %, the original RUSLE equations for *S* is:

$$S = 10.8 \sin \Phi + 0.03 \tag{3}$$

while for slope angles bigger than 9 %, the equation is:

$$S = 16.8 \sin \Phi - 0.50 \tag{4}$$

where Φ is the slope angle in degrees. Thus, the slope angles as plotted in Figure 1A have first to be converted in the right unit.

Eventhough the aforementioned equations are also applied in other global soil loss assessments (for example by Yang *et al.* (2003)), the equation used in RECODES seems more appealing:

$$S = -1.5 + \frac{17}{1 + e^{2.3 - 6.1 \sin \Phi}} \tag{5}$$

This equation was developed by Nearing (1997) and has two advantages compared to Eq. 3 and 4. First, not two but only one equation has to be applied to compute the S-factor which reduces computational time and minimizes potential sources of error. And second, “it closely follows the RUSLE relationships for the slope steepness factor for slope angles up to 22 %, and also fits existing data for slopes greater than those from which the RUSLE relationships were derived (Nearing, 1997)”. Due to these advantages and to stay in line with RECODES, the equation of Nearing has been applied to compute the slope steepness factor *S* for PCRGLOB-SET.

2.1.3. Rainfall-runoff erosivity R

Rainfall-runoff erosivity describes the potential of rainfall and resulting runoff to erode soil. The more intense the rainfall, the more soil can potentially be eroded through the impact of falling rain drops. Originally, the R-factor is determined by averaging the product of storm energy and intensity of individual storm events over long time periods (≥ 20 years) (Renard *et al.*, 1997).

Mathematically, the R-factor [MJ mm ha^{-1} h^{-1} yr^{-1}] is expressed as follows:

$$R = \frac{1}{n}\sum_{j=1}^{n}\left[\sum_{k=1}^{m} E_k I_{30,k}\right]_j \tag{6}$$

where E is the total storm kinetic energy [MJ ha^{-1}], I_{30} the maximum 30 min rainfall intensity [mm h^{-1}], n the number of years to produce the average and m the number of storms per year.

Due to the fact that such detailed information about storm events is often not available, a lot of research has focussed and still focusses on how to determine the rainfall-runoff erosivity in another way (for example Kinnell (2010), Diodato (2006) or de Santos Loureiro and de Azevedo Coutinho (2001)). Renard and Freimund (1994) derived the subsequent relation between the R-factor and annual precipitation in millimetre, based on 132 stations in the US. The annual amount of precipitation P_{year} is determined by aggregating monthly values of precipitation in millimetre (P_m)

$$P_{year} = \sum_{i=1}^{12} P_{m,i} \tag{7}$$

Depending on the total annual precipitation in each grid cell, either a linear or quadratic function is applied. If P_{year} ≤ 850 mm/year:

$$R = 0.04830 \times P_{year}^{\ 1.1610} \tag{8}$$

If P_{year} > 850 mm/year :

$$R = 587.8 - 1.219 P_{year} + 0.00415 P_{year}^{\ 2} \tag{9}$$

Eq. 2.9 has also been used by Yu and Rosewell (1996) who tested this relation against R-values obtained from 29 stations in Australia. Since the obtained results showed good correlation, the authors concluded that there might be an underlying universal nature of the relationship between rainfall-runoff erosivity and annual precipitation. Due to this, Yang *et al.* (2003) used the very same equations for a global assessment of potential soil erosion with reference to land use and climate change.

Yet, only annual R-values can be obtained with Eq. 7 to 9. In order to obtain monthly values, the monthly percentage distribution of rainfall over the year is considered. The monthly percentage distribution *Part* for each grid cell and month *i* is obtained by dividing monthly precipitation by annual precipitation. This approach is justified by the fact that the annual precipitation amount is solely the sum of monthly precipitation. Moreover, RECODES uses a similar approach to derive monthly results from a yearly value. Here, one average distribution based on monthly R-values from Northrhine-Westfalia, Bavaria and Belgium has been used to obtain monthly R-values for the entire Rhine Basin (van Dijk, 2001).

$$Part_i = P_{m,i} \big/ P_{year} \tag{10}$$

$$0 \leq Part_i \leq 1 \tag{11}$$

The final step to obtain monthly values of R is to multiply the monthly fraction distribution with the annual R-factor.

$$R_{m,i} = Part_i \times R_{year} \tag{12}$$

From the aforementioned equations it is clear that monthly precipitation is the only required input data. Moreover, the original formulation of the R-factor asks for longer period averages. In order to satisfy both requirements, mean monthly precipitation data from the Climate Research Unit (CRU) of the University of East Anglia has been used. This data covers the global land mass, is based on actual observations and has been processed in a consistent manner. For PCRGLOB-SET, the period from 1950 until 2000 has been chosen as it is consistent with the available period for temperature data from the WorldClim project (Hijmans *et al.* (2005); see chapter 2.1.4.). The data used for this model has been adopted from PCRGLOB-WB which itself uses two CRU products, namely the CRU TS 2.1 (New *et al.* (2000); New *et al.* (2002); time series between 1901 and 2002) and the CRU CLIM 1.0 (Van Remortel *et al.* (2001); climatology over 1961 until 1990) which come at a spatial resolution of 0.5° and monthly temporal resolution.

In order to visualize the input data, Figure 2 depicts the aggregated annual precipitation in millimetre (P_{year}). As it can be expected, higher precipitation occurs in equatorial zones such as in South America and especially South East Asia. In contrast, only very little precipitation occurs in the Sahara, in Australia or Central Asia.

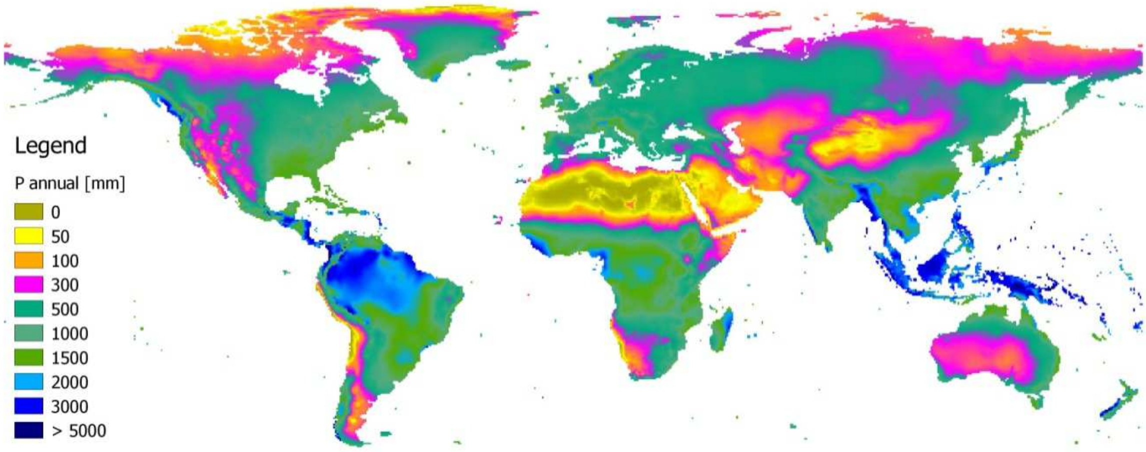

Figure 2: Aggregated annual precipitation at 0.5° resolution, computed with ERA-40 CRU products

2.1.4. Soil erodibility K

The K-factor represents the average long-term soil and soil profile response to the erosive power of rainfall which in turn triggers various hydrological and erosive processes such as soil detachment and transport due to surface shear and raindrop impact. In order to determine this response, the equation of Torri *et al.* (1997) has been chosen for two reasons: First, Yang *et al.* (2003) compared this equation with the EPIC model (Sharpley & Williams, 1990) and decided the equation of Torri *et al.* (1997) performed better. And secondly, the factors that are necessary to drive the equation can be extracted from the Harmonized World Soil Database (HWSD) (FAO *et al.*, 2012)[viii] which is the currently most up-to-date and comprehensive soil database available. For the model, the following topsoil properties (up to 30 cm soil depth) have been extracted: the fractions of sand, silt and clay per grid cell [-], the amount of organic material [%] and the soil texture classes (1 for fine, 2 for medium and 3 for coarse texture). Subsequently, each dataset has been resampled to a 0.5 degree resolution. The chosen resample mode has been bilinear for scalar values and majority for ordinal values which is a good trade-off between reducing information loss and minimizing computational time.

Torri *et al.* (1997) estimated the average annual soil erodibility K_a [T ha h ha^{-1} MJ^{-1} mm^{-1}] as a function of the soil clay fraction *Cl* [-], the Naperian logarithm of mean particle size D_g [-] and the organic matter content *OM* [%].

$$K_a = 0.0293(0.65 - D_g + 0.24 D_g{}^2)\exp\left\{-0.0021\frac{OM}{Cl} - 0.00037\left(\frac{OM}{Cl}\right)^2 - 4.02Cl + 1.72Cl^2\right\} \quad (13)$$

viii http://webarchive.iiasa.ac.at/Research/LUC/External-World-soil-database/HTML/

Here, the logarithmic expression for D_g from Torri *et al.* (1997) has been replaced by another expression applied by Yang *et al.* (2003):

$$D_g = -3.05 f_{sand} - 2.0 f_{silt} - 0.5 f_{clay} \quad (14)$$

Here f_{sand}, f_{silt} and f_{clay} represent the unitless fractions of sand, silt and clay respectively in the top soil of one grid cell.

Due to the division by *Cl* in Eq. 13, it may happen that it is not defined for some grid cells where *Cl=0*. In this case, the minimum value of the entire map has been assigned to the specific grid cell. To that end, the *"mapminimum"* function of PCRaster has been used.

Similar as for the rainfall-runoff erosivity, only annual averages can be computed with the aforementioned equations. In RECODES, soil erodibility varies in time only due to snow melt processes. Incorporating these processes is important as it was found that monthly K-factors can be up to 4.5 times higher than the annual average for coarse texture classes (Hayhoe *et al.*, 1995; Wall *et al.*, 1988).

van Dijk (2001) applied the following equation:

$$K_{m,i} = K_{ratio} MT_{fr,i} K_a + K_a (1 - MT_{fr,i}) \quad (15)$$

where K_a is the annual K-value , K_{ratio} is the ratio of seasonal to annual soil erodibilities and MT_{fr} reflects the time fraction in a month during which snowmelt occurs.

K_{ratio} can be determined using the values presented in Table 2. The values have been derived from Wall *et al.* (1988) and are used in RECODES.

Table 2: Values for K_{ratio} for five soil texture classes in RECODES

Texture class	Coarse	Medium	Med./Fine	Fine	Very fine
K_{ratio}	4.5	1.44	1.25	1.17	1.05

The application of these values requires the attribution of texture classes to soil types world-wide. This can also be managed by using the HWSD. However, the HWSD only contains three topsoil texture classes due to the scale of the map (1:5 million): coarse, medium and fine. Thus, an adapted relation between texture classes and K_{ratio} has been used in PCRGLOB-SET. For grid cells where no class has been defined, an extra class "none" has been introduced. In order to eliminate any influence of soil types without a texture class, the associated value of K_{ratio} has been set to 1.44 which is the median of the K_{ratio} values. The resulting relations are given in Table 3. The definitions of each texture class as described in the HWSD are presented in Table 4.

Table 3: Values for Kratio for three soil texture classes in PCRGLOB-WB

Texture class	**Coarse**	**Medium**	**Fine**	**None**
K_{ratio}	4.5	1.44	1.17	1.44

Table 4: Definitions of the three topsoil texture classes according to the HWSD

Texture class	**Definition**
Coarse	Sands, loamy sands and sandy loams with less than 18 percent clay and more than 65 percent sand
Medium	Sandy loams, loams, sandy clay loams, silt loams, silt, silty clay loams and clay loams with less than 35% clay and less than 65% sand; the sand fraction may be as high as 82% if a minimum of 18% is present
Fine	Clays, silty clays, sandy clays, clay loams and silty clay loams with more than 35 percent clay

In order to determine MT_{fr}, the following equation from RECODES has been applied.

$$MT_{fr,i} = \frac{MaxT - SMT}{MaxT - MinT}; \qquad 0 \leq MT_{fr,i} \leq 1 \tag{16}$$

MaxT is the monthly mean maximum daily temperature, *MinT* the monthly mean minimum daily temperature and *SMT* is the snowmelt trigger temperature (assumed to be constant at 0° C). In case that *MaxT* is below *SMT*, no melting can occur and hence MT_{fr} will be set to 0. With increasing melting time fraction, the soil erodibility and thus the soil eroded increases.

An important remark has to be made regarding the presence of snow layers. Eventhough the incorporation of a melting time fraction logically requires that snow layers are present, they have not been considered in PCRGLOB-SET. This is mostly because there is no global data on snow cover areas and their thickness. Thus, MT_{fr} solely serves as an additional factor incorporating monthly variations in soil erodibility. This can be justified by research that indicates that yields of suspended sediment increase with increasing temperature (Hovius, 1998; Jansen & Painter, 1974; Nearing *et al.*, 2004). Zhang *et al.* (2004) for example states that with increased mean temperature the soil loss can increase up to 40 %.

Values for maximum and minimum temperatures per month are taken from the “WorldClim” project (Hijmans *et al.*, 2005). Both parameters are interpolated on basis of measurements from 14.385 stations. Data is originally distributed at a 10 arc minutes spatial resolution and has been aggregated to a 0.5° resolution using GIS.

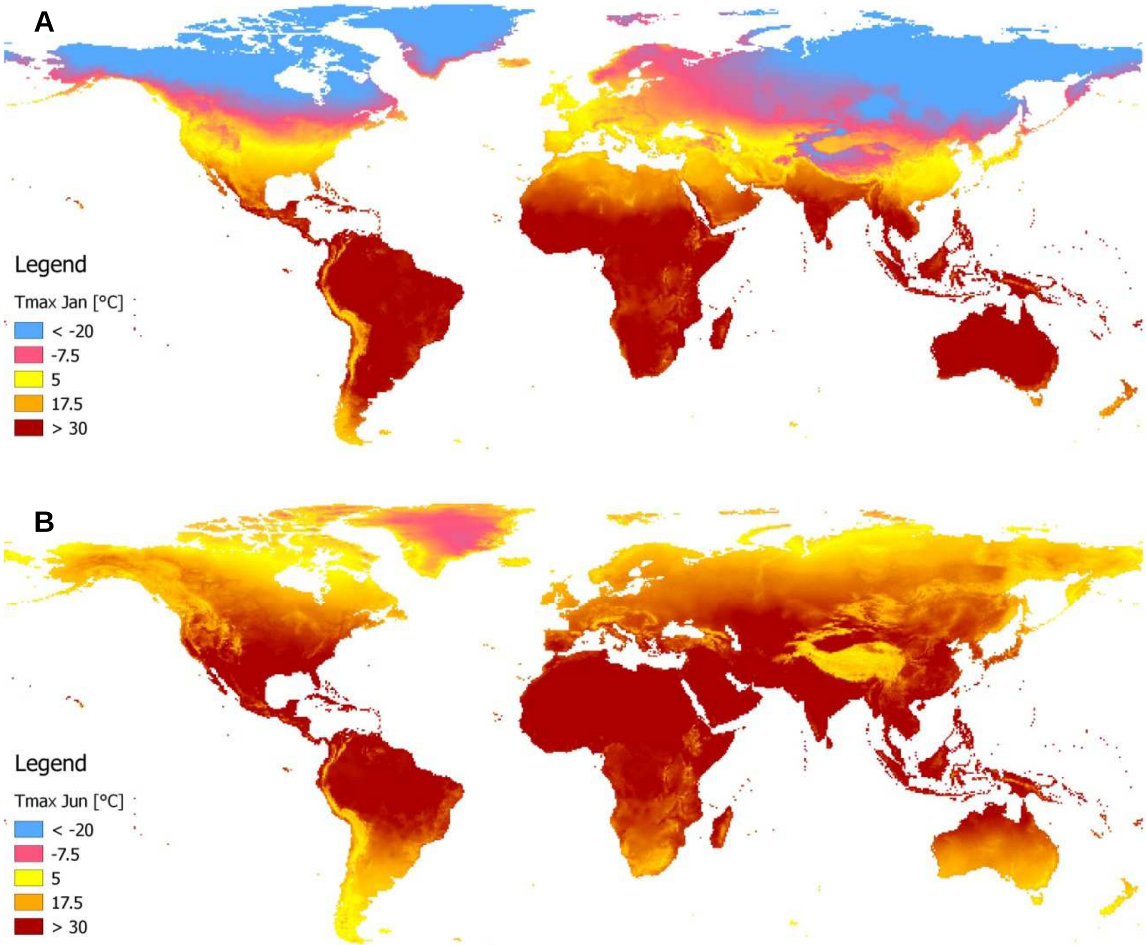

Figure 3: Mean monthly maximum temperature in degree Celsius for January (A) and June (B) with data from "WorldClim" project upscaled to a 0.5° resolution

In Figure 3, the mean monthly maximum temperature is depicted for both January and June. As it could be expected, temperatures are lower on the Northern Hemisphere in January than on the Southern Hemisphere. The lowest temperatures have been measured in Siberia. During June, temperature rises especially at the Equator and in the Northern Hemisphere while it gets colder in the Southern Hemisphere.

2.1.5. Cropping management factor C

The C-factor reflects the effect of cropping and management practices and is thus the only factor representing human interferences in the system[ix]. Due to its origin as a tool to assess the impact of these practices on soil loss, it is the C-factor which is usually varied for simulation purposes. Basically, the C-factor is determined by considering a multitude of sub-factors. First, the soil loss ratio (*SLR*) is determined as the deviation of soil loss under actual conditions compared to soil loss under reference conditions[x]. Then, the *SLR* is weighted by the fraction of rainfall and the rainfall energy-intensity *EI* associated with the time period in

[ix] Besides the Y-factor which is not accounted for in this Thesis
[x] Reference conditions refer to an area under clean-tilled continuous-fallow conditions

which *SLR* is assumed to be constant. In turn, the *SLR* is based on other sub-factors such as the impact of canopy and previous cropping management practices, just to name a few (Renard *et al.*, 1997). In RECODES, the following equation has been used:

$$C = \sum_{i=1}^{12} (\mathrm{SLR}_{m,i} \frac{R_{m,i}}{R_{year}}) \tag{17}$$

SLR_m is the monthly soil loss ratio and R_m/R is the fraction of the rainfall-runoff erosivity R in one month to the annual value. When RUSLE is applied on a monthly basis, C can be replaced by SLR_m which reduces the problem to the acquisition of adequate monthly values for *SLR* for different land use types (van Dijk, 2001).

Still, it remains difficult to obtain similarly detailed for the global scale. While van Dijk (2001) used soil loss ratios of six stages during a year for several cropping systems in Bavaria, this cannot be done on the global scale within the scope of this Thesis. Hence, other data sources had to be found. In recent research, the improvements in remote sensing technology have led to relationships between the C-factor and data from satellite missions.

Van der Knijff *et al.* (1999, 2000) proposed the following relationship:

$$C = \exp\left[-\alpha\left(NDVI / (\beta - NDVI)\right)\right] \tag{18}$$

where α and β are unitless parameters and *NDVI* is the “Normalized Difference Vegetation Index”. This index varies between -1.0 and 1.0. Water bodies and water-covered surfaces have negative values, rarely vegetated areas such as bare soils and urban areas have values of around 0 and heavily vegetated areas have values up to 1. Based on this equation, the C-factor, and as a result soil loss, decreases with increasing vegetation covers.

Kouli *et al.* (2009) chose values of 2 and 1 for α and β respectively since these values correlate well with the Corine Land Cover map 2000 of the European Environmental Agency (EEA). The same values have for example also been applied by Prasannakumar *et al.* (2011) and Prasannakumar *et al.* (2012) for a watershed in India.

One note should be made regarding the name of the C-factor. It is named the cropping management factor since the RUSLE is traditionally a tool to assess agricultural practices. However, the name might be confusing given the fact that a vegetation index is used to calculate it. The reason for that is that with the increased application for erosion modelling, the purpose of the C-factor turned from its classical agricultural one to a factor representing the influence of vegetation cover on soil loss without discrimination of different land-use or specific land-cover types. This is why recent GIS-based equations only take vegetation indices into account and hence differ strongly from the original equation.

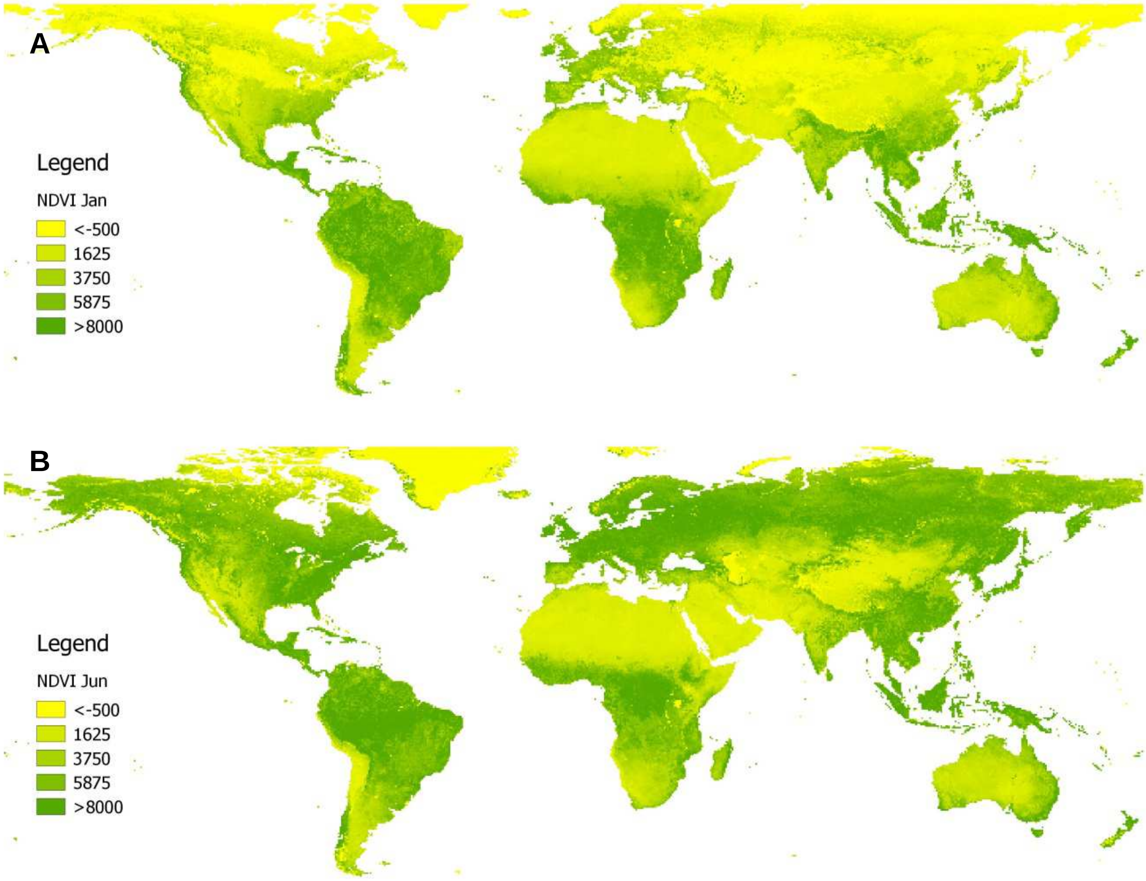

Figure 4: Global NDVI values in January (A) and June 2009 (B) upscaled to a 0.5° resolution

For PCRGLOB-SET, monthly maps of NDVI values are used. The maps are on a 0.05° spatial resolution and cover the year 2009. These data are originally distributed by the Land Processes Distributed Active Archive Center (LP DAAC), located at the U.S. Geological Survey (USGS) Earth Resources Observation and Science (EROS) Center (lpdaac.usgs.gov), and distributed in netCDF-format by the Integrated Climate Data Center (ICDC, http://icdc.zmaw.de) University of Hamburg, Hamburg, Germany.

In order to use the files in PCRaster, they have been converted from netCDF-format to GeoTiff-format using QGIS. During this step, the spatial resolution has been adjusted to 0.5°. Subsequently, files have been converted from GeoTiff-format to ASCII-format using GIS tools. Finally, it was possible to use the *"asc2map"* command of PCRaster and to create files in map-format at the correct spatial resolution.

Figure 4 exemplary shows NDVI values for both January and June 2009. The differences in vegetation cover are plainly visible. While vast areas in the Northern Hemisphere lack vegetation in winter, especially Russia and Northern America are more extensively covered with vegetation in June. Low values can then only be found in the Sahara, Australia, mountainous regions in general and Greenland. Generally, the Southern Hemisphere is more continuously covered with vegetation over the year than the Northern Hemisphere.

The fact that the NDVI does not extend that far North in January as in June is caused by snow and ice cover which do not allow the sufficient detection of wave lengths. Hence, no NDVI values could be computed.

2.2. Delivery Ratio Module

The Delivery Ratio Module yields the fraction of sediment that can actually be transported from one cell to another. Although the potential sediment supply is high, the actual amount being transported can still be relatively low. As a result, the sediment delivery would be transport-limited. The delivery ratio basically considers hydrologic and topographic properties, such as surface runoff and surface roughness. In analogy to RECODES, the monthly delivery ratio DR_m has been computed with the following equation.

$$DR_m = \tau \left(\frac{H_{c,m} s^{0.5}}{n_m l} \right)^{\xi}; \quad 0 \leq DR_m \leq 1 \tag{19}$$

Here, τ and ξ are empirical parameters of 9.53 and 0.79 respectively[xi], H_c is the hydrologic coefficient [-], s is the slope angle [%], n is Manning's roughness coefficient [s/m$^{1/3}$] and l is the length of the flow path [m]. Temporal variations are represented by varying potential to generate surface runoff (H_c) and by agricultural practices (n). Hereafter, only these factors are shortly discussed as the other two, length of flow path (which has been found to be equivalent to the slope length) and slope angle, have already been discussed before (see chapter 2.1.1 and 2.1.2).

2.2.1. Hydrologic coefficient H_c

The hydrologic coefficient was introduced because it was not possible to physically model overland flow when using a monthly time step and a grid cell size of 1 km² (van Dijk, 2001). Due to this, H_c is a relative value, proportional to surface runoff Q_s [mm] and rainfall P [mm].

$$H_{c,m} = \frac{Q_{s,m}}{P_m}; \quad 0 \leq H_{c,m} \leq 1 \tag{20}$$

[xi] In the original equation, τ is named α and ξ is named β. In order to avoid confusion with the parameters of Equation 2.19, they have been renamed.

For RECODES, the surface runoff was determined by using the CN-method which has been developed by the USDA-SCS (Soil Conservation Service; see Chow (1972)). However, this method requires a lot of computations and additional input data sets, such as the curve number CN, the available water capacity AWC or the actual free soil water SW.

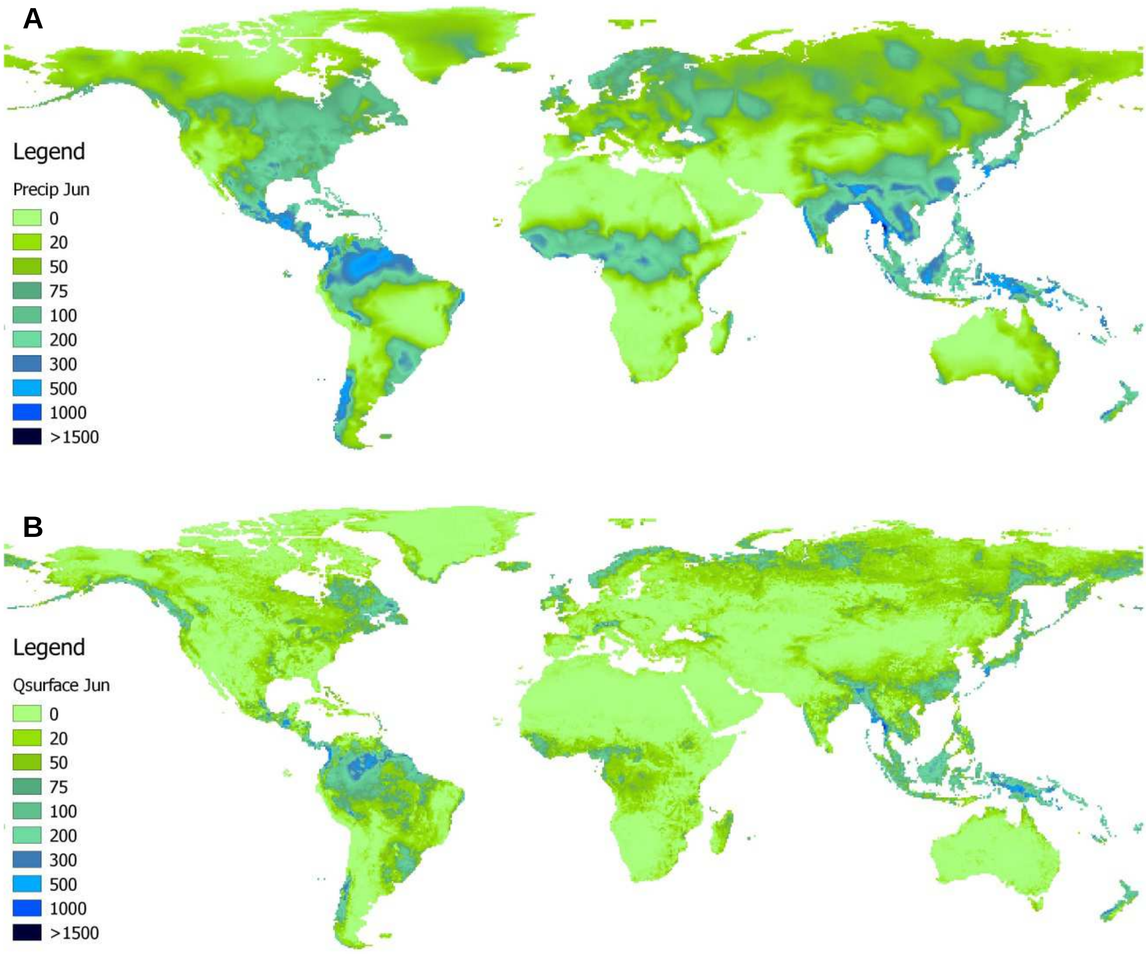

Figure 5: (A) Precipitation [mm] based on ERA-40 CRU data and (B) resulting surface discharge [mm] for June

Fortunately, PCRGLOB-WB computes surface runoff based on precipitation world-wide. Since PCRGLOB-WB model runs on the same spatial resolution (0.5°), using its output as input for the calculation of the hydrologic coefficient H_c seemed a time-saving and more accurate alternative. Moreover, this approach guarantees consistency within the model formulation in combination with the use of the corresponding precipitation data as described in chapter 2.1.3. Figure 5 shows the ERA40-CRU precipitation data and the resulting surface discharge as calculated by the aforementioned method.

2.2.2. Manning's surface roughness coefficient n

The Manning's roughness coefficient [s/m$^{1/3}$] introduces the resistance that overland discharge experiences on its path to a channel. With reduced velocity of the flow, its transport capacity decreases. Besides irregularities of the surface (n_1), factors like obstructions (n_2), changes in vegetation cover ($v_{3,,m}$) and the specific height and characteristics of vegetation (n_4) influence the hydraulic roughness. This is expressed in the following equation which is also used in RECODES:

$$n_m = n_1 + n_2 + v_{3,m} \times n_4 \tag{21}$$

For RECODES, van Dijk (2001) used tabulated values of each factor to determine n on a monthly basis. Since obtaining information about the characteristics of each grid cell would result in an extremely high workload, the approach has to be simplified. In addition, only insufficient information about Manning's roughness coefficient exists on the global scale. As a result, other ways to obtain adequate values for the resistance to flow have to be found.

As already mentioned, n_1 represents the impact of surface irregularities. Unfortunately, no measurements or data of global irregularities exist. From the data that is available, using slope as an indicator for irregularities has seemed plausible. The steeper a slope, the more irregularities can be assumed. This is because surface irregularities such as mountains, hills or valleys are always linked to a change in slope. Therefore, values of n_1 in PCRGLOB-SET have been based on the minimum and maximum values used in RECODES.

Table 5: Ranges of slope angles and associated values for surface roughness due to surface irregularities

Slope angle [%]	**≤ 1**	**> 1 - ≤ 2**	**> 2 - ≤ 3**	**> 3 - ≤ 4**	**> 4 - ≤ 5**	**> 5**
n_1	0.001	0.014	0.02	0.026	0.038	0.05

The ranges of slopes and associated roughness coefficients are given in Table 5 whereby the slope map of PCRGLOB-WB has been used as input data (see Figure 1A).

The second factor n_2 reflects the impact of obstructions to flow. Similar as for n_1, no global data is available. In RECODES, this value varies between 0 for negligible (<5% of area with obstructions) and 0.076 for appreciable (15-50% of area with obstructions) conditions. In PCRGLOB-SET, the former category has been neglected because it can be estimated that only very few grid cells at the chosen spatial resolution of 0.5° have obstructions of less than 5%. Finally, n_2 has been set to a constant value of 0.049 which is associated to obstructions of 15 % of the area. Given the rather small range between a value of 0.011 (associated to 5% obstructions) and a value of 0.076 (associated to 50% obstructions), choosing a value in between seems a reasonable compromise. Additionally, is must be taken into account that this factor is just one of four sub-factors.

As a third factor, v_3 is the only factor that is dynamic. Hence, monthly variations in Manning's surface roughness coefficient stem all from variations in vegetation cover. In RECODES, tabulated values for different land cover types have been applied. Due to the differences in model scale and spatial resolution, this approach is not feasible for PCRGLOB-SET. Since v_3 represents the vegetation cover, it makes sense to use vegetation indices instead. Therefore, the monthly NDVI maps that have already been described before (see Chapter 2.1.5) have been used to derive a value for v_3. The following rules have been applied: If $NDVI \geq 0$, then $v_3 = NDVI$. If $NDVI < 0$, then $v_3 = 0$. Thus, the maximum possible value $v_{3,max} = 1$ and the minimum possible value $v_{3,min} = 0$, representing full grid vegetation coverage and no vegetation coverage at all respectively.

Table 6: Description of available data on land cover and associated NLCD2006 categories and roughness coefficients

Data Land cover	Category NLCD2006	Number NLCD2006	n_4	Data Source
Barren Sparse	Barren land	31	0.0113	*1*
Closed Shrub	Shrub/Scrub	52	0.40	*1*
Croplands			0.04	*2*
Deciduous Broadleaf	Deciduous forest	41	0.36	*1*
Deciduous Needleleaf	Deciduous forest	41	0.36	*1*
Evergreen Broadleaf	Evergreen forest	42	0.32	*1*
Evergreen Needle	Evergreen forest	42	0.32	*1*
Grasslands	Grasslands/Herbaceous	71	0.368	*1*
Mixed Forests	Mixed Forests	43	0.40	*1*
Open Shrub	Shrub/Scrub	52	0.40	*1*
Permanent Wet	Woody wetlands	90	0.086	*1*
Savannahs	Grasslands/Herbaceous	71	0.368	*3*
Snow and Ice			0.001	*4*
Urban Built			0.015	*2*
Water bodies			0.023	*2*
Woody Savannahs	Same as "Savannahs"			*4*

Last, the specific height and characteristics of vegetation need to be considered. To that end, data about land cover types from PCRGLOB-WB have been associated with specific roughness values. The different land cover types as used in PCRGLOB-WB are listed in Table 6 under "Data Land Cover". The values of each input file range between 0 and 1 and represent the fractional coverage of the grid cell with a specific land cover type. Where possible, each cover type has been categorized using the NLCD2006[xii]. Subsequently, literature has been reviewed to obtain roughness values for each category. In Table 6, the relations between the data used, the NLCD2006 categories and the assigned surface

[xii] "National Land Cover Database" (http://www.mrlc.gov/nlcd06_leg.php)

roughness values including its source can be found. The sources for the values have mainly been Arnoldus (1977) (marked as 1), Diodato (2004) (marked as 2) and Dee *et al.* (2011) (marked as 3). Two assumptions have been made here (both marked as 4): First, it was assumed that snow and ice have relatively small roughness and hence a value of 0.001 has been assigned. And second, it was assumed that woody savannahs have the same properties as “regular” savannahs.

The resulting total Manning surface roughness coefficient n is presented in Figure 6. While in January the surface roughness is very small in the Northern Hemisphere and high values can only be found in the Southern Hemisphere and mountainous regions, the picture is changed in June. Here more resistance to flow is exerted on the Northern Hemisphere as well while no marked changes can be found for the Southern Hemisphere. This dynamic reflects the effect of vegetation coverage on surface roughness very well.

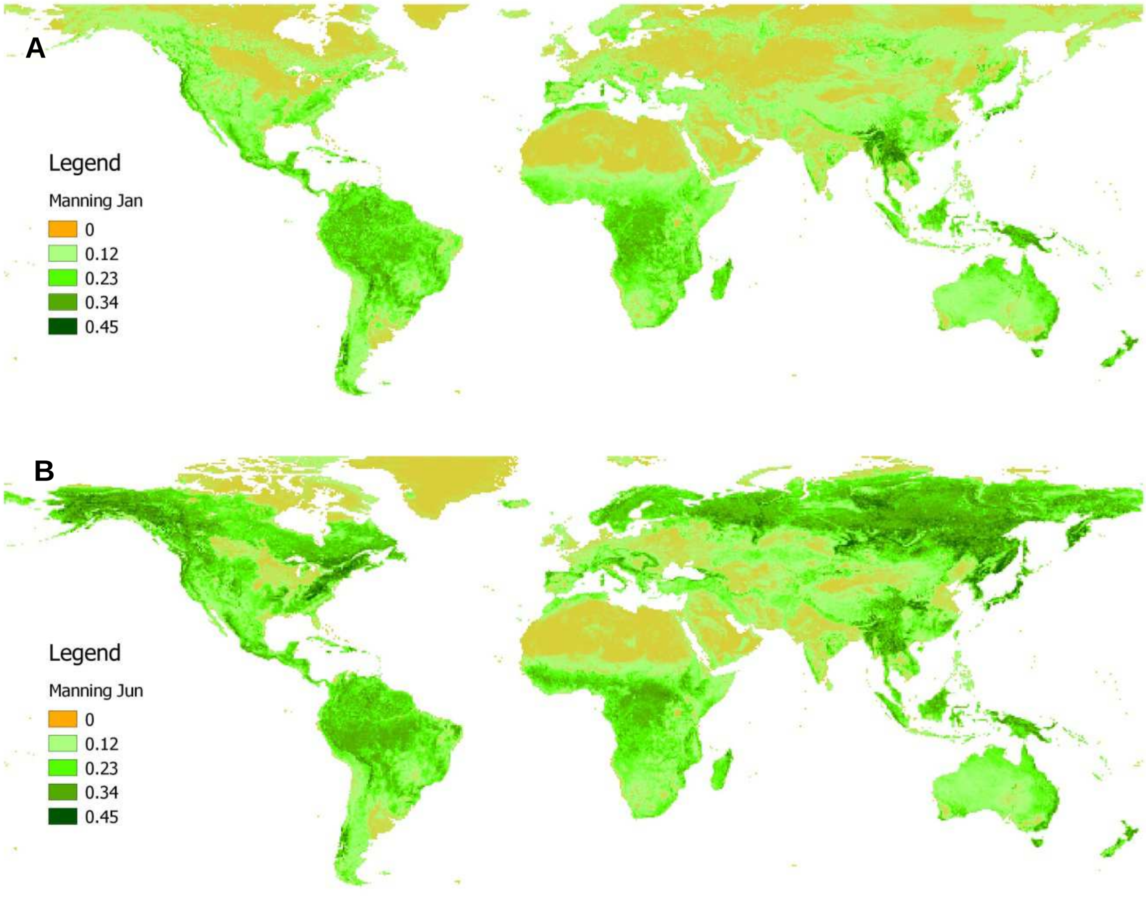

Figure 6: Computed Manning coefficients in (A) January and (B) June at a 0.5° resolution

Again, the extent of computed Manning’s coefficient differs between January and June. This is because PCRaster computes missing values (MVs) as soon as one MV occurs in an input file. As a result, the extent of surface roughness depends on the extent of its input data. In this specific case, the result considers monthly NDVI values which cannot be detected on the full range of latitudes (see Figure 4).

2.3. Hillslope Delivery Module

The Hillslope Delivery Module combines the output of both the Soil Loss Module and the Delivery Ratio Module with the following equation

$$SD_m = A_m \times DR_m \tag{22}$$

By multiplying the soil erosion A_m in T ha^{-1} month^{-1} with the unitless delivery ratio, the actual amount of sediment delivered from each grid in T ha^{-1} month^{-1} is computed.

In order to obtain accumulated amounts of sediment along the river reaches, the *"accuflux"* function of PCRaster has been applied. With this tool the sediment delivery is aggregated along its flow path on a cell-by-cell basis, yielding the sediment supply. For each cell the next downstream cell is determined and subsequently the sediment is delivered to this downstream cell. This process is continued until the sediment has reached the oceans where no further downstream transport can take place.

As a result it is possible to determine the amount of sediment supplied at the outflow points of river basins which is needed to assess the model results. For PCRGLOB-SET, basin outlets of 108 rivers are readily available[xiii] through which the sediment supply is routed.

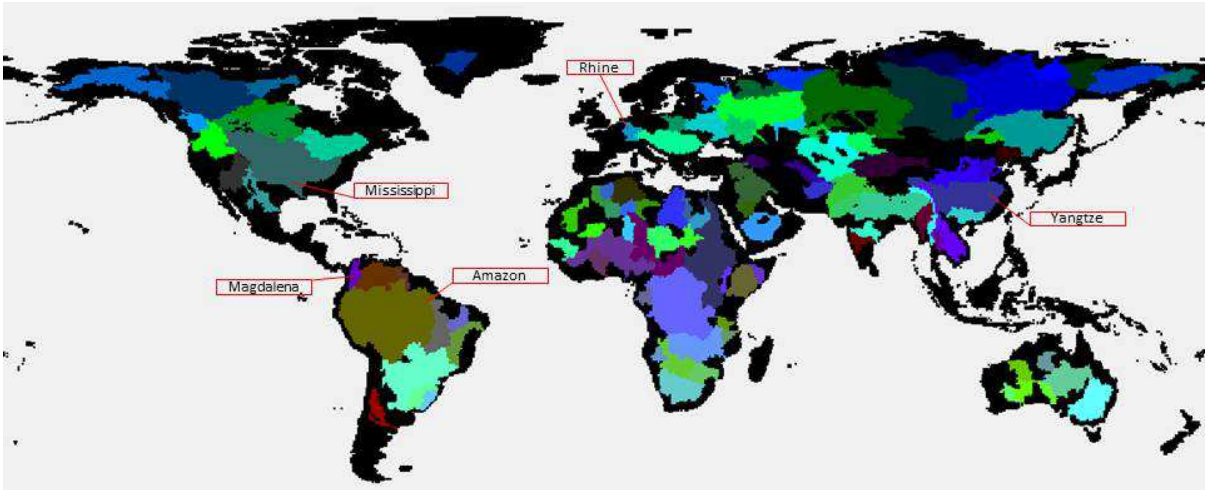

Figure 7: Raster map at 0.5° spatial resolution of 108 river basins used in PCRGLOB-SET; land surface not represented by a river basin is coloured black

[xiii] Taken from PCRGLOB-WB, resampled from drainage direction map of Döll and Lehner (2002)

3. Model results

It is the goal of the Thesis to develop a computer model that produces estimates of sediment supply into the oceans world-wide. In this chapter, the results obtained with the model as formulated in the preceding chapter are presented. First, the accumulated global sediment supply into the oceans is presented. Assessing its monthly variations needs to be done carefully as the spatial distribution of sediment supply differs strongly between each continent and even then between individual river basins. Hence, the results are apportioned for each continent and some specific river basins as well. Hereby, North and South America are treated as separate continents due to their different climates and entire Russia is added to Europe. For all spatial scales, time series and yearly totals are provided. Once again, it needs to be pointed out that computed values do show long-term values and hence cannot be considered as results for one specific year.

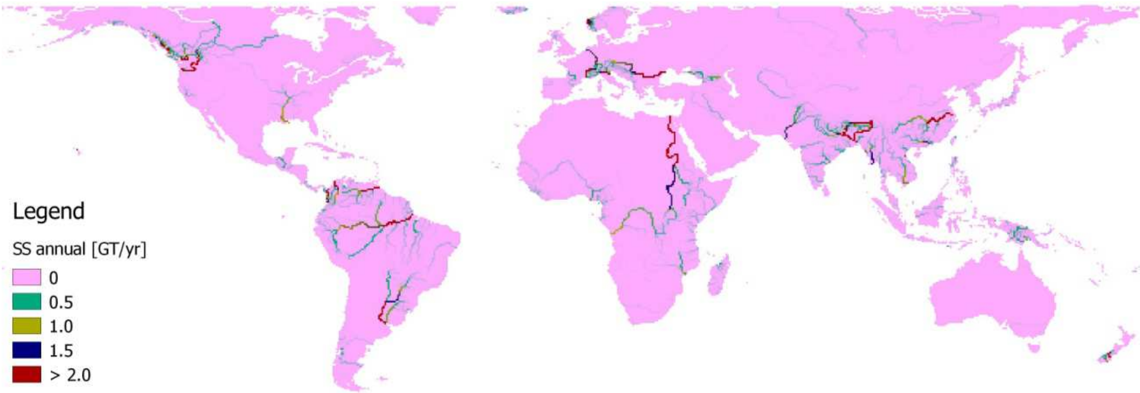

Figure 8: Annual sediment supply world-wide at a 0.5° resolution as computed with PCRGLOB-SET

3.1. Global sediment supply

Starting with global sediment supply values enables us to get a first impression of how much sediment is transported from land surfaces into the oceans. This issue has already been investigated by various researchers and is used as a major indicator for human influences on sediment transport world-wide. To that end, 68 out of the 108 rivers (see Chapter 2; Figure 7) have been identified to discharge into oceans. Due to the underrepresentation in Central Europe (visible in Figure 7), sediment supply of three more rivers has been added manually, namely of the Rhone, the Garonne and the Po River. In total, these 71 river basins drain around $6*10^7$ km^2 which is around 66% of the global land area draining into the oceans which has been estimated by Milliman and Meade (1983).

Subsequently, the calculated monthly sediment supply of these rivers has been accumulated to obtain an annual value. The rather small number of rivers defined can be related to the coarse spatial resolution of the model since it makes a more detailed representation of river basins in the model hardly feasible. After running the model and aggregating the sediment discharge of the 71 rivers, a value of 59.9 GT/year has been obtained.

In order to obtain a value representative for the entire discharging surface area, this value has to be extrapolated. When coarsely following the approach of Milliman and Syvitski (1992) who extrapolated their computed sediment supply of 8 GT/year to 20 GT/year for the entire discharging land surface area, PCRGLOB-SET would consequently yield a global annual total of around 150 GT/year. Undoubtedly, this approach contains a lot of uncertainty but its results need to be used for further processing of model output later in this Thesis.

Due to the fact that no soil loss can occur once sediment has been detached in the current set-up of PCRGLOB-SET, it is additionally possible to obtain a global value by using the *“maptotal”* command of PCRaster. Thereby the result of the Hillslope Delivery Ratio of each grid cell is accumulated for each month and the entire grid before routing it through the drainage network. As a result, an annual global sediment supply of around 195 GT/year has been computed. This approach is unfortunately only applicable as long as there are no permanent or temporal sediment sinks implemented into the model.

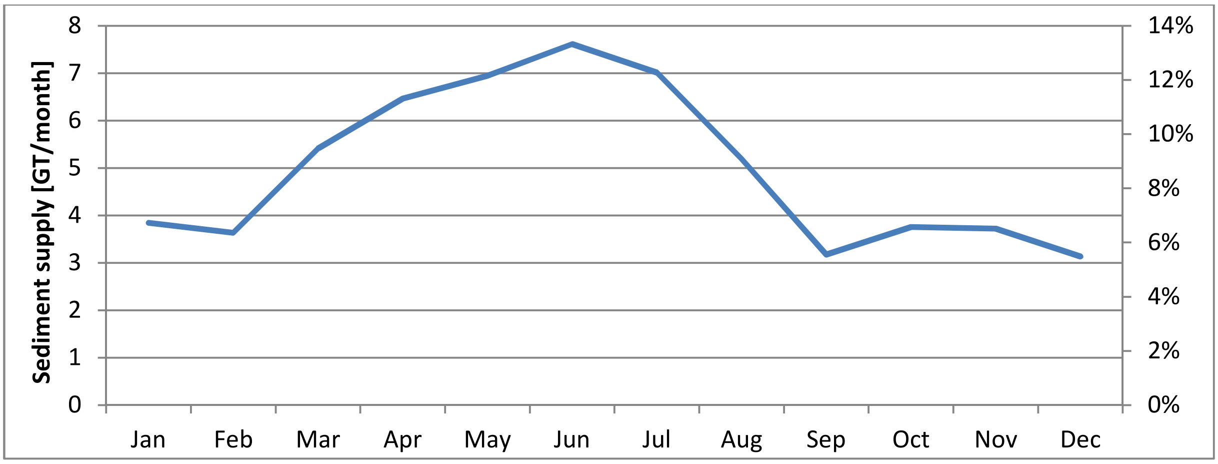

Figure 9: Course of sediment supply to the oceans over one year as computed with PCRGLOB-SET and associated monthly fractions of annual total sediment supply

Without the extrapolation, the two results computed with different approaches differ by a factor of around three. This shows that a lot of actually eroded sediment is not captured when determining global sediment supply merely based on the 71 river basins. The explanation for this discrepancy lies in the schematization of the river basins in PCRGLOB-SET. As mentioned before, the river basins plotted in Figure 7 cover only two thirds of total discharging land surface. Especially in Central America and South East Asia, schematized river basins are lacking. What is more, the small coastal strips which are not associated to any river basin apparently are important sources of sediment delivery into the ocean.

In Figure 9, the global monthly sediment supply and the monthly fractions are depicted. One can see that the major amount of sediment is thereby discharged in the period from March until August. The reason therefore is the big contribution of Asia where sediment supply is the biggest in this period (see chapter 3.2). The highest monthly amount is computed for June when 7.61 GT/month are supplied which represents 13% of the annual total. After June, the sediment supply drops until September. In December 3.13 GT/month are discharged which is the absolute minimum monthly result

3.2. Sediment supply per continent

In order to investigate how sediment supply is spatially distributed over the world, the amount of sediment supplied by individual rivers is aggregated per continent. This way a better picture can be drawn of which continent contributes more to the global sediment supply than others. First, the annual total sediment supply per continent is presented (see Figure 10 and Figure 11) and thereafter the monthly fluctuations.

As mentioned before, the total global annual sediment supply is 59.9 GT/year when solely considering the defined 71 river basins and without extrapolation. The continent with the highest annual contribution is Asia, where 24.7 GT/year or 42% of the yearly total are discharged. Asia is then followed by South America, Europe, Africa, North America and last Australia. When adding up South America and Asia, their outstanding importance for global sediment supply becomes visible as they are responsible for 64% of the total global value.

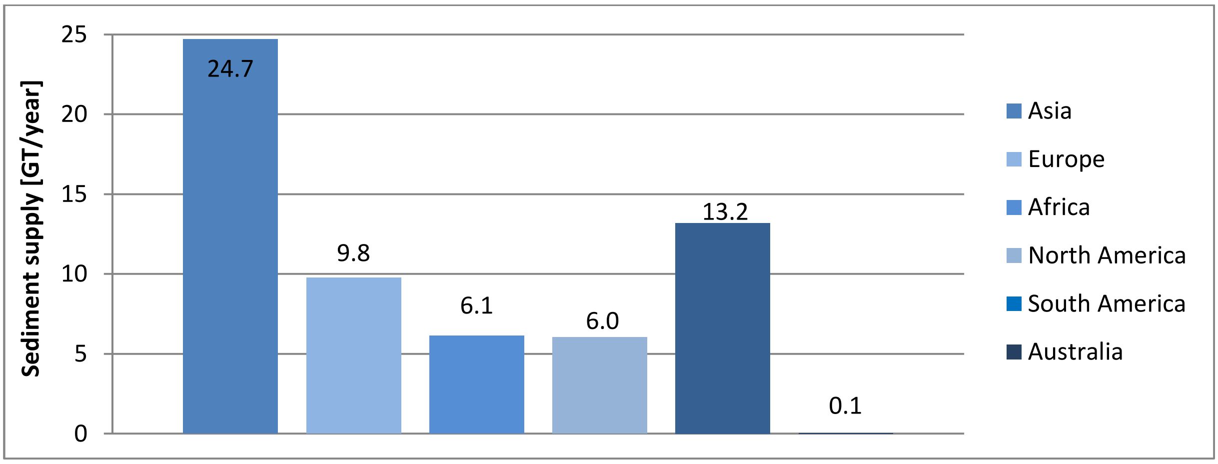

Figure 10: Annual sediment supply to the oceans for each continent as computed with PCRGLOB-SET

On each continent the sediment supply shows a different temporal pattern which is depicted in Figure 12. Hereafter, the course of sediment supply throughout a year will be presented for each continent. Table 7 shows the tabulated monthly results while Table 8 provides the ratio of maximum to minimum monthly sediment supply as well as their mean and median.

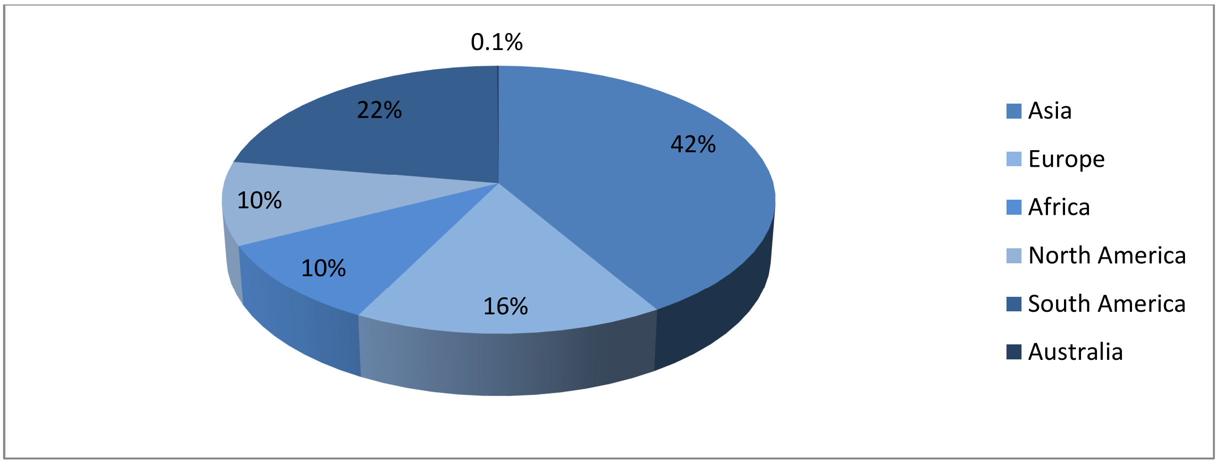

Figure 11: Fraction of total global annual sediment supply contributed by each continent

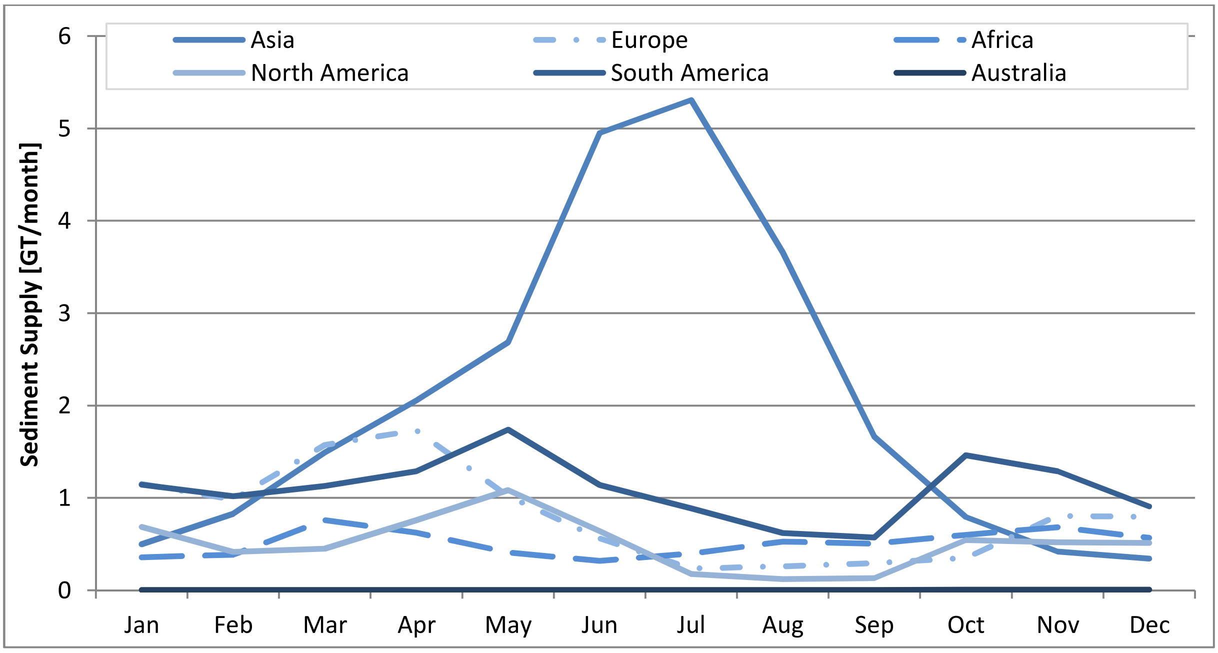

Figure 12: Monthly sediment supply to the oceans for each continent as calculated with PCRGLOB-SET

In Asia, the modelled monthly results are markedly higher than for other continents. In July 5.3 GT/month are delivered which is the overall highest monthly sediment supply of all continents. To put that value into perspective: Asia delivers in this month more than 10.000 times as much as Australia in one year, 40% of the annual total amount of North America and 9% of the total annual global supply. Generally, the months from May until August show a clear peak which is surely the main contributor to the higher sediment supply in the summer months on the global scale (see Figure 9). The driving factor behind this clear peak in the summer months is the monsoon which takes place in big parts of Asia between June/July and September/October.

Table 7: Tabulated monthly sediment supply for each continent as calculated with PCRGLOB-SET in GT/month

	Asia	Europe	Africa	North America	South America	Australia
January	0.5	1.2	0.4	0.7	1.1	$3.59*10^{-3}$
February	0.8	1.0	0.4	0.4	1.0	$3.37*10^{-3}$
March	1.5	1.6	0.8	0.5	1.1	$3.15*10^{-3}$
April	2.1	1.7	0.6	0.8	1.3	$2.46*10^{-3}$
May	2.7	1.0	0.4	1.1	1.7	$2.55*10^{-3}$
June	5.0	0.6	0.3	0.6	1.1	$1.94*10^{-3}$
July	5.3	0.2	0.4	0.2	0.9	$4.96*10^{-3}$
August	3.7	0.3	0.5	0.1	0.6	$4.50*10^{-3}$
September	1.7	0.3	0.5	0.1	0.6	$4.66*10^{-3}$
October	0.8	0.3	0.6	0.5	1.5	$6.09*10^{-3}$
November	0.4	0.8	0.7	0.5	1.3	$6.71*10^{-3}$
December	0.3	0.8	0.6	0.5	0.9	$7.59*10^{-3}$
SUM	24.7	9.8	6.1	6.0	13.2	$5.2*10^{-2}$

Sediment supply in Europe and North America shows similar patterns. First, Europe discharges a comparable amount of sediment as North America, namely 1.5 as much. Second, both continents have a comparable range in their monthly fluctuations. This is represented by the comparable ratios between maximum and minimum sediment supply. Thereby, the peaks occur during spring (April in Europe and May in North America) while the lows occur during summer (July in Europe and August in North America). And last, modelled sediment supply is slightly increased again in autumn and winter on both continents.

Modelled sediment supply in Africa is comparable to North America since both the annual total as well as the average monthly sediment supply are in the same order of magnitude. However, the sediment supply is more equally distributed throughout the year as indicated by a ratio of maximum and minimum monthly sediment supply of 1.2.

In South America, this ratio is relatively small as well with only 2.0. However, total annual and monthly average sediment supply is more than twice as high as for North America and Africa. Thus, sediment supply from South America is relatively equally distributed throughout the year at a comparatively high level.

The results obtained for Australia range between $1.94*10^{-3}$ GT/month in June and $7.59*10^{-3}$ GT/month in December. Generally, the results show two trends within the year. In the first half of the year monthly sediment supply decreases and increases in the second half. This pattern is opposite to Asia which is located on the Northern Hemisphere. Consequently, the first half of the year is responsible for only one third of the annual total sediment supply.

Table 8: The ratio of maximum monthly sediment supply (SS) to minimum monthly SS as well as the average and standard deviation (all in GT/month) of the time series as computed with PCRGLOB-SET

	Asia	Europe	Africa	N.America	S.America	Australia
Max SS / Min SS	12.7	4.9	1.2	3.9	2.0	3.9
Average SS	2.1	0.8	0.5	0.6	1.1	$4.3*10^{-3}$
Standard dev.	1.8	0.5	0.1	0.3	0.3	$1.79*10^{-3}$

3.3. Sediment supply in individual river basins

Now that global and continental values of sediment supply have been presented, values of five individual major rivers shall be given here. The chosen rivers are the Magdalena River and the Amazon River in South America, the Yangtze River in China, the Rhine River in Europe and the Mississippi River in North America. The annual sediment supply and its monthly fluctuations are shown in Figure 13 and Figure 14.

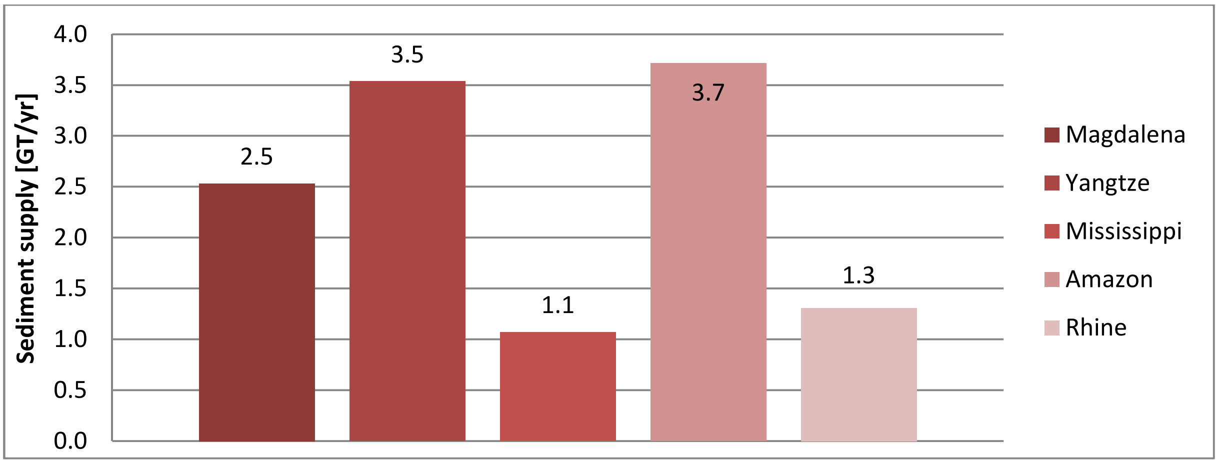

Figure 13: Annual sediment supply to the oceans for each river basin as computed with PCRGLOB-SET

Besides, the resulting temporal patterns of sediment supply are compared to the three external factors precipitation, vegetation and temperature. The last is thereby substituted by the melting time fraction MT_{fr}. Three upstream, two midstream and one downstream measuring location have been defined to derive representative time series. For the smaller river basins of the Rhine and the Magdalena, two measuring locations per sections have been selected whereas the number of locations per section has been doubled for the other river basins. This approach tries to cover as much uncertainty as possible, but due to the randomly chosen locations some error is still introduced.

Thereby positive correlation is expected between monthly precipitation and melting time fraction respectively and sediment supply while negative correlation is expected for both monthly values of vegetation cover. Especially for the river basins located in South America, the vegetation cover should not be responsible for monthly variations in sediment supply. Melting time fraction should only play a role in river basins located in colder areas. These river basins are especially the Rhine River and the Mississippi River.

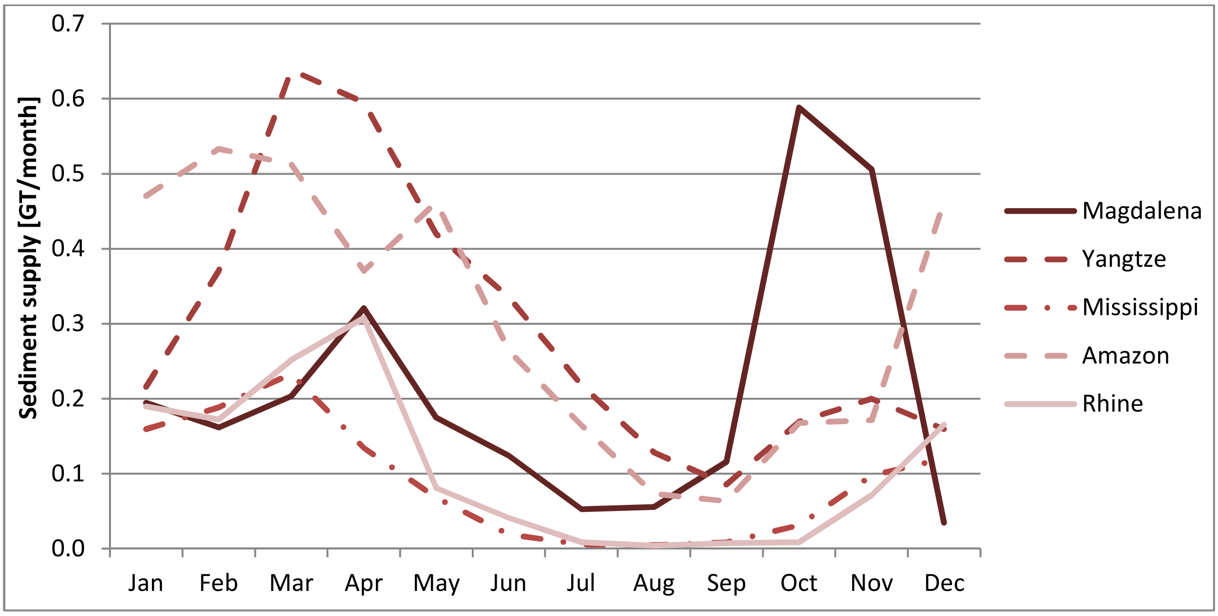

Figure 14: Monthly sediment supply for each river basin as computed with PCRGLOB-SET

3.3.1. The Magdalena River

The Magdalena River discharges 2.5 GT of sediment per year. Thereby, the highest value can be found in October when the Magdalena River discharges 0.6 GT/month. The lowest value of sediment supply in the Magdalena River is 0.03 GT/month which occurs in December. From the course over the year, two periods of increased sediment discharge with different magnitude can be identified: one around April and one around October. In contrast, the months around July and December show reduced sediment discharge.

Table 9: Coefficient of correlation between modelled sediment supply and precipitation, NDVI and MTfr for the Magdalena River Basin

	Basin-averaged	Downstream	Midstream	Upstream
Precipitation	0.64	0.35	0.23	0.83
Vegetation	-0.15	0.04	-0.58	0.07
Temperature	-	-	-	-

When assessing the impact of the environmental factors, it is found that both vegetation and temperature do not contribute to monthly variations. While melting is no issue in the basin at all, the overall coefficient of correlation between modelled sediment supply and basin-averaged NDVI is -0.15 which suggests virtually no correspondence with vegetation. This is most likely to the perennial vegetation cover of the rainforest in South America.

This is contrasted by a correlation coefficient of 0.64 between monthly values of sediment supply and basin-averaged precipitation. Especially precipitation in the upstream part of the basin explains a lot of the sediment supply fluctuations with a coefficient of 0.83. In general, the course of monthly sediment supply throughout one year is very well represented by the course of monthly basin-averaged long-term precipitation as shown in Figure 15.

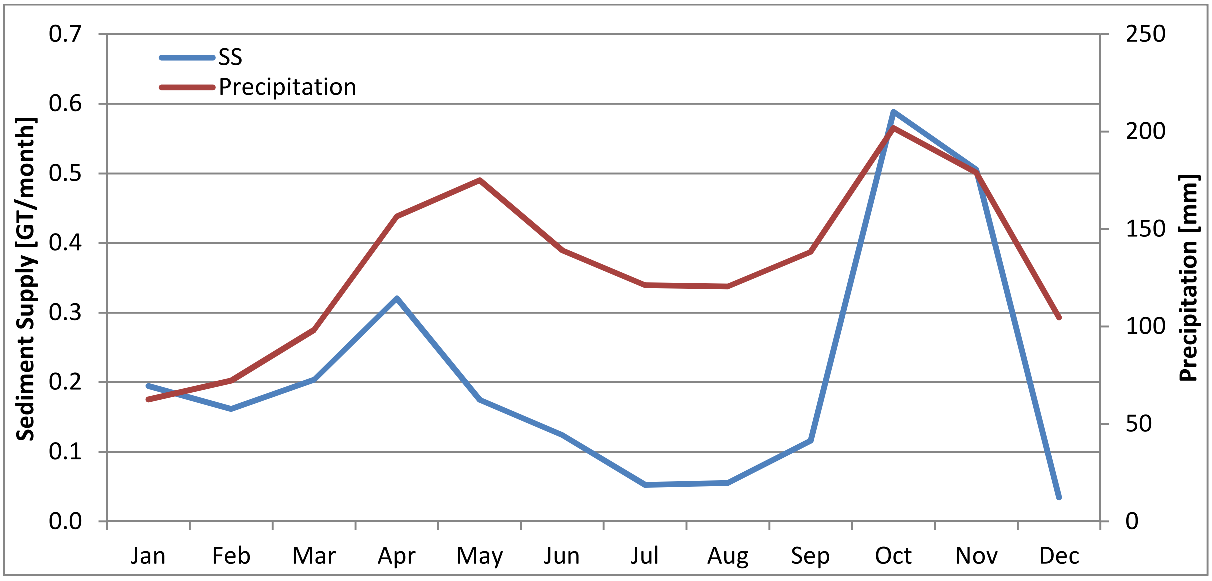

Figure 15: Modelled monthly sediment supply and observed basin-averaged long-term precipitation in the Magdalena River Basin

3.3.2. The Yangtze River

In PCRGLOB-SET, the second highest sediment supply of all rivers has been modelled for the Yangtze River. Aggregated over twelve months, the Yangtze River discharges 3.5 GT per year with a clear peak in March and clear minimum in September. While the maximum value is 0.6 GT/month, it is reduced to 0.1 GT/month some six months later – which is still the highest value of all five rivers in this specific month. Between March and September, results decline. Altogether, the months February, March, April and May are responsible for more than half of the annual total sediment supply (57%).

Table 10: Coefficient of correlation between modelled sediment supply and precipitation, NDVI and MT_{fr} for the Yangtze River Basin

	Basin-averaged	Downstream	Midstream	Upstream
Precipitation	-0.17	0.03	-0.07	-0.34
Vegetation	-0.39	-0.16	-0.39	-0.54
Temperature	-0.19	0.11	0.15	-0.23

Table 10 provides the coefficient of correlation between monthly values of modelled sediment supply and the external drivers. On the basin scale as well as only in the downstream area, no factor prevails significantly. Surprisingly, the basin-averaged correlation for both precipitation and temperature is negative. Thereby it seems as if some sections of the basin are contributing more to the monthly fluctuations than others. For instance, the changes in temperature lead to changes in sediment supply both in the down- and midstream, but not in the upstream part. The only factor that meets the expectations is vegetation, which is especially in the mid- and upstream parts of the basin the most relevant factor. Still, the basin-averaged coefficient of correlation remains low.

Due to the fact that precipitation, vegetation and temperature are the main dynamic input factors into the model, the weak and partially unexpected coefficients of correlation may be explained by the fact that sediment supply is influenced by them similarly strong. In addition, the strength of their impact differs spatially between down-, mid- and upstream part of the river basin.

3.3.3. The Mississippi River

From all rivers the Mississippi River shows the lowest sediment supply. While initially having a higher sediment supply than the Magdalena River, the obtained values of the Mississippi drop markedly after March when the maximum of 0.2 GT/month has been reached. During the summer month and parts of autumn the sediment discharge is at a low level. The absolute minimum is modelled for August when only $4.9*10^{-3}$ GT/month are discharged into the Gulf of Mexico. After October, the results increase again until December.

Table 11: Coefficient of correlation between modelled sediment supply and precipitation, NDVI and MTfr for the Mississippi River Basin

	Basin-averaged	Downstream	Midstream	Upstream
Precipitation	-0.48	0.72	-0.54	-0.71
Vegetation	-0.92	-0.88	-0.86	-0.94
Temperature	-0.77	-	-0.59	-0.82

The unexpected result that the correlation between modelled sediment supply and basin-averaged precipitation is -0.48 suggests that the erosive potential of rainfall is dominated by other factors. Indeed, the vegetation cover plays the more dominant role in the river basin. Averaged over the entire basin, the coefficient of correlation is -0.92, indicating that a decrease in vegetation cover leads to an increase in sediment supply and vice versa. In the upstream part correlation is even higher with -0.94 while it is -0.86 in the mid- and -0.88 in the downstream section, respectively.

While the melting time fraction in the downstream part is constantly at 1, it varies in the more upstream areas. However, the coefficients are negative which does not meet the formulated expectation. The reason for that remains unclear but it can be assumed that changes in the temperature cannot markedly affect monthly sediment supply but are dominated by other factors, in this case vegetation.

3.3.4. The Amazon River

In the summer months, the sediment supply shows higher values than during the winter months. For example, the highest value is obtained for February when 0.5 GT are discharged. The next lower values are found for March, January and December. These four months aggregated account for 53% of the entire aggregated annual sediment supply of 3.7 GT/year which is the highest annual value of the five rivers. The lowest value is found in September with 0.06 GT/month, followed by August and July.

Table 12: Coefficient of correlation between modelled sediment supply and precipitation, NDVI and MTfr for the Amazon River Basin

	Basin-averaged	Downstream	Midstream	Upstream
Precipitation	0.91	0.75	0.79	0.80
Vegetation	-0.16	-0.74	-0.51	0.82
Temperature	-	-	-	-

Geographically, the Amazon River Basin is adjacent to the Magdalena River Basin. As a result, the same climatic factor drives the sediment supply. The coefficient of correlation between modelled sediment supply and basin-averaged precipitation is here even higher with 0.91. Changes in temperature do not play a role due to the aforementioned conditions. In contrast to the Magdalena River, changes in vegetation can be held responsible for variations in sediment supply, especially in the down- and midstream part of the basin. The positive coefficient of correlation can mainly be attributed to the sampling error introduced by the random selection of measuring points.

3.3.5. The Rhine River

The Rhine River discharges with 1.3 GT/year the second lowest amount of sediment per year into the oceans of all river basins considered. Within a year, most sediment is supplied in the first four months. Starting in January with 0.2 GT/month, monthly output drops in February and rises in March and in April. Thereafter, monthly sediment supply rates decline and stay at a low level. The absolute minimum is reached in August when $4.1 \cdot 10^{-3}$ GT/month are discharged. After a period from July until October, supply rates increase in November and December.

Table 13: Coefficient of correlation between modelled sediment supply and precipitation, NDVI and MTfr for the Rhine River Basin

	Basin-averaged	Downstream	Midstream	Upstream
Precipitation	-0.65	-0.65	-0.52	-0.59
Vegetation	-0.66	-0.83	-0.50	-0.67
Temperature	-0.57	-0.32	-0.38	-0.64

Again, the basin-averaged correlation between precipitation and sediment supply is negative, in this case even for all parts. The same counts for the correlation with temperature which is slightly negative for the down- and midstream area and strongly negative for the upstream area. Merely changes in vegetation are affecting sediment supply in the expected way, especially in the downstream part. Thus, it appears that monthly fluctuations might be – except for vegetation – less driven by the factors investigated here but by others such as for instance the hydrologic coefficient.

4. Model verification

For the verification of the model, its output is compared to values found in the literature. In analogy to the previous chapter, the results are verified first on the global scale, then on the continental scale and subsequently on the river basins scale.

The results are compared to the so-called M&S92+ database which has been compiled by Milliman and Syvitski (1992). It is considered one of the most commonly used databases available. This database contains inter alia values of both annual sediment discharge and yield for almost 500 rivers worldwide eventhough some of them differ from values reported in other sources. It must be noted that such values are usually obtained at the most seaward gauging stations which already leads to deviations from modelled to observed sediment supply (Meade, 1996). The fractional land coverage is with two thirds comparable to the 71 river basins defined before. Assessing both datasets unveils that only 50 rivers are listed in both. This might be explained by different focusses on different areas in the world. Nevertheless, it is justifiable to employ the M&S92+ database due to the aforementioned advantages and since it is required for a consistent verification process of the results at different spatial scales.

On the global and the continental scale, model output is verified by following two different approaches. First, the absolute correctness is determined by comparing the modelled and observed amounts of sediment supply. And second, the relative correctness of the model output is assessed by ranking the rivers with the highest sediment supply per year. As a result, it is possible to verify whether the general processes are correctly modelled despite any possible over- or underestimation of absolute values.

The monthly results of PCRGLOB-SET can neither be verified on the global nor the continental scale but only at the river basin. This is done by calculating the coefficient of correlation and the Relative Mass Error (RME) between modelled and observed time series of sediment supply.

4.1. Global sediment supply

Due to the already emphasized importance of profound knowledge about sediment transport into the oceans, this process has already been assessed for a long period. Thus, numerous studies provide various values. Walling (2006) lists a number of existing estimates of suspended sediment transport to the oceans. The earliest value stems from Kuenen (1950) who estimated that 32.5 GT are annually transported into the oceans. Based on his literature study, Walling (2006) concluded that "these estimates have tended to converge on a mean annual flux in the region of 15-20 GT/year". Indeed, the value most commonly referred to as a standard of global sediment discharge is 20 GT per year and has been estimated by Milliman and Syvitski (1992). It must be carried in mind that providing a clear value of what is the actual sediment flux into the oceans is and remains a challenge. Already Milliman and Syvitski (1992) admit that by answering the question of how much sediment is carried by rivers with "we don't know".

With PCRGLOB-SET, a global annual sediment supply of 150 GT/year and 195 GT/year has been computed with different approaches. Either way, the model output systematically overpredicts reported values: when taking the maximum value found in Walling (2006) which is 51.1 GT/year and has been published by Fournier (1960), the modelled result compares acceptably well as it overpredicts by a factor of only 3 to 4. However, when comparing the result of PCRGLOB-SET with the aforementioned 15 to 20 GT/year, this factor increases to 7 to 10 which leaves space for improvements.

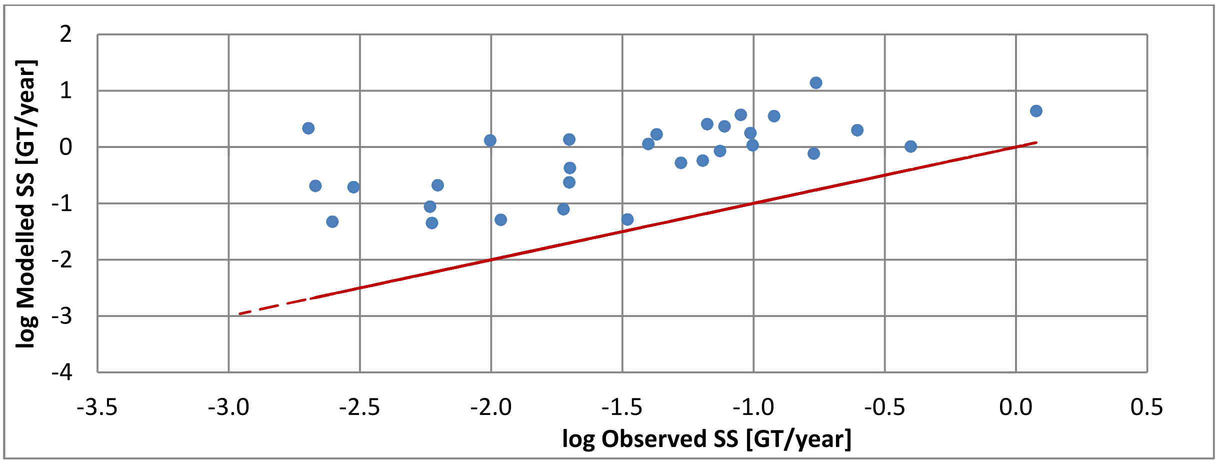

Figure 16: Scatter plot of log-scaled observed and modelled annual sediment supply into the oceans of 50 rivers including the 1:1 line in red

When considering only the 50 rivers PCRGLOB-SET has in common with the M&S92+ database, the scatter plot plotted in Figure 16 can be derived. The associated coefficient of correlation between observed and modelled sediment supply into the oceans is 0.62 which represents fairly good model performance on the global scale.

Besides the absolute quality of the model output, the relative quality is also taken into consideration. This means that not only the correct calculation of sediment delivered to the oceans is crucial but also the correct determination of the origin of the sediment in order to detect any underlying systematic error. Hence, the ten rivers with highest sediment discharge into the ocean according to the M&S92+ database and PCRGLOB-SET are ranked (see Table 14) and subsequently compared. All rivers listed occur both in the dataset used for model output and in the M&S92+ database.

Out of the ten rivers ranked according to the M&S92+ database, five are also present in the ranking according to model output: the Amazon, the Ganges, the Yangtze, the Magdalena and the Orinoco River. Especially for the first four ranks, the model output compares reasonably well eventhough for some the order is switched. Here, three out of four rivers occur on both sides with stronger overprediction for the Ganges River by PCRGLOB-SET.

The rivers that do not belong to the "top ten" according to the M&S92+ database, are comparatively high discharging rivers. For example, the Nile River ranks 12th, the Rio Parana 15th and the Rhone River 26th in the M&S92+ database. For the Po and the Columbia River, the database considers them to rank as 61st and 68th respectively.

Table 14: Ranking of the 10 rivers with globally highest sediment supply according to PCRGLOB-SET computations and to the M&S92+ database; river names in italic font occur in only one ranking

	PCRGLOB-SET		M&S92+ database	
	River name	**SS [GT/yr]**	**River name**	**SS [GT/yr]**
# 1	Ganges	13.7	Amazon	1.2
# 2	*Columbia*	*4.3*	*Huang He*	*1.1*
# 3	Amazon	3.7	Ganges	1.1
# 4	Yangtze	3.5	Yangtze	0.5
# 5	*Rhone*	*3.4*	*Mississippi*	*0.4*
# 6	Orinoco	2.7	*Irrawaddy*	*0.3*
# 7	Magdalena	2.5	*Indus*	*0.2*
# 8	*Nile*	*2.3*	Magdalena	0.2
# 9	*Po*	*2.2*	Orinoco	0.2
# 10	*Parana*	*2.1*	*Godavari*	*0.2*

4.2. Continental sediment supply

In order to verify the output of PCRGLOB-SET on the continental scale, the rivers listed in the M&S92+ database have been assigned to their corresponding continent and a continental annual value of sediment supply has been calculated by aggregation. Given the deviation of calculated to observed global annual sediment supply values, it can be expected that continental values will differ as well. In analogy to the global scale, rivers per continent are ranked according to their sediment supply and compared in order to detect any relative correctness of the model output.

In Table 15 the modelled sediment supply and the accumulated sediment supply from the database are listed for each continent. To set these values into relation, the number of rivers listed in each dataset is provided. One can see that the higher number of rivers in the M&S92+ database mainly comes from its stronger focus on rivers in Australia, Europe and North America. Moreover, the fractions of each continent from the annual global total are given including the resulting differences between both datasets. Last, the ratio between modelled and observed values is provided.

Table 15: Sediment supply for each continent including their fraction of the annual total from PCRGLOB-SET results and the M&S92+ database

	PCRGLOB-SET			M&S92+ database				
	Nr. rivers	SS [GT/yr]	global fraction	Nr. rivers	SS [GT/yr]	global fraction	Diff.	ratio
S. America	10	13.2	22 %	14	1.8	21 %	+1 %	7.4
N. America	9	6.0	10 %	52	0.9	11 %	+1 %	6.6
Europe	17	9.8	16 %	85	0.4	5 %	- 11 %	21.9
Australia	4	$5.1*10^{-2}$	0.1 %	50	0.1	2 %	+1.9 %	0.4
Asia	14	24.7	41 %	64	0.5	54 %	+ 13 %	5.4
Africa	17	6.1	10 %	29	0.5	7 %	- 3 %	11.2
SUM	71	59.9		294	8.4			7.1

From this table it can be inferred that the model generally overestimates the sediment flux for all continents but Australia where the model explains only 40 % of the published value. For the other continents, the ratios between modelled and observed sediment supply range between 5.4 for Asia and 21.9 for Europe. Except for Africa and Europe, the ratio does not exceed a factor of 7.4. On average, the output of PCRGLOB-SET overestimates the observed values by a factor of 8.8.

Another aspect to be considered is the distribution of sediment source areas. In PCRGLOB-SET, most sediment originates in Asia, followed by South America, Europe, North America and Africa and last Australia. When comparing this ranking with the one derived from the database, a similar pattern is obtained. The biggest difference hereby is found for Asia which is underestimated by PCRGLOB-SET compared to the M&S92+ database. Still, Asia is correctly modelled as the main contributor of sediment supply into the oceans. Quite the contrary, sediment supply from Europe is overestimated by the model. Apart from this, the contribution of each continent is very well represented by the model with deviations between +1.9% and -3%.

In order to achieve an idea of how the model performs within the individual continents, the rivers have been ranked in accordance to their sediment supply for each continent individually. The resulting lists are shown in Table 16.

The continents with the best agreement are South America, North America and Asia. For each of these continents, only one river is not listed in both rankings. Especially the results of South America show a good agreement.

Intermediate agreement between both datasets can be found in Africa where three out of five rivers appear both in PCRGLOB-SET output and M&S92+ database. What is more, the river with the highest supply is in both datasets the Nile and a higher sediment supply is correctly modelled for the Congo than for the Niger River.

Two continents show less good agreement, namely Australia and Europe. Still, the reasons therefore are different. For Australia, there are actually only four river basins in the database used for model output while the M&S92+ database lists 50 rivers in Australia and New Zealand. The mismatch between both rankings is therefore most likely the result of lacking definition of river basins and not solely of incorrect model output.

Table 16: Ranking of five rivers per continent with the highest sediment supply as computed with PCRGLOB-SET and listed in the M&S92+ database; rivers occurring in only one ranking are in italic font

	South America		North America		Europe	
	model	**M&S92+**	**model**	**M&S92+**	**model**	**M&S92+**
# 1	Amazon	Amazon	*Columbia*	Mississippi	Rhone	Danube
# 2	Orinoco	Magdalena	Mississippi	Colorado	*Po*	Rhone
# 3	Magdalena	Orinoco	MacKenzie	MackKenzie	Danube	*Lena*
# 4	Panana	Parana	Colorado	*Copper*	*Rhine*	*Volga*
# 5	*Uruguay*	*Chira*	Yukon	Yukon	*Garonne*	*Yesil*
	Australia		**Asia**		**Africa**	
	model	**M&S92+**	**model**	**M&S92+**	**model**	**M&S92+**
# 1	*Murray*	*Waiapu*	Ganges	*Huang*	Nile	Nile
# 2	*Streaky Bay*	*Waiapao*	Yangtze	Ganges	Congo	*Orange*
# 3	*Nullarbour*	*Hunter*	*Pearl*	Yangtze	*Zambezi*	*Tigris*
# 4	*Point Culver*	*Flinders*	Irrawaddy	Irrawaddy	Niger	Congo
# 5	-	*Fitzroy*	Indus	Indus	*Yuba*	Niger

In Europe, only the Rhone and the Danube River are correctly estimated by PCRGLOB-SET and still the sediment supply by the Rhone is overestimated compared to the Danube River. This is probably not ascribable to issues with the datasets but most likely to a more systematic deviation between model results and measurements.

4.3. Sediment supply of river basins

In the last part of model verification, the results of individual river basins are assessed. As a lot of emphasis has already been put on annual values, this aspect is treated only briefly hereafter. The focus of this chapter is to verify the temporal output of PCRGLOB-SET. This means, that time series of observed and modelled monthly sediment supply are compared.

In order to better assess the performance of the computer model, two single-objective functions have been applied. Besides the Pearson coefficient of correlation r, the Relative Mass Error RME has been calculated. This provides a better insight in general sediment balance prediction. It is determined with the following equation:

$$RME = 100 \times \frac{\sum_{i=1}^{12}(M_i - O_i)}{\sum_{i=1}^{12} O_i} \qquad (23)$$

where O_i and M_i are the observed and modelled values of sediment supply in month i, and $\overline{O}$ and $\overline{M}$ are the averages of all observed and modelled monthly values respectively.

Possible outcomes of the RME vary between -∞ and ∞ and yield the deviation of modelled to observed volume in percent. The best performance is reached when the RVE equals 0 which represents a perfect fit between observed and modelled sediment supply. Consequently, the higher or the lower the RME, the larger the deviation.

All results obtained are summarized in Table 17.

4.3.1. The Columbia River

While the annual value computed by PCRGLOB-SET is 4.33 GT/year, the value mentioned in the M&S92+ database is only $1.5*10^{-2}$ GT/year. This difference can partly be attributed to the construction of reservoirs in the Columbia River as well to the general overprediction of sediment supply by the model.

The data required for the assessment can be retrieved from the Sediment Portal of the U.S. Geological Survey (USGS) where both discrete and daily measurements of sediment concentration and load is freely available for each gauging station in the United States of America (http://cida.usgs.gov/sediment/#). Eventhough the Columbia River is a major river in North-West America, continuous time series of suspended sediment load are available for a limited period of time only. As daily sediment loads are reported only for the years 1965 and 1966, model verification could solely be based on this period.

In order to achieve monthly values, the daily values at the McNary dam (gauging station ID 14019200) have been aggregated to monthly values and subsequently the corresponding monthly values of both years have been averaged. The obtained graph is presented in Figure 17.

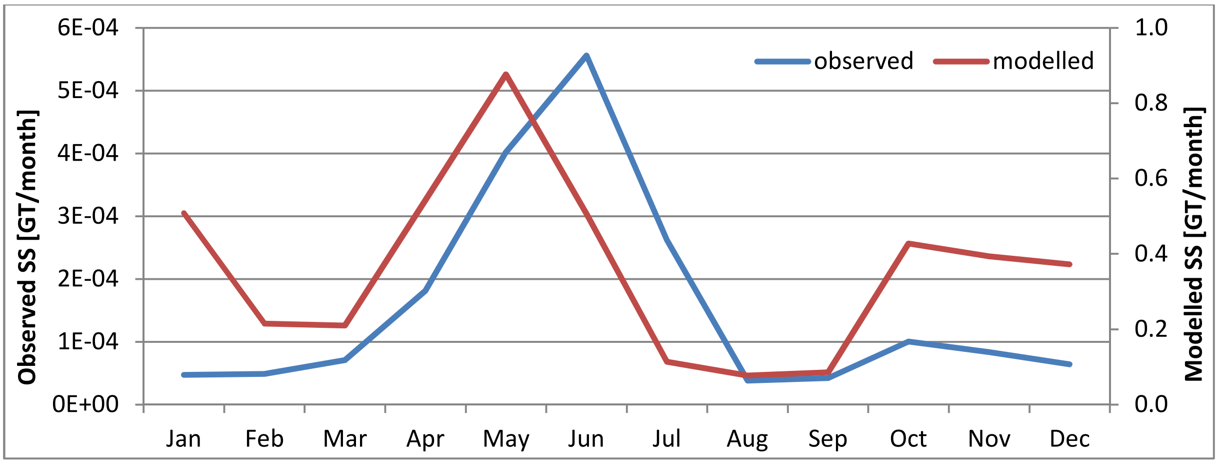

Figure 17: Observed and modelled monthly sediment supply of the Columbia River

As it could be expected, the observed and modelled results vary in their magnitude. This is indicated by a value of the RME of 228047% which stands in line with the finding made by comparing the rivers with the highest sediment supply world-wide (see Chapter 3.1; Table 14).

Still, the coefficient of correlation is 0.5. This indicates an acceptable correspondence between both time series and can also be estimated from the figure below. Here, the courses differ especially in the first month. Thereafter, the model correctly predicts a peak eventhough it occurs one month too early. After the peak, PCRGLOB-SET and actual values are lowest in August and show a minor peak again in October. Moreover, the smooth decline after the second peak is obtained for both time series.

4.3.2. The Mississippi River

The annual total sediment supply of the Mississippi River into the Gulf of Mexico is 1.07 GT/yr according to PCRGLOB-SET output. This value deviates by a factor of 2.7 from the 0.4 GT/yr mentioned in the M&S92+ database. Given all the uncertainties and important drivers that are not incorporated into the model, this deviation is acceptable. What is more, the factor of 2.7 is in the same range as the deviation of modelled and observed global annual total sediment supply.

Figure 18 shows the graphs of both modelled and observed monthly sediment supply. The observed values are thereby retrieved from the USGS Sediment Portal as well. From this portal, continuous daily suspended sediment at the gauging station Tarbert Landing (gauging station ID 07295100) is available for the period from October 1975 until September

2013. For model verification, daily values have been aggregated to monthly totals for the years 2009 until 2012. In turn, the monthly values have been averaged to gain comparable values. The resulting annual total at Tarbert Landing is comparable to values mentioned in literature, for example by Allison *et al.* (2012).

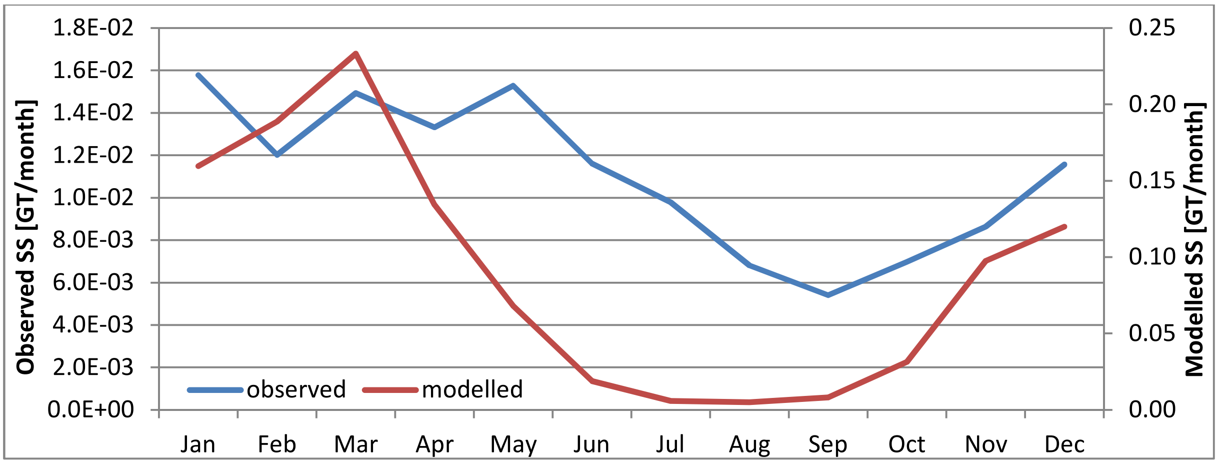

Figure 18: Observed and modelled monthly sediment supply of the Mississippi River

When comparing observed and modelled monthly sediment supply, a RME of 710% is calculated. Again, the general pattern of sediment supply overprediction by PCRGLOB-SET is confirmed.

A correlation coefficient of 0.7 is obtained which indicates that both time series are significantly related to each other. This agrees with the plotted time series in Figure 18. Especially for the months from September onwards, PCRGLOB-SET predicts the trend in sediment supply correctly. In addition, the model computes decreasing sediment supply for the period from July to August and the sharp increase from February to March in accordance to reality.

4.3.3. The Amazon River

The annual modelled sediment supply of the Amazon River is 3.7 GT/year while the observed value according the M&S92+ database is 1.2 GT/yr. This means, that the model overestimated the actual sediment load by a factor of 3.1 which is around the factor to which the model overestimated global annual sediment supply to the oceans in general. It is furthermore comparable to the factor obtained for the Mississippi River.

In order to assess the performance of PCRGLOB-SET in the Amazon River in terms of its temporal resolution, other data than the M&S92+ database had to be consulted. Therefore, the required monthly data has been downloaded from the ORE-HYBAM network (http://www.ore-hybam.org/index.php/eng/Data). Monthly observed data of water discharge and total suspended sediment concentration (SSC) in the period from 2010 until 2012 have then been merged in order to obtain a monthly sediment supply value. It is assumed that these values are representative for the sediment supply characteristics of the Amazon River.

In order to calculate the needed values, the following equation has been applied.

$$Q_s = Q \times SSC \tag{24}$$

where Q_s is the suspended sediment supply [GT/month], Q the water discharge [l/month] and SSC the suspended sediment concentration [GT/l]. Thereby it is assumed that the concentration is constant over water depth which actually does not correctly represent reality. Naturally, sediment concentrations show a logarithmic profile and vary strongly depending on where in the river bisect they have been measured. Due to the fact that no other data is available and since PCRGLOB-SET in its current form is only a first-order model, using Eq. 26 is acceptable.

Subsequently, the monthly values of the years 2010 until 2012 have been averaged to obtain 12 representative values of sediment load. The result is depicted in Figure 19 together with the modelled sediment supply for the Amazon River.

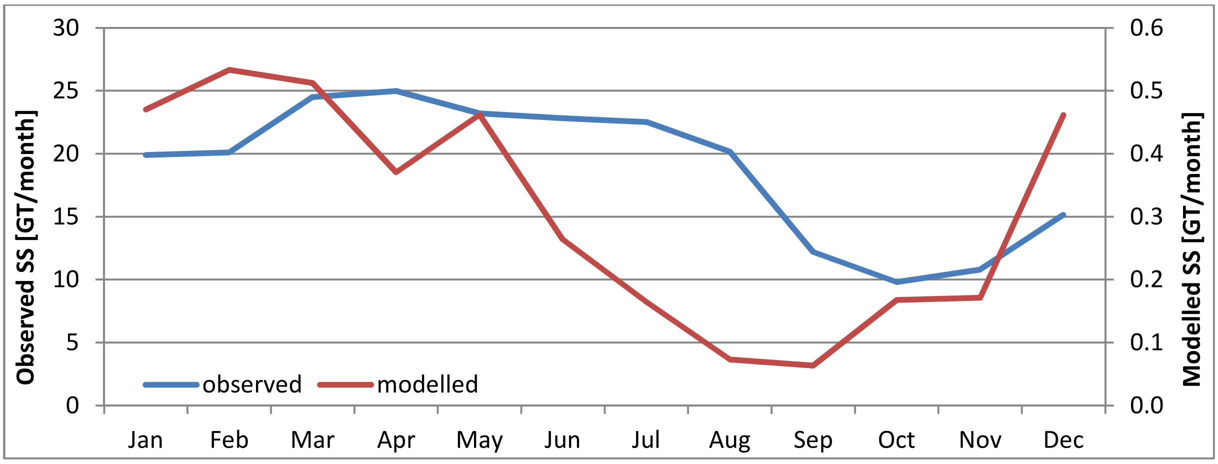

Figure 19: Observed and modelled monthly sediment supply of the Amazon River

The time series of observed and modelled sediment supply show an acceptable correlation coefficient of 0.5. Indeed, the model reproduces the monthly variations very well with a time shift of around one month in advance. More specifically, the minimum in October respectively September and the increase from November to December is well expressed. Moreover, the shape of the small peak in sediment supply from March until May is similarly reproduced by PCRGLOB-SET two months earlier.

The RME is -100% which indicates that the model underestimates the observed sediment supply. Given the systematic overprediction of sediment supply by PCRGLOB-SET, this value has to be connected to the assumptions made in the calculation process of sediment load from water discharge and SSC.

4.3.4. The Danube River

The total annual sediment supply of the Danube River into the Black Sea is, according to the M&S92+ database, $6.7 \cdot 10^{-2}$ GT/year which would make this river the highest sediment load in Europe. As already shown before, this is not the case for the PCRGLOB-SET results. Here, the Danube discharges 1.98 GT/year which is a still clearly more than reported but ranks only third behind the Rhone and the Po River.

Nevertheless, when assessing the monthly output, the results appear in a different light. The data used to obtain this value has been retrieved from Danube River Basin Water Quality database of the International Commission for the Protection of the Danube River (ICPDR). From this database, observed daily average flow in m^3/s and monthly values of suspended sediment concentration in mg/l have been taken for gauging station RO-7 which is in the Sulina River in Romania. For the years 2006 and 2007, the daily values have been processed to monthly averages. Subsequently, Eq. 26 has been applied again in order to obtain monthly values of sediment supply.

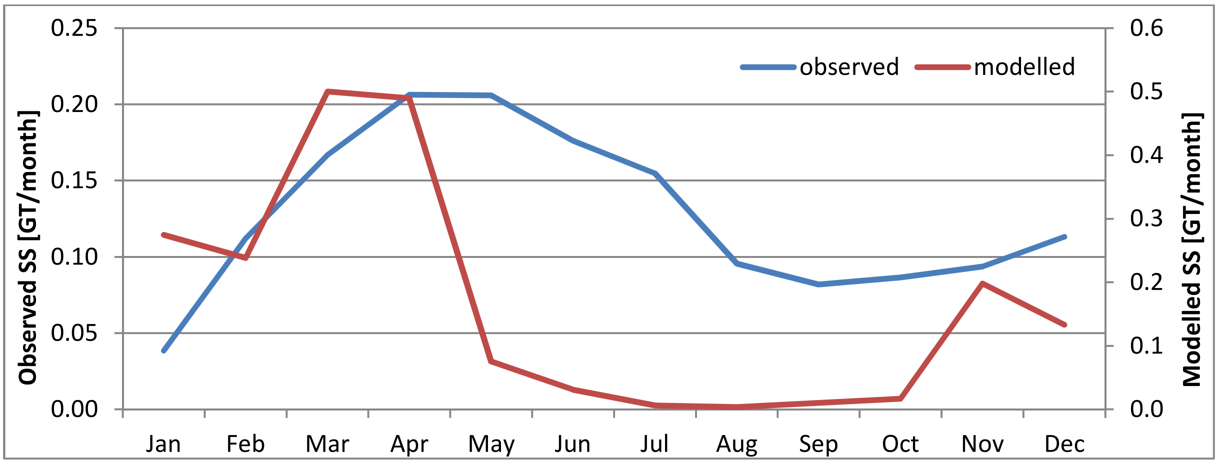

Figure 20: Observed and modelled monthly sediment supply for the Danube River

Due to the overall higher observed values of sediment supply, the RME is comparatively small with only 30% which would indicate that model output agrees better with data retrieved from the ICPRDR than from the M&S92+ database. More likely, this rather small overprediction by PCRGLOB-SET is for the biggest part owned to higher sediment supply values obtained with Eq. 26.

Table 17: *Correlation coefficient r and relative mass error RME and Nash-Sutcliffe coefficient NS for the verified rivers*

	Columbia	Mississippi	Amazon	Danube
R [-]	0.5	0.7	0.5	0.3
RME [%]	228047	710	-98	29

In terms of the correspondence between observed and modelled sediment supply, the coefficient of correlation of 0.3 indicates only little agreement. Indeed, some trends in observed sediment supply are not reproduced by the model. However, the overall fit is acceptably as the peak is correctly modelled for the months around April. Additionally, PCRGLOB-SET correctly predicts a decrease thereafter, eventhough the results decrease way to strong and early.

4.3.5. Résumé

To sum up, model outcomes of PCRGLOB-SET are overall reasonably good, given that it is only a first-order model where many decisive processes are not incorporated. One finding of this chapter is that the outcome quality differs for different scales. While the total annual global sediment supply is in a range that could be expected under the existing presumptions, agreement between observed and modelled values varies between continents and river basins. Especially the output for Europe and European rivers deviates stronger from reality than for other continents. On the other side, model output for Asia represents the real conditions with higher-than-average quality.

Regarding the temporal dimension of the model, the verification process shows that under the given limitations of PCRGLOB-SET the agreement and relation between observed and modelled time series is reasonably good. While the RME is of less importance regarding the temporal resolution of the model, the coefficient of correlation is in most cases acceptable to good except for the Danube River. Just by visual comparison of the graphs of observed and modelled sediment supply, the overall monthly fluctuations of sediment supply seem to be well represented by the model. Mostly, PCRGLOB-SET reproduces the shapes of the graph quite correctly but with a shift of one to two month in advance.

Whether the findings on the river basin scale can be transferred to the global scale is questionable. Nevertheless, they indicate that the model is more accurate in terms of monthly fluctuations than in terms of absolute mass of sediment supply. In order to better assess the applicability of an extrapolation, results need to be verified in more river basins.

5. Sensitivity analysis

Sediment supply is the result of manifold and complex processes. These processes are driven by various factors with temporally and spatially varying magnitude. Thus, it has been the aim of this sensitivity experiment to find out which input factors are more forcing on certain continents than others and how possible errors in input data can potentially influence the model output. By conducting a sensitivity analysis for RECODES, van Dijk (2001) has found that especially the slope angle, the precipitation amount and the temperature variability play an important role in soil erosion and transport. Due to its good correlation shown in chapter 3.3, the impact of changes in vegetation cover is additionally assessed. Literature indicates that variations in these factors are strongly related to the amount of soil eroded and supplied to the streams (Maina *et al.*, 2013; Nearing *et al.*, 2004; Nunes *et al.*, 2011; Osterkamp *et al.*, 2012).

For the sensitivity analysis, the four input factors have been varied separately. Four additional results have been obtained for each input factor by multiplying the original input values with the factors 0.5, 0.8, 1.2 and 1.5, respectively. These ranges do not necessarily represent actually possible values and are arbitrarily chosen. Their mere purpose is to facilitate a consistent comparison of the results. The resulting relations need to be treated carefully as some uncertainty still exits due to the unclear effective parameterization of the input factors and the non-linear relation between input factors and model output.

Results have been assessed for selected river basins. These river basins are the Amazon and Magdalena in South America, the Mississippi and Columbia in North America, the Rhine and Rhone in Europe, the Yangtze and Ganges in Asia and the Nile and the Congo River in Africa. Due to the low performance of PCRGLOB-SET in Australia, it has been prescinded from conducting a sensitivity analysis on this continent. Finally, the results are assessed for similarities and differences in sensitivity in a summarizing résumé.

5.1. Impact of variations in slope angle

Changes in the slope angle impact the outcome in various ways. First, they directly affect the magnitude both the L and the S-factor. Moreover, they influence the delivery ratio DR and hence the amount of eroded soil that can reach the streams. Thus, it can be assumed that with reduced slope angle the sediment supply decreases as well while with steeper slopes the amount increases.

Hence, the relation between slope angle and sediment delivery can mathematically be briefly expressed as follows:

$$SD = \left(a' + \frac{b'}{\arctan s} \right) \times c'^{s} \times k' \sqrt{s} \tag{25}$$

where s is the slope angle [m/m]. The other letters represent the factors that are used in slope-dependent functions and can vary in both time and space. The sign " ' " indicates that these factors have been multiplied with all other factors occurring in slope-independent equations to simplify the equation. This system will be followed in the next equations.

From Eq. 27 it can be expected that decreased slope angles will lead to slightly decreased sediment supply and vice versa.

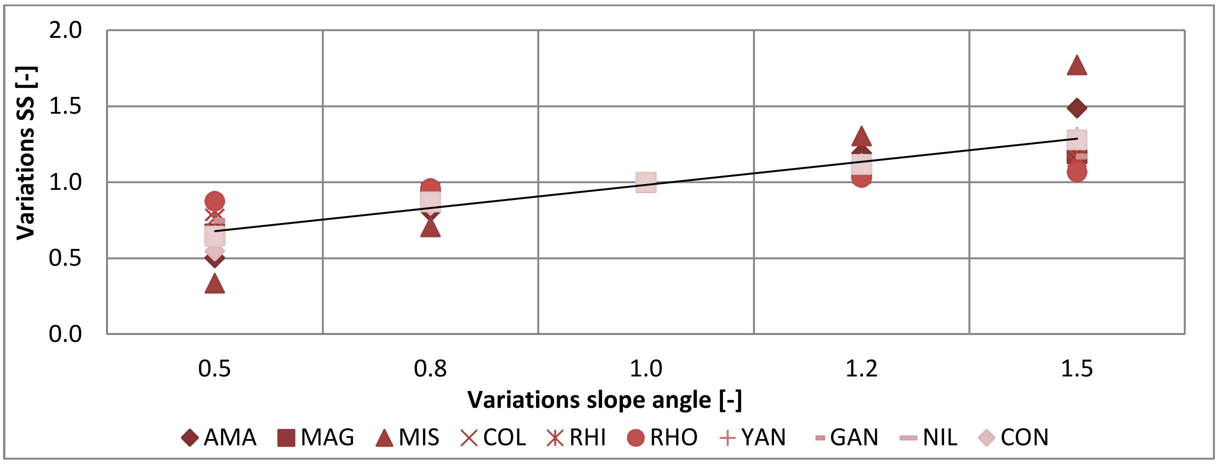

Figure 21: Scatter plot of resulting variations in sediment supply based on changes in slope angle

The strongest impact of increased slope angles has been obtained for the Mississippi where a 1.5 times steeper slope angle leads to 1.8 times more sediment supply. This is followed by the Amazon where sediment supply is almost 1:1 related to the slope angle (1.5 times the slope angle results in 1.5 times more sediment supply). An overall less visible relation has been detected for the European Rivers. For instance, increasing the slope angle by a factor 1.5 in the Rhone leads to only 1.1 times more sediment supply. For all other continents, results indicate an intermediate impact of variations in slope angle on sediment supply. In general, the findings fit to the estimation made upfront.

5.2. Impact of variations in precipitation amount

In contrast to the slope angle, variations in the precipitation amount impact the model results only at one location, namely the R-factor. Due to the binomial equation for annual precipitation higher than 850 mm this impact will presumably be stronger for an increased than for a decreased amount of precipitation. Eq. 28 gives the relation between computed sediment delivery and annual precipitation amount up to 850 mm while Eq. 29 gives the relation for amount equal or bigger than 850 mm.

$$SD = a' P_{year}^{\;1.161} \tag{26}$$

$$SD = a' P_{year}^{\;2} + b' P_{year} - c' \tag{27}$$

The impact of changes in the amount of precipitation is clearly visible in the African rivers. With reduced precipitation, the resulting sediment supply tends strongly towards zero. Only 2% of the original amount of sediment is supplied anymore in both Nile and Congo River when precipitation decreases by 50%. Quite the opposite, sediment supply strongly increases with precipitation in Asia. Here, 1.5 times more precipitation will lead to more than 4 times as much sediment supply in the Ganges and to around 3 times as much in the Yangtze River. Generally, all rivers appear to be sensitive towards changes in the amount of precipitation with the least sensitive rivers being located in Europe.

The response of computed sediment supply can be described with a binomial function which fits to Eq. 29.

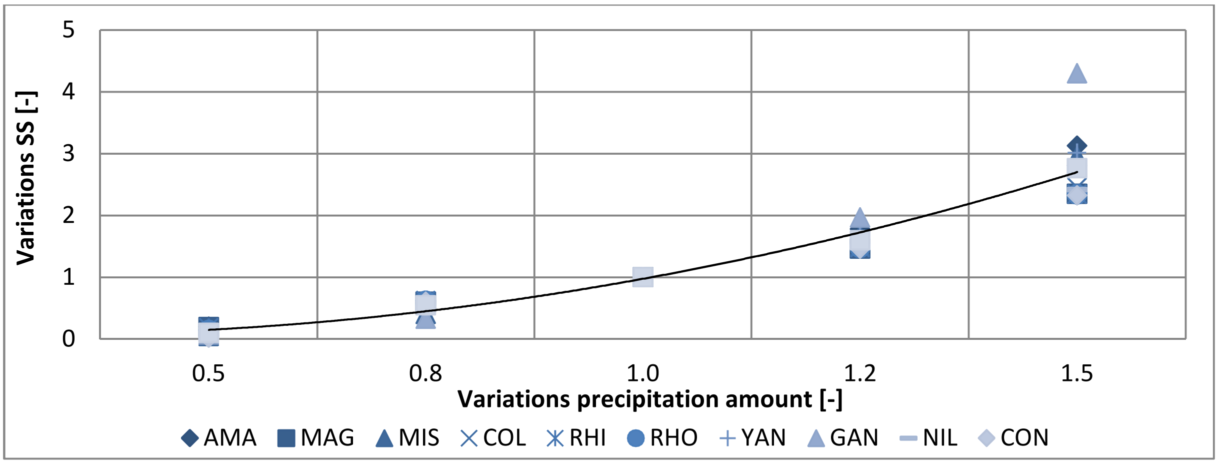

Figure 22: Scatter plot of resulting variations in sediment supply based on changes in precipitation amount

5.3. Impact of variation in temperature

Temperature plays a role only for the computation of the melting time fraction which in turn affects the soil erodibility. Eventhough literature suggests that temperature impacts the soil erosion, the analysis of correlation between monthly melting time fraction and computed monthly sediment supply did not confirm this. Hence, there is the need to determine to which extend PCRGLOB-SET is actually sensitive to temperature in its current set-up.

The simplified relation between model output and varied input factor can be expressed as follows:

$$SD = b'c'MT_{fr} + c'(1 - MT_{fr})$$
$$0 \leq MT_{fr,i} \leq 1 \tag{28}$$

Due to the upper boundary of MT_{fr}, an increased fraction should result in stagnating sediment supply. An increase in MT_{fr} will lead to an increase of the left term and simultaneously reduce the right one. Hence, variations will likely lead to only little response.

Figure 23 plots variations in computed sediment supply as a function of the variations in melting time fraction. As expected, neither smaller nor bigger fractions really influence the model output. However, the very limited response of sediment supply to reduced melting time fractions is still surprising. When reducing the fraction to 50%, the maximum decrease occurs in the Ganges River to 92%. In general, the river basins located in Europe, North America and Asia show more pronounced responses due to their exposure to generally lower temperatures.

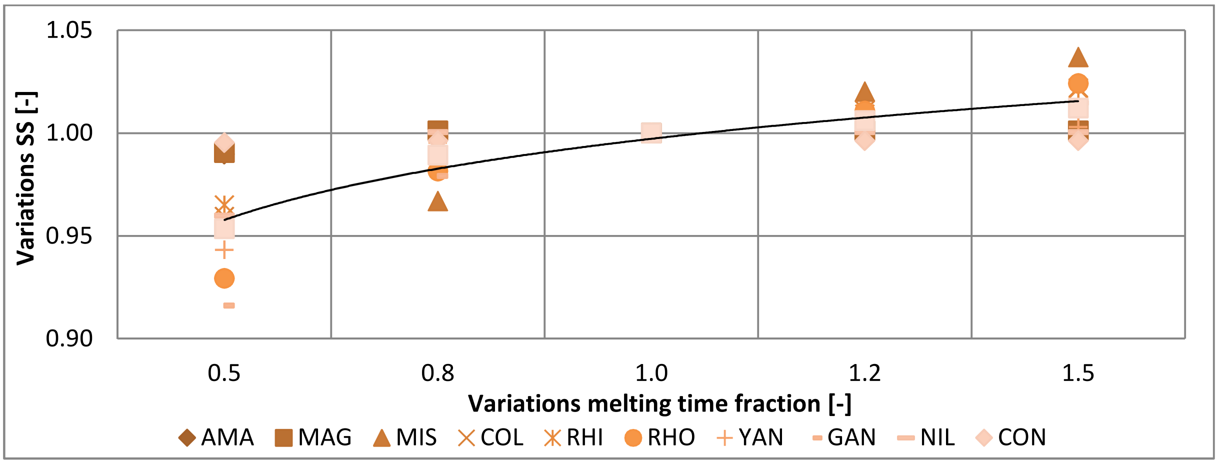

Figure 23: Scatter plot of resulting variations in sediment supply based on changes in melting time fraction

The limited sensitivity of PCRGLOB-SET to changes in the melting time fraction can explain the unexpected coefficients of correlation as computed in chapter 3.3. Obviously, melting time fraction and therefore temperature plays only a subordinate role in the computation of sediment supply.

5.4. Impact of variations in vegetation cover

While an increase in slope angle and in precipitation amount lead to more soil erosion and sediment supply, an increase in vegetation cover will lead to the opposite result. This is because vegetation cover is decisive in both diminishing soil erosion by reducing the C-factor and in decreasing the delivery ratio DR by increasing the surface roughness.

$$SD = \frac{a'}{NDVI} \exp\left(-\alpha\left(\frac{NVDI}{\beta - NDVI}\right)\right) \tag{29}$$

With increasing NDVI values, a clear exponential decrease of modelled sediment supply should be visible and vice versa. Figure 24 shows that this expectation is met by the results of the sensitivity analysis.

The river basin with the highest sensitivity to variations in the vegetation cover is the Congo River where a reduction of 50% leads to more than 6 times as much sediment supply. Moreover, the Nile shows an above-average sensitivity as well. Another continent where sediment supply is strongly coupled to the vegetation cover is South America where halving the vegetation would lead to 4.3 and 4.7 as much sediment supply in the Magdalena and Amazon, respectively. In addition, the sediment supply of the Yangtze seems to strongly depend on the vegetation cover as well whereas this clear response is not detected for the Ganges.

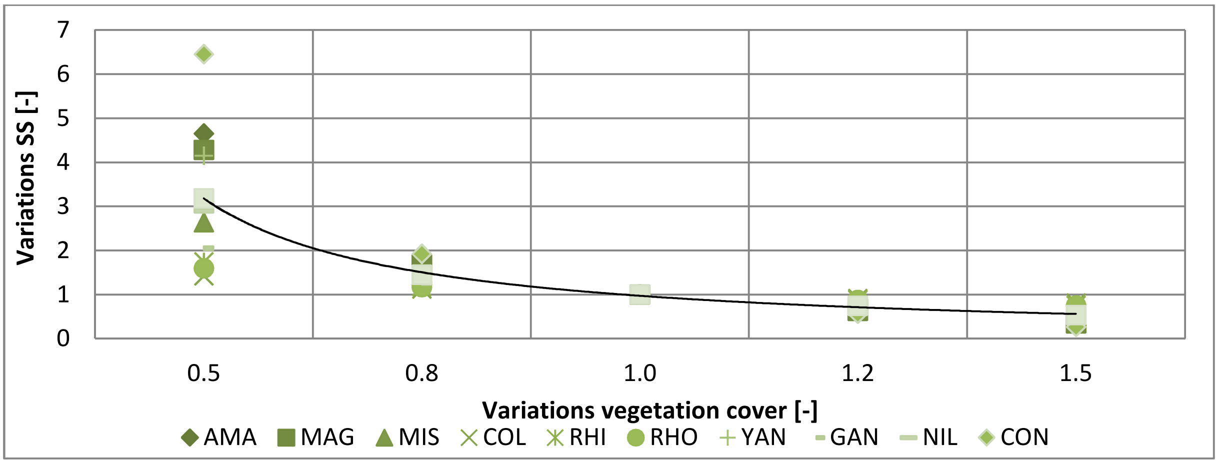

Figure 24: Scatter plot of resulting variations in sediment supply based on changes in slope angle

5.5. Résumé

Leaving the uncertainties in the model aside, clear connections between the examined factors and the resulting sediment supply exist. Yet, their significance differs between continents and even river basins. However, some trends can be defined.

Sediment supply in South America is more related to changes in vegetation cover than in the amount of precipitation. This seems plausible as precipitation is already comparatively high in South America and thus the vegetation becomes the limiting factor. Besides the vegetation cover, changes in the slope angle seem to impact sediment supply stronger than on other continents. Temperature adaptions do not play a role on this continent.

While in South America changes in the vegetation cover seem to play a key role, precipitation is the decisive factor Africa. Here, sediment supply is less sensitive to an increase in the precipitation amount than on other continents, but far more to a decrease. Besides the precipitation amount, African rivers seem to be sensitive to changes in slope angle and vegetation cover as well.

In Asia, sediment supply strongly increases with an increased amount of precipitation. The impact of vegetation cover cannot be entirely assessed but seems to be a major driving factor in some parts of the continent. The same counts for the impact of variations in the slope angle. Compared to other continents, lower temperatures seem to reduce sediment supply stronger.

In North America and Europe, no factor prevails. Here, changes in sediment supply might be equally related to changes in the slope angle, amount of precipitation and vegetation cover. Since both continents are located on the Northern Hemisphere, also changes in temperature play a role.

Based on the numbers plotted above, it can be concluded that the current model set-up of PCRGLOB-SET is most sensitive to changes in vegetation cover, especially for reduced cover. Changes in the amount of precipitation showed slightly less overall sensitivity but it appears that reduced values affect model output stronger than other factors. A basically linear response has been computed for changes in the slope angle with only little sensitivity both for increasing and decreasing angles. For all river basins, model output is least sensitive to changes in the melting time fraction per month which is partially due to the limited representation of the impact of temperature in PCRGLOB-SET.

This pattern is not comparable to the findings made by van Dijk. In the original RECODES model, sediment supply was most sensitive to the variables slope angle, precipitation amount as well as temperature while the impact of vegetation changes has not been assessed. The different results for precipitation and temperature can be explained by the absence of snowfall and snowmelt run-off in PCRGLOB-SET which can strongly affect sediment supply. For variations in the slope angle, the difference cannot entirely be explained but are most likely connected to the general uncertainty in the input data.

6. Discussion

One of the main goals of this Thesis was to develop a global sediment supply model. The verification of its annual and monthly results showed that the model is capable of estimating monthly fluctuations reasonably well but systematically overestimates the amount of sediment delivered into oceans. However, PCRGLOB-SET is only a first-order model yet. Thus, modelled sediment supply deviates from reality due to the absence of manifold important processes in soil erosion and sediment transport. Hereafter, the model results are discussed in the light of these limitations.

6.1. Model limitations and their implications

The main limitations of the current version of PCRGLOB-SET are the absence of any human interferences as well as natural factors influencing soil erosion and sediment transport. In addition, the chosen model formulation and set-up can influence the output quality. Hereafter, the significance of these limitations and their implications are discussed.

6.1.1. Human interferences with the system

Reservoirs

Vörösmarty *et al.* (2003) estimate that about half of the sediment flux on the basin scale is stored in artificial impoundments while Syvitski *et al.* (2005) associate 20% to large and another 6% to small reservoirs. Therefore, Walling (2006) correctly states that "the magnitude of this impact varies from continent to continent, in response to the spatial distribution of reservoir storage and the sediment loads of the rivers that have been dammed." Attributing these factors of 0.5 and 0.26 respectively to the annual value obtained with PCRGLOB-SET still leads to a major overprediction. Based on the two different approaches, the resulting annual global sediment supply would then be 75 GT/year and 110 GT/year, respectively.

Rivers that are excessively dammed are amongst others the Nile River (see Biswas and Tortajada (2012); Gu *et al.* (2011); Woodward *et al.* (2007)), the Yangtze River (see Liu *et al.* (2007); Wang *et al.* (2008); Xiqing *et al.* (2005); Yang *et al.* (2014)) and the Columbia River (see Naik and Jay (2011); Vörösmarty *et al.* (2003)). Not surprisingly, it has been found that results strongly overestimate reality in these rivers by a factor of 19.3, 7.4 and 289, respectively.

In order to investigate the impact of sediment trapping in reservoirs at the river basin scale, the reservoirs of the Global Reservoir and Dam (GRanD) database (Lehner *et al.*, 2011)[xiv] have been associated to their corresponding river basins as schematized in PCRGLOB-SET. Subsequently, the representative maximum storage capacity for each of those 50 river basins where both observed and modelled values are available is computed. It is hypothesized that computed sediment supply in river basins with higher maximum storage capacity will deviate stronger from observed values.

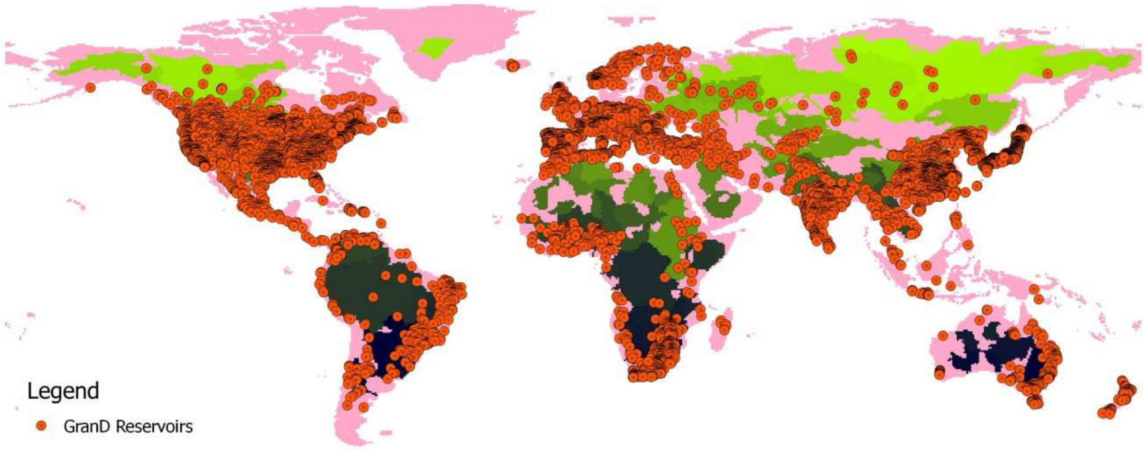

Figure 25: Reservoirs of the GRanD database (orange dots) and 108 river basins (coloured green to blue) used in PCRGLOB-SET

Figure 26 shows the resulting scatter plot. The results actually show a slight positive trend towards higher differences with more maximum storage capacity which confirms the hypothesis. However, the overall correlation of 0.14 which is rather weak.

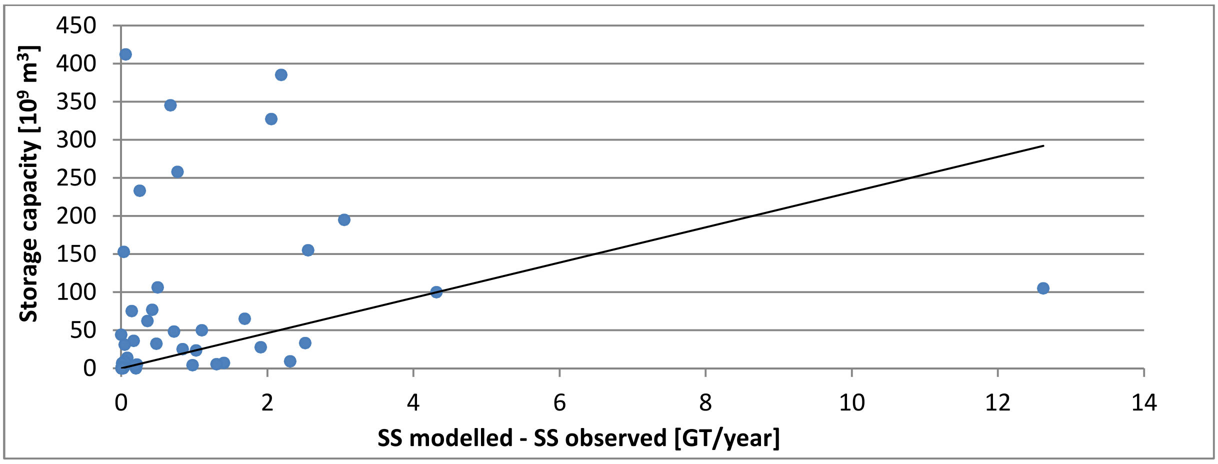

Figure 26: Scatter plot of difference between modelled and observed SS and maximum storage capacity including trend line

[xiv] The GRanD database is online accessible on http://sedac.ciesin.columbia.edu/data/set/grand-v1-dams-rev01

When considering only the ten biggest deviations which contribute most to the general model error, the coefficient of correlation turns out to be 0.26 which indicates a slight tendency towards bigger deviations in river basins with more storage capacity. The aforementioned rivers Nile, Yangtze and Columbia indeed occur all within the top ten of dammed rivers with maximum storage capacities of 385×10^9 m^3 (2^{nd}), 195×10^9 m^3 (7^{th}) and 105×10^9 m^3 (10^{th}) respectively. On the other side, the coefficient of correlation for the river basins with the ten smallest differences is markedly reduced (r=0.13).

These findings suggest that sediment retention is one but not the only one factor influencing the fate of sediment. Especially in river basins with bigger differences between modelled and observed sediment supply, dams and reservoirs seem to play a more decisive role than in river basins where the model performance is already good.

Soil Conservation Practices

Besides reservoirs, the application of soil conservation practices such as terracing has been disregarded in the model as well by setting the P-factor to 1 eventhough their impact is well documented (for example in Dai *et al.* (2009) or Xiqing *et al.* (2005)). For the Huang (Yellow) River, Wang *et al.* (2007) estimate that soil conservation practices are responsible for around 28% of the total decrease in sediment supply which clearly illustrates the impact of soil conservation practices.

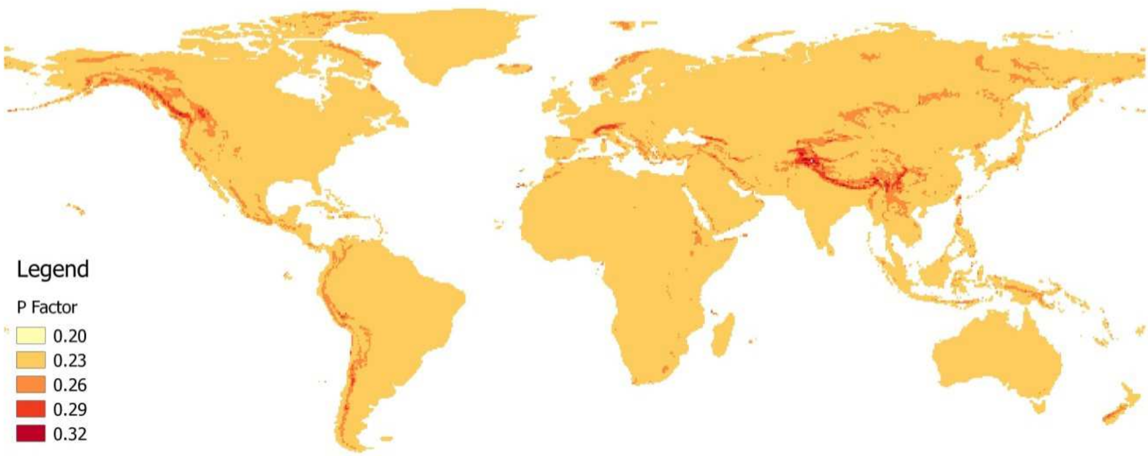

Figure 27: Values for the P-factor world-wide at a 0.5° resolution

For large scale applications, the Wener method (Wener, 1981) is rather straightforward and easily applicable to obtain values for the Y-factor globally. Admittedly, this approach rather poorly represents the variety and heterogeneity of soil conservation practices but serves well as a first estimate of the impact of the Y-factor.

$$Y = 0.2 + 0.3s \qquad (30)$$

where Y is dimensionless and s the slope angle [m/m]. Resulting values for the Y-factor vary between 0.2 and 0.32 with higher values found in mountainous areas (see Figure 27).

The resulting annual global sediment supply would then be reduced by 76 %. Moreover, the impact of soil conservation practices appears to be stronger in North America and Asia, where the continental fraction of global sediment supply is reduced by 1%. On the other side, Europe is responsible for a bigger part of sediment supply since its share increases 2% which means that the application of soil conservation practices is less efficient here.

Land-Use Change

While both reservoirs and soil conservation practices reduce sediment supply, on-going land-use change increases it. Especially in countries with growing population, land surface is cleared and used for increased agriculture and urban areas. On the global scale, the precise impact of land-use change is hardly to determine. Bakker *et al.* (2008) showed that intensification of agriculture leads to increased soil loss. Case studies in various river basins world-wide strongly agree with this finding (Alkharabsheh *et al.*, 2013; Martínez-Casasnovas & Sánchez-Bosch, 2000). Besides, sediment supply is increased due to increased surface run-off (Olang & Fürst, 2011). Given the anticipated rise in population, the associated increased demand will most likely fuel the intensification process. Tilman *et al.* (2011) estimate that with current practice around 1 billion ha of land will be cleared by 2050. One might remark here that land-use change is already accounted for with the C-factor. This is not entirely correct since the used vegetation index NDVI solely expresses the degree to which the surface is covered with vegetation but neither the actual land-use nor its intensity.

In the light of the massive influence of human actions on soil erosion and sediment transport, the results of PCRGLOB-SET appear to be in a reasonable magnitude. Assuming that soil conservation practices are applied only on 50% of land in each river basin, the associated reduction of sediment supply would drop from 76% to 38% which is around the value published by Wang *et al.* (2007). Hence, when applying a factor of 0.26 for reservoir and 0.38 for soil conservation practices, total global sediment supply is reduced from 195 GT/year to around 19 GT/year without consideration of the increasing effects of land-use change. For PCRGLOB-SET being only a first-order model and for human interferences representing only one cause for reduced sediment supply, this theoretical value is absolutely acceptable.

6.1.2. Natural factors affecting sediment supply

Sediment transport capacity

Another aspect that is not accounted for in PCRGLOB-SET is the impact of alluvial processes. Currently, it is assumed that all rivers are in equilibrium state and no morphological processes take place. This however has only little connection with reality as transported sediment might be deposited in reaches with insufficient transport capacity. Indeed, Ali *et al.* (2011) link the sediment transport capacity to unit stream power which is comparable to other equations in scientific literature, for instance in Celik and Rodi (1991) or Prosser *et al.* (2001).

With good reason it can be assumed that the slope does not play a superior role because for rivers reaching from their mountainous source until the ocean it will be, with some exceptions, in similar ranges. Additionally, actually erodible sediment will probably range within small margins as well. As a result, the sediment transport capacity is related the strongest to water discharge.

It is more than obvious, that the sediment transport capacity is not equal for all streams as assumed in the PCRGLOB-SET formulation. For instance, the Amazon River has a discharge of around 200.000 m^3/s, the Nile River of 3.500 m^3/s and the Rhine River only 2.000 m^3/s (values according to the M&S92+ database). In order to underline this, Table 18 provides the five rivers with highest sediment and highest water discharge. Thereby especially the rivers occurring only in one list are of special interest. For instance, the Zaire/Congo River which ranks second regarding the highest water discharge is listed on rank 30 in terms of sediment discharge. The other way around, the Yellow River can even be found on rank 54 for water discharge.

Table 18: Ranking of five rivers with highest sediment and water discharge according to the M&S92+ database

	Sediment discharge	Water discharge
# 1	Amazon	Amazon
# 2	Yellow River	Zaire / Congo
# 3	Ganges	Orinoco
# 4	Yangtze	Ganges
# 5	Mississippi	Yangtze

These numbers and examples perfectly illustrate that the absence of any sediment transport capacity in the model formulation clearly leads to overprediction of sediment supply especially in rivers with little water discharge.

A related issue is the discrimination between suspended sediment load and bed load. Eventhough PCRGLOB-SET computes merely suspended load, it may happen in reality that it is converted to bed load under certain discharge regimes and vice versa. Implementing these small scale processes at the global scale will however be challenging.

Overbank deposition

The temporal storage of sediment due to sedimentation on floodplains is not represented by PCRGLOB-SET but it assumes that all sediment that has been eroded and delivered to a stream will reach the mouth of this stream.

The importance of these processes in temporal storage of sediment is undoubted in scientific literature. Asselman and van Wijngaarden (2002) for instance determined that about 13% of total annual suspended sediment supply is deposited on the floodplains of the main branches of the Rhine River. Middelkoop and Asselman (1994) estimated that around 19% of suspended sediment load has been deposited on floodplains during a flood in the Waal River.

However, overbank deposition rates appear to be highly site dependent. While Walling and He (1998) measured values between 0.1 to 5.4 mm/year in four English rivers, Pierce and King (2008) published rates of 0.9 to 6.7 mm/year in unchannelized sites in the Lower Mississippi Valley. In other sites, they found rates of even 3.4 to 62 mm/year.

Prosser *et al.* (2001) provide an equation for computing overbank deposition of a river reach in dependence of inter alia floodplain area, water discharge and settling velocity. In their modelling approach, Asselman and van Wijngaarden (2002) applied a more straightforward approach but linked the overbank deposition rate to the same parameters.

While the settling velocity varies only little, water discharge differs strongly between river basins as already shown above. Similarly, available floodplain area in river basins varies world-wide as well. It even has to be separately considered for up-, mid- and downstream parts of each river. The complex task of determining these factors might be one reason why overbank deposition has not been implemented in other global sediment supply models such as WBMsed (Cohen *et al.*, 2013) or Pelletier (2012).

Having the aforementioned deposition potential in mind, it becomes clear that the absence of this important alluvial process leads to overprediction. Compared to the other factors discussed, overbank deposition plays only a minor role in terms of annual sediment storage but probably a more decisive one regarding the temporal fluctuation of sediment load in rivers.

Temporal variations

Sediment supply shows temporal variations at different scales which makes a good long-term estimation rather difficult. On the big scale, sediment supply differs between today and glacial ages with reduced sediment supply nowadays (Hay, 1994; Milliman & Syvitski, 1992; Syvitski, 2003). Some research even suggests that Milankovitch-scale climatic forcing impacts sediment supply (Van der Zwan, 2002). On the intermediate scale, seasonal differences in temperature, vegetation and precipitation strongly impact the amount of sediment supply as well. And on the small scale, individual short extreme events are decisive in soil erosion and sediment transport (Bookhagen, 2010; Coppus & Imeson, 2002; Korup, 2012; Restrepo & Kjerfve, 2000; Vanmaercke *et al.*, 2010). While the intermediate scale is incorporated into PCRGLOB-SET except for snowmelt processes, both big and small scale dynamics cannot be incorporated. While on the big scale extremely long time-series would be required, it is hardly feasible to incorporate a module that predicts the magnitude, location and timing of extreme events such as the La Niña phenomenon for instance. Findings of Inman and Jenkins (1999) suggest that this regularly recurring event results in 27 times higher average sediment flux than during normal conditions.

Given these complexities, it is not feasible to incorporate either long- nor short-term variations in such global models but their influence on actual sediment supply must be carried in mind when assessing any modelled sediment supply values.

6.1.3. Model characteristics and formulation

Schematization of river basins

Regardless the model formulation, the spatial resolution influences the model output as well. With the chosen 0.5° resolution, PCRGLOB-SET runs at the same spatial resolution as other recent global sediment supply models as for instance the "WBMsed" model by Cohen *et al.* (2013). Since one raster cell at a 0.5° resolution covers an area of 55 km to 55 km at the Equator, it is possible that the model output is biased towards bigger river basins due to the aggregation of smaller river basins.

In order to investigate this, the catchment area has been calculated for each river basin and subsequently been compared to values listed in the M&S92+ database. Given the coarse spatial resolution of PCRGLOB-SET and the limited number of only 108 river basins, it can be expected that the schematization unsatisfactory represents the actual extend and shape of the river basins. Computed sediment supply would be wrongly attributed to a river basin eventhough it actually occurs at a different river mouth. Consequently, model results would be higher or lower for over- or underrepresentation of the actual catchment area, respectively.

Thereafter the difference between modelled and observed sediment supply and the difference in model and database catchment area have been correlated. The resulting coefficient is 0.06 which indicates that there is virtually no correspondence between difference in sediment supply and in catchment area. This is underlined by the scatter plot which plots the difference between schematized and reported catchment areas in relation to difference between modelled and observed sediments supply. Thus, the schematization of the river basins used in PCRGLOB-SET cannot be held responsible for the computed deviation in sediment supply.

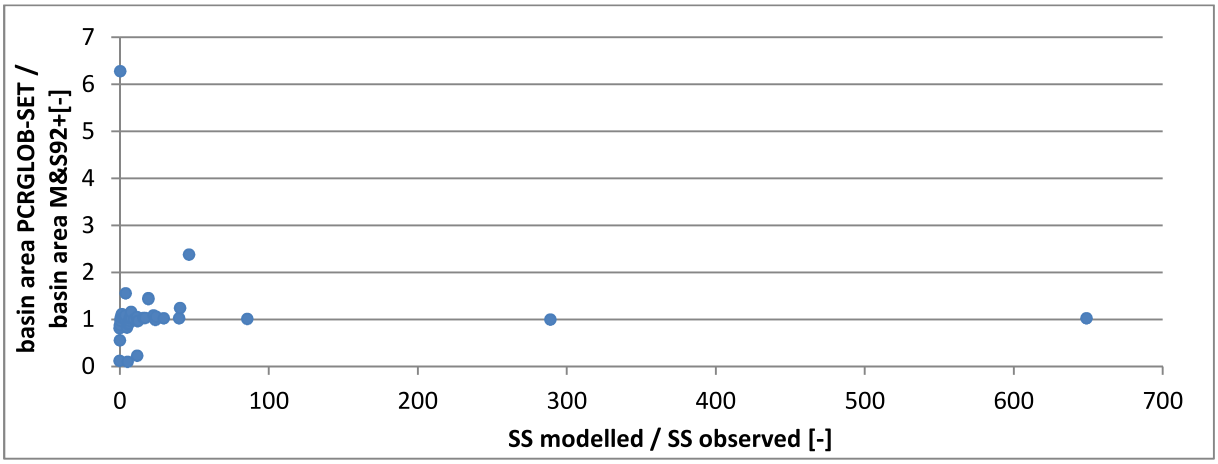

Figure 28: Scatter plot of factorized difference between modelled and observed SS and factorized difference between reported (M&S92+) and catchment area as schematized in PCRGLOB-SET

In Appendix D the river basins defined in PCRGLOB-SET and by HydroSHEDS[xv] are provided. Originally, this map ought to be solely for visualization of the investigated issue. Thereby it has been found that the catchment areas from HydroSHEDS partially differ markedly from those mentioned in the M&S92+ database. For instance, the schematized Nile River Basin is in PCRGLOB-SET 1.43 times bigger than according to the database but when comparing it to HydroSHEDS, this value drops to 0.99 which is almost perfect fit. When comparing with catchment areas of HydroSHEDS instead, the number of catchments deviating +/- 20% of the value in PCRGLOB-SET is strongly diminished. This unintended finding does however not affect the statement made before that the catchment area in PCRGLOB-SET is not related to the occurring difference between modelled and observed sediment supply.

<u>*Soil loss or delivery ratio module?*</u>

What makes PCRGLOB-SET unique is the application of RUSLE on the global scale. Moreover, only very few studies combine RUSLE with a sediment transport component (for example Mhangara *et al.* (2012) in a South African watershed). What is more, the underlying

[xv] HYDROlogical data and maps based on SHuttle Elevation Derivatives at multiple Scales

model RECODES has not yet been applied to other basins but for the Rhine River. Given the systematic overprediction of sediment supply by PCRGLOB-SET, it should be discussed whether one of the modules can be held responsible.

To that end, three recent case studies have been assessed in which the RUSLE has been applied for soil erosion modelling on the catchment scale. The range of soil loss published (A_{publ}) is then compared to values computed with PCRGLOB-SET (A_{calc}). Due to the spatial resolution of PCRGLOB-SET, a representative value has been compared to published values.

Table 19: Published and calculated values of soil loss for different case studies

Reference	Country	A_{publ} [t/ha/yr]	A_{calc} [t/ha/yr]
Demirci and Karaburun (2012)	Turkey	102	~ $0.35*10^6$
Ranzi *et al.* (2012)	Vietnam	32	~ $8*10^6$
Prasannakumar *et al.* (2012)	India	18	~ $2*10^6$

The differences between calculated and published values are massive. Obviously, the RUSLE approach as formulated and implemented here cannot adequately produce soil loss but overestimates it surprisingly strongly. Given the magnitude of difference in soil loss and the comparatively small magnitude in sediment supply, it appears as if the values produced by the Delivery Ratio Module are actually too low.

Due to the different spatial resolutions of PCRGLOB-SET and case studies, a more detailed look on which parameter within the Soil Loss Module causes the deflection is not feasible. For example, the entire watershed investigated by Demirci and Karaburun (2012) has an area of around 600 km^2 which can be represented by 20% of one raster cell in PCRGLOB-SET. In this specific case, it becomes even more complicated because the watershed is distributed in two raster cells whose computed soil erosion differs by a factor of 0.75. Thus, comparing the erosion rates in Table 19 need to be carefully compared.

The sensitivity analysis unravels that sediment supply is in some river basins strongly related to variations in precipitation, vegetation and slope angle. Due to the fact that more detailed input data had to be resampled to a coarser spatial resolution, its correctness may have been reduced. As a result, only small deviations in input data lead to linear or exponential changes in computed sediment supply.

Besides, the chosen equations need to be discussed. Three aspects are thereby of importance. First, the equations directly taken from RUSLE are not to be applied on big scales eventhough this is regularly done. Second, other equations taken from scientific literature are only rarely applied for bigger catchments. Third, new approaches and many assumptions have to be made in order to apply these equations with available input data to the global scale. For instance, monthly R-values have never been calculated as in PCRGLOB-SET and the attribution of values to the sub-factors of Manning's surface roughness coefficient is mostly based on assumptions not on actual data. What is more, the impact of temperature on soil erosion is hardly captures as shown in the sensitivity analysis and in the weak or even opposite correlation to computed sediment supply. Last, it is shown that the absence of snowfall and snowmelt strongly limits the potential impact of temperature changes. Especially in river basins where temperature changes are expected to influence sediment supply, no such correlation could be found. This is underlined by the outcome of the sensitivity analysis where the current model did not show any significant response to variations in the melting time fraction.

Another important aspect thereby is the concept of the "effective parameter" which describes the impact of the large scale application of equations derived for small scale processes as erosion is. As a result of a large scale application, modelling output can be determined by the spatial correlation of the processes driving soil detachment and transport. However, no equations that account for these scale-depending processes have been published yet and thus the resulting implications have to be accepted and accounted for in the interpretation of model results.

Grid cell size of input data

As briefly indicated above, the chosen spatial resolution influences the accuracy of the data input. Soil erosion is a complex and spatially heterogeneous process. Hence, a coarse spatial resolution even garbles this complexity. In the scientific discourse, the impact of coarser resolution on derivatives from DEMs is an important issue, especially the impact on slope, basin area channel length and drainage density (Armstrong & Martz, 2003; Kienzle, 2004; Sørensen & Seibert, 2007; Vaze *et al.*, 2010).

The general impact of different spatial resolution on other hydrologic or sediment-related parameter is not that intensively discussed. Jetten *et al.* (2003) state that in raster-based models "the grid cell determines everything", for instance land use patterns. In order to visualize this statement, Figure 29 plots NDVI values in a randomly chosen area in South America both at the original 0.05° and the 0.5° resolution as used in PCRGLOB-SET. The spatial heterogeneity of the original values is clearly diminished due to the reduction to only 1% of the original number of raster cells.

Hessel (2005) researched how different grid cell sizes and time steps influence results in another sediment detachment model (LISEM). He varied grid sizes from 5 m up to 100 m and found that the sediment yield decreases with increasing grid size. This is most likely because coarser grid sizes result in smaller maximum and average slopes and thus to less transport capacity. While Jetten *et al.* (2003) agree on the inverse relation between discharge and cell size, they come to a different conclusion regarding erosion and net soil loss. For these, they state that "the variation […] with grid cell size is even fairly unpredictable". Additionally, they point out the relatively large impact of isolated pixels. Rojas *et al.* (2008) in addition recommend grid sizes smaller than 150 m for proper simulation results because sediment sources become less appropriately depicted and calculated sediment delivery ratios became unrealistically high. Modelling approaches using RUSLE have thus way finer spatial resolutions than PCRGLOB-SET. For instance Mhangara *et al.* (2012) and Prasannakumar *et al.* (2012) apply a 20 m resolution while Cohen *et al.* (2005) and Chen *et al.* (2011) use a 30 m resolution.

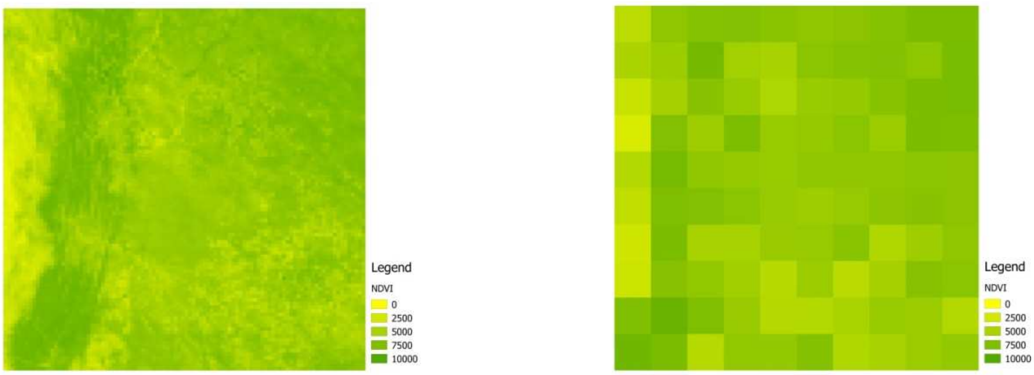

Figure 29: NDVI at the original 0.05° resolution (A) and a 0.5° resolution as used in PCRGLOB-SET (B)

These different opinions perfectly show the complexity and spatial heterogeneity of soil erosion and sediment transport. Therefore a clear and quantified judgement about the impact of grid cell size on model results cannot be made. However, most recent research strongly suggests that modelled sediment supply and yield decrease with finer resolution. Besides Hessel (2005) with LISEM, Wu *et al.* (2005) report the same using USLE in a watershed in Virginia, USA, Goulden *et al.* (2014) using SWAT in a Canadian catchment and Chaplot (2014) based on various basins world-wide. In the latter study, the impact of changes in spatial resolution is even more precisely elaborated. Especially the number of watershed sub-divisions and the resolution of soil data appear to play an important role. The findings made in the sensitivity analysis stand in line as decreasing slope (representing coarser resolution) results in less sediment supply in PCRGLOB-SET. More generally, the sensitivity analysis provides clear evidence that changes in input factors can lead to strong responses in model output. This is of special importance as a lot of data sets have been resampled to a coarser spatial scale which indeed leads to changes of the original input values.

6.2. Comparison to other global sediment supply models

In this section, PCRGLOB-SET is compared to two other recently developed global sediment supply models, namely WBMsed by Cohen *et al.* (2013) and one (nameless) model developed by Pelletier (2012). Thereby the model formulation is briefly outlined and the spatial and temporal resolution as well as the results are assessed.

6.2.1. WBMsed

The WBMsed model is able to run at a temporal resolution of 0.1° degree and a daily temporal resolution. However, global results are solely determined at a 0.5° and annual resolution.

It consists of three parts, namely the WBMplus module (Wisser *et al.*, 2010), the BQART module (Syvitski & Milliman, 2007) and the Psi module (Morehead *et al.*, 2003). BQART stands thereby for the different influences parameterized by the module: geological and human factors (B), discharge (Q), area (A), relief (R) and temperature (T). Through the implementation of the B-factor, the model results do not represent pre-human conditions which is a major difference to PCRGLOB-SET.

The BQART computes long-term average suspended sediment loads for each grid cell. Thereby, each basin-average parameter needs to be dynamically calculated for each pixel within the basin. This is because BQART is originally a large-scale distributed and not a spatially explicit module.

$$\overline{Q_s} = \omega B \overline{Q}^{0.31} A^{0.5} R T \text{ for } \mathrm{T} \geq 2°\mathrm{C} \tag{31}$$

$$\overline{Q_s} = 2\omega B \overline{Q}^{0.31} A^{0.5} R \text{ for } \mathrm{T}<2°\mathrm{C} \tag{32}$$

where ω is a coefficient of proportionality and $\overline{Q}$ is the long-term average discharge per cell.

Using the Psi-module resolves long-term sediment flux on a daily time step. Moreover, it is capable of capturing the intra- and interannual variability.

$$\left(\frac{Q_{s[i]}}{\overline{Q_s}}\right) = \psi_{[i]} \left(\frac{Q_{[i]}}{\overline{Q}}\right)^{C_{(a)}} \tag{33}$$

where ψ describes a lognormal random distribution, [i] refers to a daily time step and $C_{(a)}$ is a normally distributed annual rating exponent.

In contrast to PCRGLOB-SET, this represents more a “bottom-up” approach as parameters are determined for each river basin separately before basin-averaging for each pixel. In total, 15 different datasets have been compiled to run the model which is due to the broad range of factors considered. Thus, this approach will most likely cost more time than the “top-down” approach where global datasets are directly applied.

However, climatic factors such as precipitation and temperature are not directly part of WBMsed but externally computed in the WBMplus module which calculates water balances and thus also surface and groundwater run-off. Here, PCRGLOB-SET links resulting sediment supply more directly to important drivers such as precipitation, surface run-off, temperature and vegetation.

The resulting coefficient of correlation of 0.66 between modelled and observed sediment yields indicates that WBMsed models sediment load acceptable well. This coefficient is based on results in 95 river basins and is in the same range as the one of PCRGLOB-SET (r=0.62). This appears to be rather surprising as with the more complex and “bottom-up” model set-up of WBMsed a better result is intuitively expected. Next to the output on the river-basin scale, no continental or global value of sediment supply is published.

The areas where the model uniformly underrepresents observed values are East Asia, the Mediterranean basin and North America. In other areas, the model overpredicts observed values. The most prominent rivers are thereby the Amazon and the Mekong River. Unfortunately, no values are published for a more in-depth comparison of model results.

6.2.2. Pelletier’s model

The model developed by Pelletier (2012) aims to compute natural/pre-dam long-term suspended sediment discharge. In contrast to WBMsed and similar to PCRGLOB-SET, his model is spatially distributed and globally applicable and does not use upscale river basin results.

It works at a spatial resolution of 5 arc-minutes or a width of 10 km at the Equator. Thus, the chosen spatial resolution in PCRGLOB-SET is by a factor 30 coarser. The temporal resolution is monthly to obtain a better annual result. Thereby, the factor temperature is not incorporated and only changes in vegetation and precipitation lead to monthly dynamics in sediment supply. This approach is partially equal to PCRGLOB-SET but does not provide time series of sediment supply throughout the year.

Another parallel is the structure of the model which consists of two components as well. The first component determines the detachment rate D [kg/m/yr] which is computed at every location (x,y) and every grain diameter (d).

$$D(x,y,d) = c_1 \rho_b f_d S^{5/4} \sum_{k=1..12} R_k e^{-L_k} \tag{34}$$

where c_1 is a free dimensionless parameter (calibrated), ρ_b the bukl density of soil [kg/m^3], f_d the fraction of the soil within each soil texture bin of grain diameter d [-], S the lope [-], R_k the mean monthly rainfall [m/yr] and L_k the mean monthly Leaf Area Index LAI [-].

Second a Rouse-number dependent transport component is implemented. Transport only takes place when the computed threshold of 1.2 is exceeded.

$$R_{\#}(x,y,d) = c_2 \frac{w_s}{S^{1/2}} \tag{35}$$

where c_2 is a free calibrated parameter [s/m] and w_s is the settling velocity [m/s].

Correlating the model output with observed values in 128 rivers yields a coefficient of 0.79 which indicates good agreement. Eventhough this model is also raster based and hence computes sediment supply for all grid cells, no global value has been published eventhough it would have been possible to compute it.

Some of the rivers strongly overestimated by PCRGLOB-SET are also found to be strongly overestimated by Pelletier's model as well. For instance, the Sao Francisco is computed to produce 10, the Rhine 6.8 and the Columbia River 6.6 more sediment than reported.

In addition, some river basins are simultaneously underpredicted as for example the Orange River in South Africa. Most interestingly, both models underrepresent observed values models in the Huang River and compute only 7% of the reference value 1.1 GT/year.

In order to complete the complex picture, results in some rivers are contradictory. Thereby especially the Mississippi River (only 12%) stands out as it has been overpredicted by PCRGLOB-SET (269%). Another example is the Godavari River which is underrepresented by Pelletier (16%) but overrepresented by PCRGLOB-SET (382%)

7. Conclusion

Sediment supply modelling was, is and probably will be a challenging task due to the complex nature of soil erosion and sediment transport processes. In order to better assess the impact of mankind on sediment flux, global models are required. Amongst others, the supply of sediment to the oceans determines the rate of coastal erosion and is decisive for the survival of important ecosystems.

The raster model applied in this Thesis consists of three modules. One computes the soil loss per grid cell based on RUSLE while the second estimates the delivery ratio. The third module finally combines them and routes the eroded sediment through the drainage network. Applying such a construct on the global scale is both innovative and consequent as RUSLE has been so far applied in individual sub-catchments, entire river basins and countries. Besides, the temporal variability of sediment supply is modelled which is another added value of this research.

Thereby, the absolute annual values produced are in most river basins strongly overestimating reported values. In total, PCRGLOB-SET computes 59.9 GT/year of sediment supply into oceans based on the schematized river basins. Since only two third of land surface discharging into oceans is covered by these river basins, the actual amount of sediment delivered is higher. Different calculation approaches yield values of 150 GT/year and 195 GT/year. Temporally, most of the sediment is discharge in the period from March until August. Spatially, most sediment is delivered from Asia, followed by South America. In general, the spatial distribution of sediment sources is correctly resembled by PCRGLOB-SET which allows for the conclusion that the heterogeneity of soil erosion and sediment transport is well captured with the current version of the model.

The systematic overprediction of sediment supply is most likely due to the fact that PCRGLOB-SET is only a first-order model yet, lacking important external influences on soil erosion and sediment transport. Amongst other minor influences, the following important external influences on sediment supply have been detected: the damming of rivers, the absence of soil conservation practices, sediment transport capacity and overbank deposition of sediment. When coarsely assessing the impact of these factors, the modelled value would be reduced to a more reasonable value which leads to the conclusion that the model has the potential to produce applicable results.

Comparing observed and modelled annual values for different river basins, the computed coefficient of correlation indicates acceptable agreement. It is a throwback thereby that only

50 rivers are both schematized in PCRGLOB-SET and listed in the M&S92+ database. However, the ranking of sediment supply computed in river basins agrees acceptably well with reality. While the model computed the three highest values for the Ganges, Columbia and Amazon River, the M&S92+ database used for model verification lists the Amazon, Huangh and Ganges River as rivers with highest sediment discharge.

River basins where modelled sediment supply strongly overestimates observed values are the Rhine, the Columbia and the Uruguay River. Eventhough PCRGLOB-SET overpredicts in most cases, it underpredicts in some rivers as for instance the Huangh, the Orange and the Colorado River. Reasons for occurrence and different magnitudes of overprediction and underpredictions in river basins cannot unambiguously be named. The sensitivity analysis showed that some river basins are more sensitive to certain input factors than others. Moreover, the sensitivity analysis unravelled that variations in some input factors lead to stronger variations in modelled sediment supply than other. For instance, changes in precipitation generally lead to stronger responses in sediment supply than changes in slope angle. At the same time, changes in precipitation are more effective in African than in South American river basins. This suggests the conclusion that errors in input data may locally lead to stronger deviations in the model result. Such errors can for example result from resampling data sets to different spatial resolutions.

Based on the outcome of the sensitivity analysis, it can be concluded that it is important to incorporate snowfall and snowmelt in the model formulation as these processes markedly influence both the absolute value as well as the temporal fluctuations of sediment supply.

The monthly output of PCRGLOB-SET shows reasonably good correlation with measured values. From the four rivers investigated, three have a coefficient of correlation between 0.7 and 0.5. Hence, it is demonstrated that the dynamic section of PCRGLOB-SET is capable of re-producing the patterns of monthly variations in sediment supply. This is a major addition as current research mainly focusses on annual totals than on the monthly fluctuations of sediment supply. It furthermore facilitates the future implementation of intra-annual processes such as temporal sediment storage due to overbank deposition and erosion.

Based on the comparison of PCRGLOB-SET with other models in terms of their formulation and output quality, it can be concluded that – regardless their set-up, spatial and temporal resolution as well as complexity – no model globally computing sediment supply is capable of correctly estimate basin-scale values. Additionally, it can be inferred from the comparison that some river basins seem to be more challenging than others in terms of correctly modelling sediment loads.

8. Recommendations

PCRGLOB-SET is only a first-order model and thus many important factors are not yet implemented. This limits the quality of the model output. In order to obtain a more realistic picture, it is recommended to consider the impact of reservoirs, soil conservation practices and other external factors. For instance, the PCRGLOB-WB model contains information on both floodplains and reservoirs. Going even beyond this, coupling both the PCRGLOB-WB and the -SET model would create an even more powerful tool to assess the interactions between water discharge and sediment transport such as the impact of stream power on sediment transport capacity.

The current results lead to the conclusion that the temporal output of PCRGLOB-SET represents reality well. However, in order to substantiate this finding, model output needs to be compared to more river basins and better data for model verification is needed. Eventhough the employed M&S92+ database provides a lot of valuable data, its timeliness can be doubted more than 20 years after its creation. Admittedly, this would require a combined effort of scholars to obtain, process and combine relevant data on sediment transport rates in rivers world-wide.

Besides, some recommendations have to be made regarding the model set-up and formulation. A major recommendation is to refine the spatial resolution of PCRGLOB-SET. Regarding the input data, this is no problem since most of the required parameters have been resampled from global data sets at a finer resolution anyway. As a result, errors introduced by data manipulation could be heavily minimized or even eradicated.

A finer spatial resolution would not only increase model accuracy. A more detailed resolution would moreover facilitate a better schematization of smaller river basins and hence increase the number of rivers where model results can be obtained and verified. Generally, the schematization of river basins as used in the current version of PCRGLOB-SET needs to be improved. Especially the extent of river basins schematized has to be increased to areas so far underrepresented. At the moment, model output in Central Europe and South East Asia cannot sufficiently be taken into consideration.

The impact of temperature on soil erosion is not fully accounted for in PCRGLOB-SET. This is because snow cover could not be implemented on the global scale. Another factor is the transformation from rain- to snowfall which does not contribute to soil erosion. Implementing respective equations in the model as for example in RECODES would reflect real dynamics much more accurately.

References

Ali, M., Sterk, G., Seeger, M., Boersema, M., & Peters, P. (2011). Effect of hydraulic parameters on sediment transport capacity in overland flow over erodible beds. *Hydrology and Earth System Sciences Discussions, 8*(4), 6939-6965.

Alkharabsheh, M. M., Alexandridis, T. K., Bilas, G., Misopolinos, N., & Silleos, N. (2013). Impact of Land Cover Change on Soil Erosion Hazard in Northern Jordan Using Remote Sensing and GIS. *Procedia Environmental Sciences, 19*(0), 912-921. doi: http://dx.doi.org/10.1016/j.proenv.2013.06.101

Allison, M. A., Demas, C. R., Ebersole, B. A., Kleiss, B. A., Little, C. D., Meselhe, E. A., . . . Vosburg, B. M. (2012). A water and sediment budget for the lower Mississippi–Atchafalaya River in flood years 2008–2010: Implications for sediment discharge to the oceans and coastal restoration in Louisiana. *Journal of Hydrology, 432–433*(0), 84-97. doi: http://dx.doi.org/10.1016/j.jhydrol.2012.02.020

Armstrong, R. N., & Martz, L. W. (2003). Topographic parameterization in continental hydrology: a study in scale. *Hydrological Processes, 17*(18), 3763-3781. doi: 10.1002/hyp.1352

Arnold, J. G., Srinivasan, R., Muttiah, R. S., & Williams, J. R. (1998). Large area hydrologic modeling and assessment part I: Model development1: Wiley Online Library.

Arnold, J. G., Williams, J. R., Nicks, A., & Sammons, N. (1990). *SWRRB; a basin scale simulation model for soil and water resources management*: Texas A & M University Press.

Arnoldus, H. M. J. (1977). Methodology used to determine the maximum potential average annual soil loss due to sheet and rill erosion in Morocco. *FAO Soils Bulletins (FAO)*.

Asselman, N. E. M., Middelkoop, H., & van Dijk, P. M. (2003). The impact of changes in climate and land use on soil erosion, transport and deposition of suspended sediment in the River Rhine. *Hydrological Processes, 17*(16), 3225-3244. doi: 10.1002/hyp.1384

Asselman, N. E. M., & van Wijngaarden, M. (2002). Development and application of a 1D floodplain sedimentation model for the River Rhine in The Netherlands. *Journal of Hydrology, 268*(1), 127-142.

Bakker, M. M., Govers, G., van Doorn, A., Quetier, F., Chouvardas, D., & Rounsevell, M. (2008). The response of soil erosion and sediment export to land-use change in four areas of Europe: The importance of landscape pattern. *Geomorphology, 98*(3–4), 213-226. doi: http://dx.doi.org/10.1016/j.geomorph.2006.12.027

Biswas, A. K., & Tortajada, C. (2012). Impacts of the High Aswan Dam. In C. Tortajada, D. Altinbilek & A. K. Biswas (Eds.), *Impacts of Large Dams: A Global Assessment* (pp. 379-395): Springer Berlin Heidelberg.

Bookhagen, B. (2010). Appearance of extreme monsoonal rainfall events and their impact on erosion in the Himalaya. *Geomatics, Natural Hazards and Risk, 1*(1), 37-50. doi: 10.1080/19475701003625737

Brugnach, M., Tagg, A., Keil, F., & de Lange, W. J. (2007). Uncertainty matters: computer models at the science–policy interface. *Water resources management, 21*(7), 1075-1090.

Celik, I., & Rodi, W. (1991). Suspended sediment-transport capacity for open channel flow. *Journal of Hydraulic Engineering, 117*(2), 191-204.

Chaplot, V. (2014). Impact of spatial input data resolution on hydrological and erosion modeling: Recommendations from a global assessment. *Physics and Chemistry of the Earth, Parts A/B/C, 67–69*(0), 23-35. doi: http://dx.doi.org/10.1016/j.pce.2013.09.020

Chen, T., Niu, R.-q., Li, P.-x., Zhang, L.-p., & Du, B. (2011). Regional soil erosion risk mapping using RUSLE, GIS, and remote sensing: a case study in Miyun Watershed, North China. *Environmental Earth Sciences, 63*(3), 533-541. doi: 10.1007/s12665-010-0715-z

Chow, V. T. (1972). *Handbook of Applied Hydrology*. New York: McGraw-Hill.

Cohen, M. J., Shepherd, K. D., & Walsh, M. G. (2005). Empirical reformulation of the universal soil loss equation for erosion risk assessment in a tropical watershed. *Geoderma, 124*(3–4), 235-252. doi: http://dx.doi.org/10.1016/j.geoderma.2004.05.003

Cohen, S., Kettner, A. J., Syvitski, J. P. M., & Fekete, B. M. (2013). WBMsed, a distributed global-scale riverine sediment flux model: Model description and validation. *Computers & Geosciences, 53*(0), 80-93. doi: http://dx.doi.org/10.1016/j.cageo.2011.08.011

Coppus, R., & Imeson, A. C. (2002). Extreme events controlling erosion and sediment transport in a semi-arid sub-andean valley. *Earth Surface Processes and Landforms, 27*(13), 1365-1375. doi: 10.1002/esp.435

Dai, S. B., Yang, S. L., & Li, M. (2009). The sharp decrease in suspended sediment supply from China's rivers to the sea: anthropogenic and natural causes. *Hydrological Sciences Journal, 54*(1), 135-146. doi: 10.1623/hysj.54.1.135

de Santos Loureiro, N., & de Azevedo Coutinho, M. (2001). A new procedure to estimate the RUSLE EI30 index, based on monthly rainfall data and applied to the Algarve region, Portugal. *Journal of Hydrology, 250*(1–4), 12-18. doi: http://dx.doi.org/10.1016/S0022-1694(01)00387-0

Dee, D. P., Uppala, S. M., Simmons, A. J., Berrisford, P., Poli, P., Kobayashi, S., . . . Vitart, F. (2011). The ERA-Interim reanalysis: configuration and performance of the data assimilation system. *Quarterly Journal of the Royal Meteorological Society, 137*(656), 553-597. doi: 10.1002/qj.828

Demirci, A., & Karaburun, A. (2012). Estimation of soil erosion using RUSLE in a GIS framework: a case study in the Buyukcekmece Lake watershed, northwest Turkey. *Environmental Earth Sciences, 66*(3), 903-913. doi: 10.1007/s12665-011-1300-9

Dickinson, W., Rudra, R., & Clark, D. (1986). A delivery ratio approach for seasonal transport of sediment. *IAHS-AISH publication*(159), 237-252.

Dickinson, W., Rudra, R., Sharma, D., & Ahmed, S. (1992). Planning sediment monitoring programs using a watershed model. *Erosion and sediment transport monitoring programs in river basins. IAHS Publication*(210).

Diodato, N. (2004). Estimating RUSLE's rainfall factor in the part of Italy with a Mediterranean rainfall regime. *Hydrology and Earth System Sciences, 8*(1), 103-107.

Diodato, N. (2006). Predicting RUSLE (Revised Universal Soil Loss Equation) Monthly Erosivity Index from Readily Available Rainfall Data in Mediterranean Area. *Environmentalist, 26*(1), 63-70. doi: 10.1007/s10669-006-5359-x

Döll, P., & Lehner, B. (2002). Validation of a new global 30-min drainage direction map. *Journal of Hydrology, 258*(1), 214-231.

FAO, IIASA, ISRIC, ISS-CAS, & JRC. (2012). Harmonized World Soil Database (version 1.2). Rome, Italy; Laxenburg, Austria: FAO;IIASA.

Fournier, F. (1960). *Climat et érosion: la relation entre l'érosion du sol par l'eau et les précipitations atmosphériques*: Presses universitaires de France.

Goode, J. R., Luce, C. H., & Buffington, J. M. (2012). Enhanced sediment delivery in a changing climate in semi-arid mountain basins: Implications for water resource management and aquatic habitat in the northern Rocky Mountains. *Geomorphology, 139*, 1-15.

Goulden, T., Jamieson, R., Hopkinson, C., Sterling, S., Sinclair, A., & Hebb, D. (2014). Sensitivity of Hydrological Outputs from SWAT to DEM Spatial Resolution. *Photogrammetric Engineering & Remote Sensing, 80*(7), 639-652. doi: 10.14358/PERS.80.7.639

Gu, J., Chen, Z., & Salem, A. (2011). Post-Aswan dam sedimentation rate of lagoons of the Nile Delta, Egypt. *Environmental Earth Sciences, 64*(7), 1807-1813. doi: 10.1007/s12665-011-0983-2

Hay, W. W. (1994). Pleistocene-Holocene fluxes are not the Earth's norm. *Material Fluxes on the Surface of the Earth*, 15-27.

Hayhoe, H., Pelletier, R., & Coote, D. (1995). Estimating snowmelt runoff erosion indices for Canada. *Journal of soil and Water Conservation, 50*(2), 174-179.

Hessel, R. (2005). Effects of grid cell size and time step length on simulation results of the Limburg soil erosion model (LISEM). *Hydrological Processes, 19*(15), 3037-3049.

Hijmans, R. J., Cameron, S. E., Parra, J. L., Jones, P. G., & Jarvis, A. (2005). Very high resolution interpolated climate surfaces for global land areas. *International Journal of Climatology, 25*(15), 1965-1978. doi: 10.1002/joc.1276

Hovius, N. (1998). Controls on sediment supply by large rivers. In K. W. Shanley & P. J. McCabe (Eds.), *Relative Role of Estuary, Climate, and Tectonism in Continental Rocks* (pp. 2-16).

ICPDR. (2014). International Commission for the Protection of the Danube River. Retrieved 15 09, 2014, from http://www.icpdr.org/main/

Inman, D. L., & Jenkins, S. A. (1999). Climate change and the episodicity of sediment flux of small California rivers. *The Journal of Geology, 107*(3), 251-270.

Jansen, I. M. L., & Painter, R. B. (1974). Predicting sediment yield from climate and topography. *Journal of Hydrology, 21*(4), 371-380.

Jetten, V., Govers, G., & Hessel, R. (2003). Erosion models: quality of spatial predictions. *Hydrological Processes, 17*(5), 887-900.

Kienzle, S. (2004). The effect of DEM raster resolution on first order, second order and compound terrain derivatives. *Transactions in GIS, 8*(1), 83-111.

Kinnell, P. I. A. (2010). Event soil loss, runoff and the Universal Soil Loss Equation family of models: A review. *Journal of Hydrology, 385*(1–4), 384-397. doi: http://dx.doi.org/10.1016/j.jhydrol.2010.01.024

Korup, O. (2012). Earth's portfolio of extreme sediment transport events. *Earth-Science Reviews, 112*(3–4), 115-125. doi: http://dx.doi.org/10.1016/j.earscirev.2012.02.006

Kouli, M., Soupios, P., & Vallianatos, F. (2009). Soil erosion prediction using the Revised Universal Soil Loss Equation (RUSLE) in a GIS framework, Chania, Northwestern Crete, Greece. *Environmental Geology, 57*(3), 483-497. doi: 10.1007/s00254-008-1318-9

Kuenen, P. H. (1950). *Marine Geology*. New York: John Wiley & Sons.

Lehner, B., Reidy Liermann, C., Revenga, C., Vorosmarty, C., Fekete, B., Crouzet, P., . . . Wisser, D. (2011). High-Resolution Mapping of the World's Reservoirs and Dams for Sustainable River-Flow Management. *Frontiers in Ecology and the Environment, 9*, 494-502.

Liu, J. P., Xu, K. H., Li, A. C., Milliman, J. D., Velozzi, D. M., Xiao, S. B., & Yang, Z. S. (2007). Flux and fate of Yangtze River sediment delivered to the East China Sea. *Geomorphology, 85*(3–4), 208-224. doi: http://dx.doi.org/10.1016/j.geomorph.2006.03.023

Maina, J., de Moel, H., Zinke, J., Madin, J., McClanahan, T., & Vermaat, J. E. (2013). Human deforestation outweighs future climate change impacts of sedimentation on coral reefs. *Nat Commun, 4*. doi: 10.1038/ncomms2986

Martínez-Casasnovas, J. A., & Sánchez-Bosch, I. (2000). Impact assessment of changes in land use/conservation practices on soil erosion in the Penedès–Anoia vineyard region (NE Spain). *Soil and Tillage Research, 57*(1–2), 101-106. doi: http://dx.doi.org/10.1016/S0167-1987(00)00142-2

Meade, R. H. (1996). River-sediment inputs to major deltas. In J. D. Milliman & B. U. Haq (Eds.), *Sea-Level Rise and Coastal Subsidence* (pp. 63-85). Bosten, MA: Kluwer Academic Publishing.

Mhangara, P., Kakembo, V., & Lim, K. (2012). Soil erosion risk assessment of the Keiskamma catchment, South Africa using GIS and remote sensing. *Environmental Earth Sciences, 65*(7), 2087-2102. doi: 10.1007/s12665-011-1190-x

Miao, C., Ni, J., Borthwick, A. G., & Yang, L. (2011). A preliminary estimate of human and natural contributions to the changes in water discharge and sediment load in the Yellow River. *Global and Planetary Change, 76*(3), 196-205.

Middelkoop, H., & Asselman, N. E. M. (1994). *Spatial and temporal variability of floodplain sedimentation in the Netherlands*: Department of Physical Geography, Faculty of Geographical Sciences, Utrecht Univ.

Milliman, J. D., & Meade, R. H. (1983). World-wide delivery of river sediment to the oceans. *The Journal of Geology*, 1-21.

Milliman, J. D., & Syvitski, J. P. M. (1992). Geomorphic/Tectonic Control of Sediment Discharge to the Ocean: The Importance of Small Mountainous Rivers. *The Journal of Geology, 100*(5), 525-544.

Millward, A. A., & Mersey, J. E. (1999). Adapting the RUSLE to model soil erosion potential in a mountainous tropical watershed. *CATENA, 38*(2), 109-129. doi: http://dx.doi.org/10.1016/S0341-8162(99)00067-3

Morehead, M. D., Syvitski, J. P., Hutton, E. W., & Peckham, S. D. (2003). Modeling the temporal variability in the flux of sediment from ungauged river basins. *Global and Planetary Change, 39*(1), 95-110.

Morris, G. L., & Fan, J. (1998). *Reservoir sedimentation handbook: design and management of dams, reservoirs, and watersheds for sustainable use* (Vol. 9): McGraw-Hill New York.

Mukundan, R., Pradhanang, S. M., Schneiderman, E. M., Pierson, D. C., Anandhi, A., Zion, M. S., . . . Steenhuis, T. S. (2013). Suspended sediment source areas and future climate impact on soil erosion and sediment yield in a New York City water supply watershed, USA. *Geomorphology, 183*(0), 110-119. doi: http://dx.doi.org/10.1016/j.geomorph.2012.06.021

Naik, P. K., & Jay, D. A. (2011). Distinguishing human and climate influences on the Columbia River: Changes in mean flow and sediment transport. *Journal of Hydrology, 404*(3–4), 259-277. doi: http://dx.doi.org/10.1016/j.jhydrol.2011.04.035

Nearing, M. (1997). A single, continuous function for slope steepness influence on soil loss. *Soil Science Society of America Journal, 61*(3), 917-919.

Nearing, M., Pruski, F. F., & O'Neal, M. R. (2004). Expected climate change impacts on soil erosion rates: A review. *Journal of soil and Water Conservation, 59*(1), 43-50.

New, M., Hulme, M., & Jones, P. (2000). Representing twentieth-century space-time climate variability. Part II: Development of 1901-96 monthly grids of terrestrial surface climate. *Journal of Climate, 13*(13), 2217-2238.

New, M., Lister, D., Hulme, M., & Makin, I. (2002). A high-resolution data set of surface climate over global land areas. *Climate research, 21*(1), 1-25.

Nunes, A. N., de Almeida, A. C., & Coelho, C. O. A. (2011). Impacts of land use and cover type on runoff and soil erosion in a marginal area of Portugal. *Applied Geography, 31*(2), 687-699. doi: http://dx.doi.org/10.1016/j.apgeog.2010.12.006

Olang, L. O., & Fürst, J. (2011). Effects of land cover change on flood peak discharges and runoff volumes: model estimates for the Nyando River Basin, Kenya. *Hydrological Processes, 25*(1), 80-89. doi: 10.1002/hyp.7821

ORE-HYBAM. Data. Retrieved 09 13, 2014, from http://www.ore-hybam.org/index.php/eng/Data

Osterkamp, W. R., Hupp, C. R., & Stoffel, M. (2012). The interactions between vegetation and erosion: new directions for research at the interface of ecology and geomorphology. *Earth Surface Processes and Landforms, 37*(1), 23-36. doi: 10.1002/esp.2173

Palmieri, A., Shah, F., & Dinar, A. (2001). Economics of reservoir sedimentation and sustainable management of dams. *Journal of Environmental Management, 61*(2), 149-163. doi: http://dx.doi.org/10.1006/jema.2000.0392

Pelletier, J. D. (2012). A spatially distributed model for the long-term suspended sediment discharge and delivery ratio of drainage basins. *Journal of Geophysical Research: Earth Surface (2003–2012), 117*(F2).

Pierce, A. R., & King, S. L. (2008). Spatial dynamics of overbank sedimentation in floodplain systems. *Geomorphology, 100*(3), 256-268.

Prasannakumar, V., Shiny, R., Geetha, N., & Vijith, H. (2011). Spatial prediction of soil erosion risk by remote sensing, GIS and RUSLE approach: a case study of Siruvani river watershed in Attapady valley, Kerala, India. *Environmental Earth Sciences, 64*(4), 965-972. doi: 10.1007/s12665-011-0913-3

Prasannakumar, V., Vijith, H., Abinod, S., & Geetha, N. (2012). Estimation of soil erosion risk within a small mountainous sub-watershed in Kerala, India, using Revised Universal Soil Loss Equation (RUSLE) and geo-information technology. *Geoscience Frontiers, 3*(2), 209-215. doi: http://dx.doi.org/10.1016/j.gsf.2011.11.003

Prosser, I. P., Rutherfurd, I. D., Olley, J. M., Young, W. J., Wallbrink, P. J., & Moran, C. J. (2001). Large-scale patterns of erosion and sediment transport in river networks, with examples from Australia. *Marine and Freshwater Research, 52*(1), 81-99.

Ranzi, R., Le, T. H., & Rulli, M. C. (2012). A RUSLE approach to model suspended sediment load in the Lo river (Vietnam): Effects of reservoirs and land use changes. *Journal of Hydrology, 422–423*(0), 17-29. doi: http://dx.doi.org/10.1016/j.jhydrol.2011.12.009

Renard, K. G., Foster, G. R., Weesies, G. A., McCool, D., & Yoder, D. (1997). Predicting soil erosion by water: a guide to conservation planning with the revised universal soil loss equation (RUSLE). *Agriculture Handbook (Washington)*(703).

Renard, K. G., & Freimund, J. R. (1994). Using monthly precipitation data to estimate the R-factor in the revised USLE. *Journal of Hydrology, 157*(1–4), 287-306. doi: http://dx.doi.org/10.1016/0022-1694(94)90110-4

Restrepo, J. D., & Kjerfve, B. (2000). Magdalena river: interannual variability (1975–1995) and revised water discharge and sediment load estimates. *Journal of Hydrology, 235*(1–2), 137-149. doi: http://dx.doi.org/10.1016/S0022-1694(00)00269-9

Rojas, R., Velleux, M., Julien, P., & Johnson, B. (2008). Grid Scale Effects on Watershed Soil Erosion Models. *Journal of Hydrologic Engineering, 13*(9), 793-802. doi: doi:10.1061/(ASCE)1084-0699(2008)13:9(793)

Sharpley, A. N., & Williams, J. R. (1990). EPIC-erosion/productivity impact calculator: 1. Model documentation. *Technical Bulletin-United States Department of Agriculture*(1768 Pt 1).

Sørensen, R., & Seibert, J. (2007). Effects of DEM resolution on the calculation of topographical indices: TWI and its components. *Journal of Hydrology, 347*(1–2), 79-89. doi: http://dx.doi.org/10.1016/j.jhydrol.2007.09.001

Stahl, G., Koschmann, T., & Suthers, D. (2006). Computer-supported collaborative learning: An historical perspective. *Cambridge handbook of the learning sciences, 2006*.

Syvitski, J. P. M. (2003). Supply and flux of sediment along hydrological pathways: research for the 21st century. *Global and Planetary Change, 39*(1–2), 1-11. doi: http://dx.doi.org/10.1016/S0921-8181(03)00008-0

Syvitski, J. P. M. (2008). Deltas at risk. *Sustainability Science, 3*(1), 23-32. doi: 10.1007/s11625-008-0043-3

Syvitski, J. P. M., & Milliman, J. D. (2007). Geology, Geography, and Humans Battle for Dominance over the Delivery of Fluvial Sediment to the Coastal Ocean. *Journal of Geology, 115*, 1-9.

Syvitski, J. P. M., Vörösmarty, C. J., Kettner, A. J., & Green, P. (2005). Impact of Humans on the Flux of Terrestrial Sediment to the Global Coastal Ocean. *Science, 308*(5720), 376-380. doi: 10.1126/science.1109454

Tilman, D., Balzer, C., Hill, J., & Befort, B. L. (2011). Global food demand and the sustainable intensification of agriculture. *Proceedings of the National Academy of Sciences, 108*(50), 20260-20264. doi: 10.1073/pnas.1116437108

Torri, D., Poesen, J., & Borselli, L. (1997). Predictability and uncertainty of the soil erodibility factor using a global dataset. *CATENA, 31*(1–2), 1-22. doi: 10.1016/S0341-8162(97)00036-2

U.S. Geological Survey. (2004). *HYDRO1k Elevation Derivative Database*

U.S. Geological Survey. (2014). Sediment Portal. Retrieved 13 09, 2014, from http://cida.usgs.gov/sediment/#

van Beek, L. P. H., & Bierkens, M. F. P. (2008). The Global Hydrological Model PCR-GLOBWB: Conceptualization, Parameterization and Verification. Utrecht, The Netherlands: Department of Physical Geography.

Van der Knijff, J., Jones, R., & Montanarella, L. (1999). *Soil erosion risk assessment in Italy*: European Soil Bureau, European Commission.

Van der Knijff, J., Jones, R., & Montanarella, L. (2000). *Soil erosion risk assessment in Europe*: European Soil Bureau, European Commission.

Van der Zwan, C. J. (2002). The impact of Milankovitch-scale climatic forcing on sediment supply. *Sedimentary Geology, 147*(3–4), 271-294. doi: http://dx.doi.org/10.1016/S0037-0738(01)00130-0

van Dijk, P. M. (2001). *Soil erosion and associated sediment supply to river. Seasonal dynamics, soil conservation measures and impacts of climate change.* (PhD Thesis), University of Amsterdam, Amsterdam.

Van Remortel, R. D., Hamilton, M. E., & Hickey, R. J. (2001). Estimating the LS Factor for RUSLE through Iterative Slope Length Processing of Digital Elevation Data within ArcInfo Grid. *Cartography, 30*(1), 27-35. doi: 10.1080/00690805.2001.9714133

Vanmaercke, M., Zenebe, A., Poesen, J., Nyssen, J., Verstraeten, G., & Deckers, J. (2010). Sediment dynamics and the role of flash floods in sediment export from medium-sized catchments: a case study from the semi-arid tropical highlands in northern Ethiopia. *Journal of Soils and Sediments, 10*(4), 611-627. doi: 10.1007/s11368-010-0203-9

Vaze, J., Teng, J., & Spencer, G. (2010). Impact of DEM accuracy and resolution on topographic indices. *Environmental Modelling & Software, 25*(10), 1086-1098.

Vörösmarty, C. J., Meybeck, M., Fekete, B., Sharma, K., Green, P., & Syvitski, J. P. M. (2003). Anthropogenic sediment retention: major global impact from registered river impoundments. *Global and Planetary Change, 39*(1–2), 169-190. doi: http://dx.doi.org/10.1016/S0921-8181(03)00023-7

Wall, G. J., Dickinson, W. T., Rudra, R. P., & Coote, D. R. (1988). Seasonal soil erodibility variation in Southwestern Ontario. *Canadian Journal of Soil Science, 68*(2), 417-424. doi: 10.4141/cjss88-038

Walling, D. E. (2006). Human impact on land–ocean sediment transfer by the world's rivers. *Geomorphology, 79*(3–4), 192-216. doi: http://dx.doi.org/10.1016/j.geomorph.2006.06.019

Walling, D. E., & He, Q. (1998). The spatial variability of overbank sedimentation on river floodplains. *Geomorphology, 24*(2), 209-223.

Wang, H., Yang, Z., Saito, Y., Liu, J. P., Sun, X., & Wang, Y. (2007). Stepwise decreases of the Huanghe (Yellow River) sediment load (1950–2005): Impacts of climate change and human activities. *Global and Planetary Change, 57*(3–4), 331-354. doi: http://dx.doi.org/10.1016/j.gloplacha.2007.01.003

Wang, H., Yang, Z., Wang, Y., Saito, Y., & Liu, J. P. (2008). Reconstruction of sediment flux from the Changjiang (Yangtze River) to the sea since the 1860s. *Journal of Hydrology, 349*(3–4), 318-332. doi: http://dx.doi.org/10.1016/j.jhydrol.2007.11.005

Wener, C. G. (1981). *Soil Conservation in Kenya, Nairobi*: Ministry of Agriculture, Soil Conservation Unit.

Wesseling, C. G., Karssenberg, D.-J., Burrough, P. A., & Deursen, W. P. A. (1996). Integrating dynamic environmental models in GIS: the development of a Dynamic Modelling language. *Transactions in GIS, 1*(1), 40-48.

Wischmeier, W. H., & Smith, D. D. (1978). Predicting rainfall erosion losses-A guide to conservation planning. *Predicting rainfall erosion losses-A guide to conservation planning*.

Wisser, D., Fekete, B., Vörösmarty, C. J., & Schumann, A. H. (2010). Reconstructing 20th century global hydrography: a contribution to the Global Terrestrial Network-Hydrology (GTN-H). *Hydrology and Earth System Sciences, 14*(1), 1-24.

Wisser, D., Frolking, S., Hagen, S., & Bierkens, M. F. P. (2013). Beyond peak reservoir storage? A global estimate of declining water storage capacity in large reservoirs. *Water Resources Research, 49*(9), 5732-5739. doi: 10.1002/wrcr.20452

Woodward, J. C., Macklin, M. G., Krom, M. D., & Williams, M. A. (2007). The Nile: evolution, Quaternary river environments and material fluxes. *Large rivers: geomorphology and management, 13*, 712.

Wu, S., Li, J., & Huang, G. (2005). An evaluation of grid size uncertainty in empirical soil loss modeling with digital elevation models. *Environmental Modeling & Assessment, 10*(1), 33-42. doi: 10.1007/s10666-004-6595-4

Xiqing, C., Erfeng, Z., Hongqiang, M., & Zong, Y. (2005). A Preliminary Analysis of Human Impacts on Sediment Discharges from the Yangtze, China, into the Sea. *Journal of Coastal Research*, 515-521. doi: 10.2112/03-0034.1

Yang, D., Kanae, S., Oki, T., Koike, T., & Musiake, K. (2003). Global potential soil erosion with reference to land use and climate changes. *Hydrological Processes, 17*(14), 2913-2928. doi: 10.1002/hyp.1441

Yang, S. L., Li, M., Dai, S. B., Liu, Z., Zhang, J., & Ding, P. X. (2006). Drastic decrease in sediment supply from the Yangtze River and its challenge to coastal wetland management. *Geophysical Research Letters, 33*(6), L06408. doi: 10.1029/2005GL025507

Yang, S. L., Milliman, J. D., Xu, K. H., Deng, B., Zhang, X. Y., & Luo, X. X. (2014). Downstream sedimentary and geomorphic impacts of the Three Gorges Dam on the Yangtze River. *Earth-Science Reviews, 138*(0), 469-486. doi: http://dx.doi.org/10.1016/j.earscirev.2014.07.006

Yang, S. L., Zhang, J., & Xu, X. J. (2007). Influence of the Three Gorges Dam on downstream delivery of sediment and its environmental implications, Yangtze River. *Geophysical Research Letters, 34*(10), L10401. doi: 10.1029/2007GL029472

Yu, B., & Rosewell, C. (1996). A robust estimators of the R-reaction for the Universal Soil Loss Eequation. *Transactions of the ASAE, 39*(2), 559-561.

Zhang, X.-C., Nearing, M. A., Garbrecht, J. D., & Steiner, J. L. (2004). Downscaling Monthly Forecasts to Simulate Impacts of Climate Change on Soil Erosion and Wheat Production. *Soil Science Society of America Journal, 68*(4), 1376-1385. doi: 10.2136/sssaj2004.1376

Appendices

A) Input data

Data	Distributed by	Original spatial resolution	Original temporal resolution
Slope map	PCRGLOB-WB	0.5°	-
Slope length	PCRGLOB-WB	0.5°	-
Precipitation	CRU TS 2.1/ CRU CLIM 1.0	0.5°	Monthly
Temperature	WorldClim	10’	Monthly
Soil properties	HWSD	30’’	-
NDVI	MODIS/ ICDC	0.05°	Monthly
Surface runoff	PCRGLOB-WB	0.5°	Daily
Land use and cover	PCRGLOB-WB	0.5°	-

B) Model parameters

Symbol	Description	Unit	Dynamic/ Static
L	Slope length factor	-	S
l_c	Contributing slope length	m	S
s	Slope angle	$m\ m^{-1}$	S
S	Slope steepness factor	-	S
Φ	Slope angle	°	S
P_{year}	Annual precipitation	$mm\ year^{-1}$	S
R	Annual rainfall-runoff erosivity factor	$MJ\ mm\ ha^{-1}\ h^{-1}\ year^{-1}$	S
Part	Monthly fraction of precipitation	-	D
P	Monthly precipitation	$mm\ month^{-1}$	D
R	Monthly rainfall-runoff erosivity factor	$MJ\ mm\ ha^{-1}\ h^{-1}\ month^{-1}$	D
K_a	Annual soil erodibility factor	$T\ ha\ h\ ha^{-1}\ MJ^{-1}\ mm^{-1}$	S
OM	Organic matter content in top soil	%	S
Cl	Fraction of clay in top soil	-	S
D_g	Naperian logarithm of mean particle size	-	S
f_{sand}	Fraction of sand in top soil	-	S
f_{silt}	Fraction of silt in top soil	-	S
f_{clay}	Fraction of clay in top soil	-	S
MaxT	Maximum monthly temperature	°C	D
MinT	Maximum monthly temperature	°C	D
SMT	Snow melting temperature	°C	S
MT_{fr}	Melting time fraction	-	D
K_{ratio}	Factor representing impact of soil texture on soil erodibility	-	S
K_m	Monthly soil erodibility factor	$T\ ha\ h\ ha^{-1}\ MJ^{-1}\ mm^{-1}$	D
C	Land cover and management factor	-	D
NDVI	Normalized Differentiated Vegetation Index	-	D
Y	Soil conservation factor	-	S
A	Monthly soil loss	$T\ ha^{-1}\ month^{-1}$	D
l	Distance to channel	m	S
H_c	Hydrologic coefficient	-	D
Q_s	Monthly surface water discharge	$mm\ month^{-1}$	D
n	Manning's surface roughness coefficient	$s/m^{1/3}$	D
n_1	Roughness due to irregularities	$s/m^{1/3}$	S
n_2	Roughness due to obstacles	$s/m^{1/3}$	S
v_3	Changes in vegetation cover	-	D
n_4	Roughness due to vegetation cover	$s/m^{1/3}$	S
DR	Delivery ratio	-	D
SD	Sediment delivery	$T\ ha^{-1}\ month^{-1}$	D

C) PCRGLOB-SET code for PCRaster

```
##############################################
# Model: PCRGLOB-SET                          #
# Date: 07.11.2014                            #
# Version: 1.0                                #
# Author: Jannis Hoch                         #
#       B.Sc. Civil Engineering               #
#       University of Twente                  #
##############################################
```

binding

```
    #### INPUT ####

    ## TOPOGRAPHY ##
    slopeGRA= $1\topography\globalgradslope.map; # slope angle in m/m (from PCRGLOB-WB)
    slopeLENGTH= $1\topography\globalbcat.map; # slope length in m (from PCRGLOB-WB)
                                               # also length of flow path
    LDD= $1\topography\glwd130m_ldd.map; # local drainage direction (from PCRGLOB-WB)
    CellArea= $1\topography\CellArea.map; # total surface (m2) covered per grid cell (from PCRGLOB-WB)

    ## CLIMATE ##
    Precipitation= $1\climate\Precip00; # mean monthly CRU precipitation (1950-2000)
    Pannual= $1\climate\Pannual.map; # calculated in pre-step from CRU precipitation data (1950-2000)
    Tmaximum= $1\climate\Tmax05dg; # mean monthly max. temperature from WorldClim project (1950-2000)
    Tminimum= $1\climate\Tmin05dg; # mean monthly min. temperature from WorldClim project (1950-2000)

    ## HYDROLOGY ##
    Qs= $1\hydrology\Qsurface; # monthly surface discharge, calculated in PCRGLOB-WB (1950-2000)
    RiverLOCS= $1\hydrology\rivers_maximumarea_selected.map; # locations of river basin outlets

    ## VEGETATION ##
    NDVImaps= $1\vegetation\NDVI2009; # monthly NDVI values for 2009 from MODIS
     barrensparse= $1\vegetation\barrensparse.map; # relative values of land cover types per grid cell (from PCRGLOB-WB)
    closedshrub= $1\vegetation\closedshrub.map; #...
    crop= $1\vegetation\croplands.map; #..
    decbroad= $1\vegetation\decbroadleaf.map; #.
    decneedle= $1\vegetation\decneedleleaf.map;
    evergrbroad= $1\vegetation\evergrbroadleaf.map;
    evergrneedle= $1\vegetation\evergrneedle.map;
    grass= $1\vegetation\grasslands.map;
    mixforests= $1\vegetation\mixedforests.map;
    openshrub= $1\vegetation\openshrub.map;
    permanentwet= $1\vegetation\permanentwet.map;
    savannas= $1\vegetation\savannas.map;
    snowice= $1\vegetation\snowice.map;
```

```
urban= $1\vegetation\urbanbuilt.map;
water= $1\vegetation\waterbodies.map;
woodysavannas= $1\vegetation\woodysavannas.map;

## SOIL PROPERTIES ##
Text0= $1\soil\Texture0_05deg.map; # maps with soil texture classes 0 until 3 (0=no texture) (from HWSD)
Text1= $1\soil\Texture1_05deg.map; # (1=fine texture)
Text2= $1\soil\Texture2_05deg.map; # (2=medium texture)
Text3= $1\soil\Texture3_05deg.map; # (3=coarse texture)
fsand= $1\soil\fsand_05deg.map; # fractions of sand, silt and clay (from HWSD)
fsilt= $1\soil\fsilt_05deg.map;
fclay= $1\soil\fclay_05deg.map;
OM= $1\soil\OM.map;

## CONSTANTS ##
SMT=scalar(0); # snow melt temperature
n2=scalar(0.049); # Manning's surface roughness coefficient n2
ALPHA=scalar(9.53);
BETA=scalar(0.79);
THETA=scalar(2);
ZETA=scalar(1);

## TABLES ##
gammaTBL= $1\tbl\gamma.tbl; #table relating slope angles to gamma-values
N1TBL= $1\tbl\manningN1.tbl; #table relating slope angles to irregularities

#### OUTPUT ####

slopeDEG=$2\slopeDEG.map; # map with slope angle in degree

R1= $2\maps\Erosion\Rfactor\R1.map;
R2= $2\maps\Erosion\Rfactor\R2.map;
Ryear= $2\maps\Erosion\Rfactor\Rannual.map; # annual R-value
L= $2\maps\Erosion\LSfactor\Lfactor.map;
S= $2\maps\Erosion\LSfactor\Sfactor.map;
LS= $2\maps\Erosion\LSfactor\LSfactor.map;
Part= $2\maps\Erosion\Rfactor\Part0000; # Monthly fraction of precipitation
R= $2\maps\Erosion\Rfactor\Rfactor0; # monthly R-values
MTfr= $2\maps\Erosion\Kfactor\MTFR0000; # melt time fraction per month
KratioTOT= $2\maps\Erosion\Kfactor\Kratio.map;
Kyear= $2\maps\Erosion\Kfactor\Kyear.map;
Dg= $2\maps\Erosion\Kfactor\Dg.map;
K= $2\maps\Erosion\Kfactor\Kfactor;
C= $2\maps\Erosion\Cfactor\Cfactor;
A= $2\maps\Erosion\Erosion0; # total soil loss per month [MT/month/cell]
AHectare= $2\maps\Erosion\ErosHect; # total soil loss per month [MT/month/hectare]
```

```
Aaccu= $2\maps\Erosion\ErosAccu; # accumulated soil loss [MT/month]
Ayear= $2\maps\Erosion\ErosionAnnual.map; # annual aggregate of soil loss [MT/year]

Manning= $2\maps\DeliveryRatio\Manning0; # total manning coefficient [-]
Hc= $2\maps\DeliveryRatio\HydrCoef; # hydrologic coefficient [-]
DR= $2\maps\DeliveryRatio\DelRatio; # delivery ratio per cell [-]

SSgrid= $2\maps\SedimentSupply\SSgrid00; # hillslope sediment delivery [MT/month/cell]
SSgridANNUAL= $2\maps\SedimentSupply\SSgridANNUAL.map; # annual aggregate of sediment supply [MT/year]
SSHectare= $2\maps\SedimentSupply\SSHectar; # hillslope sediment delivery [MT/month/hectare]
SSAccu= $2\maps\SedimentSupply\SedAccu0; # accumulated sediment delivery [MT/month]
SSOceansTSS= $2\tss\Sed2OCEAN.tss; # time series of sediment delivery at basin outlets [MT/month]
```

areamap

```
globalclone.map; (from PCRGLOB-WB)
```

timer

```
1 12 1;
```

initial

```
slopeDEG1=atan(slopeGRA); # changing units from m/m to degree
report slopeDEG=scalar(slopeDEG1);
slopeGRA=slopeGRA*100; # calculating "full" percentage values (i.e. m/m to %)

# TOPGRAPHIC FACTOR LS #
gamma=lookupscalar(gammaTBL,slopeGRA); # associating slopes to gamma-values
report L=(slopeLENGTH/22.13)**gamma; # calculating L, S and LS-factor
report S=-1.5+(17/(1+exp(2.3-(6.1*slopeDEG))));
report LS=L*S;

report R1=if(Pannual le 850 then (0.04830*Pannual**1.1610) else 0); # applying equations from Renard & Freimund
report R2=if(Pannual gt 850 then (587.8-1.219*Pannual+0.004105*Pannual**2) else 0);
report Ryear=R1+R2; # "overlay" of both R values to obtain one combined map

# SOIL ERODIBILITY K #
Kratio0=if(Text0 eq 1 then 1.44 else 0); # asscociating soil texture to Kratio values
Kratio1=if(Text1 eq 1 then 1.17 else 0);
Kratio2=if(Text2 eq 1 then 1.44 else 0);
Kratio3=if(Text3 eq 1 then 4.50 else 0);
report KratioTOT=Kratio0+Kratio1+Kratio2+Kratio3; # unifying Kratio values to one map

fsand=fsand/100; # converting percentage content of sand, silt and clay to fraction
fsilt=fsilt/100;
fclay=fclay/100;
OMC=OM/fclay;
report Dg=-3.5*fsand-2.0*fsilt-0.5*fclay; # Naperian logarithm of geometric mean
EXP=(-0.0021*OMC-0.00037*(OMC)**2-4.02*fclay+1.12*fclay**2); # calc Kyear
Kyear=0.0293*(0.65-Dg+0.24*Dg**2)**EXP;
```

```
report Kyear=cover(Kyear,mapminimum(Kyear)); # covering MVs with minimum of all Kyear values in map

# MANNING SURFACE ROUGHNESS #
Bar=barrensparse*0.0113; # associating roughness values to various land cover types
ShrubCl=closedshrub*0.4; #...
Crp=crop*0.04; #..
DecBrd=decbroad*0.36; #.
DecNdl=decneedle*0.36;
EgrBrd=evergrbroad*0.32;
EgrNdl=evergrneedle*0.32;
Grs=grass*0.368;
For=mixforests*0.4;
ShrubOp=openshrub*0.4;
Wet=permanentwet*0.086;
Sav=savannas*0.368;
SnI=snowice*0.00001;
Urb=urban*0.015;
Wtr=water*0.023;
SavWdy=woodysavannas*0.365;
n4=Bar+ShrubCl+Crp+DecBrd+DecNdl+EgrBrd+EgrNdl+Grs+For+ShrubOp+Wet+Sav+SnI+Urb+Wtr+SavWdy; # summing individual roughnesses

SSgridANNUAL=scalar(0);
```

dynamic

```
Precip=timeinput(Precipitation); # importing various mapstacks
Qsurface=timeinput(Qs);
Qsurface=Qsurface*1000;
Tmax=timeinput(Tmaximum);
Tmax=Tmax/10; # due to scaling factor in input
Tmin=timeinput(Tminimum);
Tmin=Tmin/10; # due to scaling factor in input
NDVI=timeinput(NDVImaps);
NDVI=NDVI/10000; # due to scaling factor in input

## RUSLE MODULE ##

# TOPGRAPHIC FACTOR LS #
# see initial section

# RAINFALL-RUNOFF EROSIVITY R #
Part=Precip/Pannual; # relative monthly precipitation to annual precipitation
report Part=cover(Part,0);
R=Ryear*Part; # calculating monthly R-values
report R=cover(R,windowmaximum(R,1));
```

```
# SOIL ERODIBILITY K#
MTfr=if(Tmax gt SMT then ((Tmax-SMT)/(Tmax-Tmin)) else 0); # calculating melt time fraction per month
MTfr=if(MTfr lt 0 then 0 else MTfr);
MTfr=if(MTfr gt 1 then 1 else MTfr);
report MTfr=cover(MTfr,windowminimum(MTfr,1));

report K=KratioTOT*MTfr*Kyear+Kyear*(1-MTfr);

# MANAGEMENT FACTOR C #
C=exp(-THETA*(NDVI/(ZETA-NDVI))); # calculating C-factor according to van Knijff
report C=cover(C,windowmaximum(C,1));

# SOIL LOSS A #
report A=LS*R*K*C; # applying RUSLE and reporting soil loss (T month-1 gridcell-1)
report Aaccu=accuflux(LDD,((1E-6)*A)); # accumulated erosion in MT per month
report Ayear=Ayear+A*(1E-6); # aggregating each month to a yearly erosion value

## DELIVERY RATIO MODULE ##

# MANNING SURFACE ROUGHNESS #
n1=lookupscalar(N1TBL,slopeGRA); # associating Manning sub-factor to slopes
n1=cover(n1,0); #covering MVs
v3=NDVI; # associating Manning sub-factor v3 to monthly NDVI values
v3=if(v3 le 0 then 0 else v3); # excluding negative NDVI values (no negative roughness possible)
report Manning=n1+n2+v3*n4; # calculating total Manning's surface roughness coefficient

# HYDROLGIC COEFFICIENT Hc #
Hc=Qsurface/Precip;
Hc=max(0,Hc);
Hc=min(1,Hc);
report Hc=cover(Hc,0.0001); # covering MVs

# DELIVERY RATIO DR #
DR=ALPHA*((Hc*sqrt(slopeGRA))/(Manning*slopeLENGTH))**BETA; # applying DR equation
report DR=if(DR gt 1 then 1 else DR);

## HILLSLOPE DELIVERY MODULE ##

report SSgrid=(1E-6)*A*DR; # applying equation (result in MT/month/gridcell)
report SSgridANNUAL=SSgridANNUAL+SSgrid; # aggregating each month to a yearly sediment supply value
report SSHectare=SSgrid*CellArea/10000; # converting to MT/month/hectare

report SSAccu=accuflux(LDD,SSHectare); # accumulating delivered sediment along channels/rivers (MT/month)
report SSOceansTSS=timeoutput(RiverLOCS,SSAccu); # creating timeseries of sediment delivery at ouflows to oceans
```

D) Global river basins map